https://doi.org/10.1016/j.compfluid.2019.04.009

Progress in the Development of a New Lattice Boltzmann Method

R. M. C. So[1], R. C. K. Leung[2,] *, E. W. S. Kam[3], S. C. Fu[4]

Abstract

A new modeled Boltzmann equation (MBE) with four improvements made to conventional MBE is formulated. The first improvement is to include the particle internal rotational degree of freedom in the derivation of a continuous equilibrium velocity distribution function f^{eq}; thus, rendering the MBE applicable to diatomic gas. The second improvement is made in the expansion assumed for f_α^{eq} in the lattice Boltzmann equation (LBE). This expansion is expressed in terms of the particle velocity vector ($\boldsymbol{\xi}$) alone; hence, the LBE is no longer limited by a very low Mach number (M) assumption, and it also allows the LBE to correctly satisfy the zero divergence of the velocity field for incompressible flow. The third improvement is made to eliminate the bounce-back rule used to model no-slip wall boundary condition for f_α because the rule leads to leakage at solid walls and mass conservation is compromised. The fourth improvement is carried out to render the modeled LBE truly valid for hydrodynamic flow simulation. Thus improved, the new lattice Boltzmann method (LBM) is no longer subject to the $M << 1$ condition and can be confidently extended to hydrodynamic simulations where the flow is truly incompressible. The f_α^{eq} expansion coefficients are found to be functions of the primitive variables, their derivatives and their products. In this LBE, fluid properties are inputs, and boundary values of f_α are deduced from the primitive variables at the boundaries. Only a D2Q9 and a D3Q15 lattice model are required for 2-D and 3-D flow simulation, respectively. A finite difference splitting method is used to solve the new LBM; the scheme is labeled FDLBM, and it has been used to simulate widely different laminar flow of gas and liquid; incompressible with/without heat transfer, compressible with/without shocks, aeroacoustics with/without scattering, thermo-aeroacoustics, buoyant and double diffusive flow, and non-Newtonian flow, as well as blood flow in arteries with/without blockage. Accurate results are obtained, and they agree with other finite-difference numerical simulations of the same problems, and experimental and theoretical results whenever available. Furthermore, the aeroacoustics results are in agreement with those obtained from direct aeroacoustics simulations of the same problems.

[1] Professor Emeritus, Hong Kong Polytechnic University, Kowloon, HK, HKSAR
[2] Associate Professor, Hong Kong Polytechnic University, Kowloon, HK, HKSAR
*Corresponding author email address: Randolph.leung@polyu.edu.hk
[3] Lecturer, Rensselaer Polytechnic Institute, Troy, NY, USA
[4] Research Assistant Professor, Hong Kong University of Science and Technology, Clearwater Bay, HK, HKSAR

Contents

Nomenclature

BE	Boltzmann equation
c	speed of sound
C_p	specific heat at constant pressure
$\left(C_p\right)_r$	macroscopic reference C_p
CFD	computational fluid dynamics
D	problem dimension
D_T	translational degree of freedom of the particle
D_R	rotational degree of freedom of the particle
DAS	direct aeroacoustics simulations
DNS	direct numerical simulations
e	internal energy
e_t	total internal energy
f	particle distribution function
f^{eq}	equilibrium particle distribution function
$f^{(n)}$	n^{th} element of f
FDLBM	finite difference lattice Boltzmann method
$\boldsymbol{g}$	gravitational acceleration vector
IBM	immersed boundary method
Kn	Knudsen number
L	characteristic length
LBE	lattice Boltzmann equation
LBM	lattice Boltzmann method
M	Mach number
MBE	modeled Boltzmann equation
p	pressure
Pr	Prandtl number
R	universal gas constant
Re	Reynolds number
T	gas temperature
S	salinity
t	time
$\boldsymbol{u}$	fluid velocity vector
u	stream velocity component

v	normal velocity component
$\boldsymbol{x}$	position vector
x	stream coordinate
$x^{(i)}$	i^{th} element of x
y	normal coordinate
γ	specific heat ratio
θ	normalized temperature (= RT)
κ	fluid conductivity
μ	fluid shear viscosity
$\boldsymbol{\xi}$	particle velocity vector
ρ	fluid density
σ	lattice velocity magnitude
τ	relaxation time
Subscripts	
i, j	vector and/or tensor indices
o	microscopic reference condition
r	macroscopic reference condition
α	index for the lattice velocity
∞	upstream reference condition
Superscripts	
$\wedge$	hat denotes dimensional quantities
n	indicates the order of a term in Chapman-Enskog expansion in terms of Kn

1. Introduction

1.1 Background

In the past several decades, the continuous Boltzmann equation (BE) has been proposed as an alternative to the Euler and Navier-Stokes (N-S) equations for gas dynamic, and fluid dynamic studies [1, 2, 3]. The BE describes the evolution of the particle distribution function $\hat{f}$ as a result of particle streaming and collisions [4, 5]. Once the transport of $\hat{f}$ is known, the macroscopic properties of the fluid medium, such as density, momentum, internal energy, and their fluxes, can be determined from the integral of the moments of $\hat{f}$. From a transport viewpoint, it appears that the BE approach has advantages over that of the Euler and N-S equations. For example, the BE is applicable even when the medium cannot be treated as a

continuum, such as in rarefied gas flow; also, the BE can be used to derive the gas equation of state, viscous stresses, and heat conduction of the fluid for monatomic gas, even though the applicability of these expressions might not be valid for diatomic and polyatomic gas. Furthermore, the attractiveness of the BE approach is derived from the fact that the BE can be solved by implementing the Bhatnagar, Gross, and Krook (BGK) model [6] and the Chapman-Enskog [7] expansion for $\hat{f}$ in terms of the Knudson number *Kn* to enable full recovery of the Euler [3, 4] and N-S [8, 9, 10, 11] equations in the limit of small *Kn*. This equation is designated as the modeled BE or MBE. In the lattice approach to solve the MBE, typically, the equilibrium particle distribution function f_α^{eq} is expanded in terms of the inner product of the particle velocity ($\boldsymbol{\xi}$) and the mean flow velocity ($\boldsymbol{u}$) [12, 13]. Thus formulated, a lattice Boltzmann method (LBM) like that obtained from the lattice gas automata [5, 8, 9, 10] is derived. The resulting LBM is discrete in the velocity space and can be used to simulate the evolution of fluid particles. The equations in the LBM are essentially linear [2, 3, 8]; therefore, the numerical code developed could exploit the lack of second order gradient terms in the LBM model, and their intrinsic feature of parallelism [11, 12]. Since then, a variety of finite difference LBM techniques (FDLBM) have been proposed for different types of flow, including single component gas dynamic and aerodynamic studies, multiphase and multicomponent flows, particle suspension in fluids, and flow through porous media in two and three dimensions [1, 2, 3, 13]. On the other hand, the gas equation of state, the Stokes viscous hypothesis, and the Fourier heat conduction relation must be specified in any numerical solution of the N-S equations. Furthermore, special consideration is necessary in the treatment of the second order gradient terms in the N-S equations and the numerical method employed to treat these terms if artificial dissipation in numerical simulations were to be kept to a minimum. These requirements render the development of a general numerical code, where artificial dissipation is kept to a minimum and yet is relatively accurate, rather challenging.

As attractive as the FDLBM might be, inherent weaknesses can be found in conventional LBM that could render the FDLBM less desirable compared to numerically solving the Euler and

N-S equations directly. For example, current FDLBM is essentially based on the assumption that a Maxwellian distribution function can be used to represent the equilibrium distribution function f^{eq} in the BE [7] with only the translational degree of freedom of gas particles taken into account. This assumption renders the modeled BE valid for monatomic gas only. Consequently, *Re*, *Pr*, γ, κ, and viscous stresses, etc., thus calculated are not correct for diatomic gas, and the recovered Euler and N-S equations are subject to this limitation. This inadequacy of the LBM is quite undesirable and needs to be addressed if the FDLBM were to be valid for diatomic gas and can recover the state equation, γ, κ, *Re*, *Pr*, etc. correctly. Another inadequacy originates from the expansion of the lattice f_α^{eq}. A mean flow velocity $\boldsymbol{u}$ is included in this expansion. Consequently, if the expansion were to converge properly, the resulting *M* has to be very small, thus subjecting the LBM to limited applications. A third inadequacy is given rise by the fact that it is very difficult, if not impossible, to correctly evaluate f_α at a solid wall such that the no-slip condition at the wall is satisfied exactly. This inability to determine the wall value of f_α correctly leads to mass leakage at the wall. The fourth inadequacy is also related to the $M << 1$ assumption. Quite often, the LBM is used to tackle hydrodynamic problems. Since the LBM is subject to the $M << 1$ condition, strictly speaking, it is not suitable for hydrodynamic flow simulation because liquid is truly an incompressible fluid. Therefore, if the LBM approach were used to treat hydrodynamic flow, it is necessary to show that a discrete flux representation approach used to derive the Euler and N-S equations could lead to an equation that is similar to the MBE and fluid density can again be defined by the summation of f^{eq}, which is now used to represent a group of masses of fluid (instead of gas particles); thus, the LBM approach could be extended to treat hydrodynamic flow problems. Improvements to these inadequacies are necessary before the FDLBM can be made viable and attractive for aeroacoustics, aerodynamics hydrodynamics and other flow problems.

For ease of reference in the following, these improvements are labeled: (i) a new Maxwellian distribution function, (ii) relaxation of the $M << 1$ condition, (iii) eliminate mass leakage at solid boundary, and (iv) extension to hydrodynamic flows. Before embarking on the

development of a truly valid and viable FDLBM, it is prudent to examine the origin of the inadequacies and seek improvements and corrective measures to address each and every one.

1.2 Proposed Improvements

The rationale, and physical arguments and justification on why the improvements are necessary are outlined below.

1.2.1 *A New Maxwellian Distribution Function*

The first improvement is carried out to seek an alternative to the Maxwellian distribution function used for f^{eq} in conventional MBE. In deriving the Maxwellian distribution function, only the internal translational degree of freedom of the particles is considered [7]. This assumption is quite restrictive and limits the validity of the distribution function to monatomic gas only. In aerodynamic and aeroacoustics studies, it is important to consider the kinetic theory of diatomic and polyatomic gases; therefore, it is necessary to broaden the approach to diatomic and polyatomic gas no matter how difficult is the task. This requires considering multi-energy modes to describe particle motion. If this approach were to apply to the modeled BE, a generalization to include as many energy modes as mathematically possible is necessary. Such an approach, where multi-energy modes are used to describe particle motion, has been adopted in gas dynamic schemes [14, 15, 16], but not in an attempt to enable the BE to correctly resolve aeroacoustics and aerodynamics problems. The difficulty is illustrated by examining the effort took to include the internal rotational angular momentum in the derivation of f^{eq} [17]; the resulting theory thus derived is very complicated, especially for numerical purposes. As a result, a WCUB equation, coined by Wang Chang et al. [17], was derived by introducing a set of particle distribution function f for each quantum mode to represent the internal state of the particles. In order to describe the dynamics of the polyatomic gas properly, the equation is constructed by assuming a spherically symmetric inter-particle potential. Since then, other researchers have attempted to use this equation as a base to formulate different models and approaches. Even though the degenerate rotational states do play an important role in angular momentum polarizations, this was neglected in the derivation of the WCUB equation.

An attempt has been made by Morse [18] to improve the WCUB approach by simplifying the equation using a BGK-type modeled BE. The approach was further improved by Holway [19] through the construction of an ellipsoidal statistical BGK model and used it to broaden the applicability of the equation derived by Morse [18] such that a correct fluid conductivity κ can be deduced. The key to this success was in replacing the Maxwellian distribution function by an anisotropic Gaussian distribution. The WCUB and its improvements have one thing in common; their proposed distribution function for f^{eq} is a set of Maxwellian distribution functions corresponding to different internal states. If the velocity lattice approach were used to solve the modeled BE, it is not at all clear how a corresponding lattice f^{eq} could be derived. Consequently, these approaches are seldom used to solve practical problems. The present paper aims to pursue a new approach where at least one other degree of freedom of the particle, besides the translational degree, is employed to construct a different distribution function for f^{eq}. The resulting distribution function should be practical enough to warrant application to multiple flow dynamics problems. Therefore, the objective is to extend the formulation to cover both monatomic and diatomic gas, such that the resulting f^{eq} would asymptote correctly to the monatomic gas limit and is equally applicable to diatomic gas.

1.2.2 *Relaxation of the M << 1 Condition*

The second improvement attempts to relax the $M << 1$ condition in the MBE formulation. This condition is a direct consequence of the proposed expansion for f_α^{eq}, which is expressed in terms of the inner product of $\boldsymbol{\xi}$ and $\boldsymbol{u}$ [20, 21]. After proper normalization using the sound speed as the reference velocity, M appears naturally in the expansion series for f_α^{eq}. Therefore, it follows that if the expansion series for f_α^{eq} were to converge properly, the $M << 1$ assumption must be invoked. Strictly speaking, this assumption restricts the validity of the LBM to compressible flow with very small M. As a result, most studies using the LBM to simulate fluid dynamics, including incompressible flow, are subject to the $M << 1$ condition [20, 22, 23, 24, 25, 26], and the solutions for incompressible flows are taken to be valid even though the zero divergence of the velocity field condition is not met [22].

Although this condition ($M << 1$) does not seem to have much effect on the simulated incompressible flow results [3, 20], its mere existence in the LBM formulation compromises the integrity of the incompressible flow definition. Most studies claimed that the N-S equations for incompressible flows are recovered correctly [22, 24]; however, the exact incompressible N-S equations cannot be deduced from the full set of recovered N-S equations by allowing $M \to 0$ in these equations. The reason is that even if the $M << 1$ condition is satisfied, a gas equation of state is still present in the formulation, and the fluid density is determined from the state equation once the pressure is known or vice versa. On the other hand, fluid density is constant in an incompressible flow and should be so specified in any numerical simulation. Therefore, the continuity equation thus deduced from the full set of N-S equations will give rise to the zero divergence of the velocity field condition in the whole flow field. In the LBM formulation reported in past studies, this divergence condition is not exactly satisfied. Consequently, mass leakage would develop as calculation proceeds; this leakage is often explained away as a consequence of the compressibility effect [2, 20, 22]. This mass leakage is not the same as that given rise by stipulating a no-slip condition at solid boundary. The latter mass leakage occurs because of the bounce-back method used to evaluate the boundary values of f_α [26] to satisfy the no-slip condition at solid boundary. In view of this, conventional LBM will give rise to two separate sources of mass leakage; one derived from the $M << 1$ assumption, which is inevitable from the conventional expansion of f_α^{eq} arising from the Maxwellian distribution function, and another from the method used to evaluate the boundary value of f_α at a solid wall so that the no-slip condition is satisfied. If an LBM absent of these mass leakages were to be formulated for correct incompressible and compressible flow simulation, then the $M << 1$ assumption must be eliminated from the formulation, and a more accurate method to evaluate f_α at solid boundary has to be developed.

1.2.3 *Eliminate Mass Leakage at Solid Boundary*

The third improvement attempts to replace the proposed bounce-back condition [26] used to evaluate the behavior of f_α at a solid boundary. According to Mei et al. [27], as f_α

approaches a wall node it scatters back to the fluid node along its incoming normal link while reflection along the tangential link is normally neglected. Therefore, the bounce-back boundary condition only considers the normal bounce back part and ignores the tangential part of the contribution. This treatment is only correct to 1st order numerical accuracy, thus leading to mass leakage at the wall [20, 22] that is 2nd order and higher. Consequently, the continuity equation is not quite satisfied [20], and the drawback renders the LBM less attractive compared to other simulation methods used to solve the Euler and/or N-S equations for any flow problems with solid boundaries.

Many improvements have been proposed to eliminate the mass leakage at a solid boundary. For example, Verberg and Ladd [28] proposed a way to implement the bounce-back condition for LBM such that mass conservation is maintained. In this method, a new continuous variable is defined for all points, and distance from points on a solid boundary to grids on fluid or solid points are stored in the new continuous variable so that the information can be applied to the distribution function as needed. As proposed, the method is quite cumbersome. Rohde et al. [29] put forward an improved bounce-back boundary condition, which is mass conservative in the propagation step but not in the collision step. In order to eliminate mass leakage error, Chun and Ladd [30] suggested an improved bounce-back boundary condition; however, the proposed method still has mass leakage, though very small, and no side effects were noticed in the velocity results. Bao et al. [31] had carried out a detailed assessment of the mass leakage problem and then proposed a mass conserving boundary condition that is 2nd order accurate. In their study, mass leakage agent is searched first, then, the calculated mass leakage is assigned to a particular term. The next step is to propose certain relations for mass leakage elimination. It should be noted that after applying their proposed method to simulate a channel flow problem, the mass flow converges to a constant value that is not necessarily equal to the initial value. In other words, mass leakage has not been eliminated. Furthermore, they also analyzed the grid refinement remedy method proposed in [32], which they named the FH method, and a 2nd order accurate correction method in [27], which they designated as the MLS method. They concluded

that the FH and MLS methods do not quite remedy the problem because mass leakage is not eliminated. The reason is that when the FH or MLS method is applied, mass leakage converges to a constant rate, but not necessarily to a constant value. In other words, a constant value of mass still leaks in each time step.

In the work of Krüger et al. [25], the mass leakage problem was investigated using new concepts. In their paper mass leakage was labeled mass increase; however, they suggested that mass change could be increased or decreased. On further examination of the channel flow problem, they found that if velocity boundary conditions at both inlet and outlet were used, mass increase occurred and could only be reduced by choosing a smaller value for the Mach number. This observation seems to suggest that mass leakage due to the $M << 1$ assumption has a compensating effect on mass leakage derived from the bounce-back condition. Chen et al. [33] examined the mass leakage problem and concluded that numerical instability of the interpolation boundary schemes was responsible for the mass non-conservation effect in the bounce-back boundary condition. Therefore, they proposed a new mass conserving bounce-back boundary condition. In order to remove the drawback of mass loss and numerical instability in the proposal of [33], Coupance and Verschaeve [34] put forward a mass conserving bounce-back boundary condition. In their proposed method [34], the particle distribution function f_α was divided into an equilibrium and a non-equilibrium part, and they proposed certain relations for use in their method. They showed that the mass was indeed conserved up to round off error during the simulations using their proposed method. Even then, the suggested remedy is not completely satisfactory because its extension to a wider class of problems might not produce the same kind of results. Consequently, the proposed remedy might not be generally applicable to a wide range of fluid dynamics problems.

1.2.4 *Extension to Hydrodynamic Flows*

The fourth improvement is made to eliminate the presence of a state equation in the MBE formulation. Most MBE based numerical methods requires either a specification of a pressure-density relation or a state equation [20] in the formulation, even for incompressible flow

simulation. Usually, the explanation is attributed to the $M << 1$ assumption and that the solution of the MBE is accurate to 2nd order of M. There is no need to specify any state equation in hydrodynamic flow simulation because the medium is a liquid. For incompressible flow the fluid density is constant. The use of a conventional FDLBM to simulate such flows, even though the results are reasonably correct, raise concern about whether the approach is conceptually correct and hence its validity [35]. This implies that if the FDLBM were to be used to simulate hydrodynamic flows, the simulation results must exactly satisfy $\nabla \bullet \boldsymbol{u} = 0$, i.e. zero divergence of the velocity field. A recent attempt to alleviate this concern in the use of conventional FDLBM to simulate incompressible flow has been made by Chen et al. [35]. In their approach, the vorticity-stream-function form of the NS equation is used. As a result, the pressure term does not appear anywhere in the vorticity equation and the continuity equation is satisfied through the stream function definition. This approach has two disadvantages: (a) it is limited to flows where a stream function can be defined, and (b) it is difficult to specify the boundary condition for vorticity. Consequently, the approach cannot be easily applied to just any flow; thus, limiting its applicability.

In order to demonstrate that the MBE approach could be extended to treat hydrodynamic flows, a discrete flux distribution function f, similar in nature to that for gas particles [6], used to represent mass and momentum transport in the flow has to be found. Then, it is shown that the derived transport equation for f is similar to the BE. The next step is to show that this transport equation, subject to certain conditions, could be used to recover the Euler and N-S equations correctly. Once demonstrated, the transport equation for f can be solved using the lattice method adopted for the solution of the LBE. When this equivalence has been established, doubts on using an LBE to simulate hydrodynamic flow problems would not be present any more.

1.3 Work Completed on Improvements

Studies carried out in [36-40] seemed to suggest that if the FDLBM were to be valid for monatomic as well as diatomic gas, the rotational degree of freedom of the gas has to be considered. Therefore, the first improvement was carried out along the line to include both the

internal translational and rotational degree of freedom of the particles in the energy model used to evaluate internal energy. In order to derive a new continuous distribution function for f^{eq}, the idea put forward in [4, 17, 18, 19] is adopted. The first term in this new f^{eq} is given by a modified Maxwellian distribution function constructed such that, when only the translational degree of freedom of the particle is considered, the Maxwellian distribution is recovered exactly for monatomic gas. Other terms in the new f^{eq} are constructed to take into account the contributions given by the rotational degree of freedom and its interaction with other energy modes of the particle. Since only the translational and the rotational degree of freedom of the particle are considered, the improvement is applicable only to monatomic and diatomic gas. This approach deviates from that assumed in the BGK model [6]. Consequently, the specific heat ratio could be recovered with no dependence on problem dimensions, and the approach allows the equation of state for diatomic gas to be recovered correctly. Realization of this objective would ensure the first improvement to be addressed, and achieved completely and correctly.

The early work of Philippi et al. [41] and the newly derived continuous f^{eq} [42] suggests that the expansion for the corresponding lattice distribution function f_α^{eq} can be made in terms of the particle velocity $\boldsymbol{\xi}$ alone. Therefore, M would not appear anywhere in the new LBM formulation, and the solution would not be subjected to the $M << 1$ condition. The coefficients in the f_α^{eq} expansion are determined by imposing the condition that the Euler and/or the N-S equations can be recovered correctly. As a result, the coefficients are functions of the primitive variables, their derivatives, and their products. Thus formulated, the boundary conditions for f_α could be determined from the primitive variables evaluated at the boundaries, and the need to evaluate the boundary values of f_α at any solid boundary is avoided. However, there is a disadvantage to this approach and that is determination of the fluid properties. Properties such as μ, κ, etc., and Newton's definition for μ, the Sutherland and Fourier law for viscosity dependence on temperature and heat conduction, respectively, are treated as inputs to the problem. Therefore, this approach renders the new LBM more likely to be a numerical

technique used to solve the Euler and N-S equations, while the original intent of the Boltzmann approach, where recovery of fluid properties is inherent in the formulation, is compromised.

In the present approach, it can be seen that the new LBM can address and accomplish the three improvements outlined above; namely, (i) a different Maxwellian distribution function, (ii) relaxation of the $M << 1$ condition, and (iii) eliminate mass leakage at solid boundary. The fourth improvement (iv) can be achieved by extending the above treatment to simulate hydrodynamic flows. If improvement (iv) were to be achieved, it is necessary to show equivalence between the new LBM approach for gas flow and the discrete flux approach for liquid flow to derive the transport equations and their eventual recovery of the Euler and N-S equations. Once this equivalence has been established, the new LBM can be extended to treat hydrodynamics where the flow is truly incompressible and a state equation is not required.

1.4 Present Objective

Overall, the LBM project took a number of years to arrive at the present point. This project began by attempting to extend a conventional LBM to simulate aeroacoustics problems through modification of existing LBM to include rotational degree of freedom in the evaluation of internal energy in the formulation [36, 37], and by implementing nonreflecting boundary conditions [38]. Even with these improvements, it was found that, depending on the problem considered, the modifications might work for some aeroacoustics simulations; however, it is necessary to modify the changes made if the approach were to be applied to another class of similar flow problems. Therefore, the modifications are problem dependent, and this lack of generality in the proposed modifications prompted a different approach to improve existing LBM and FDLBM. The effort led to multiple publications [42-54], and two PhD theses [55, 56] in the Mechanical Engineering Department of The Hong Kong Polytechnic University.

The type of flows investigated includes aeroacoustics, incompressible flows with and without heat transfer, compressible flows with and without shocks, and hydrodynamics flows with and without buoyancy effect, while fluid medium treated include diatomic gas, Newtonian and non-Newtonian fluids, and nanofluids. This way of disseminating the new LBM/FDLBM

ideas and results might be timely, but is less focused. Further, it renders attempt to concisely outline the analysis and the concomitant new ideas appear piecemeal. As such, the generality of the new LBM/FDLBM and its uniqueness might be lost in the process. In order to rectify this inadequacy, the objectives of the current paper are to detail the rationale and to provide a solid theoretical foundation for the new LBM, to present a coherent development of the relevant equations for different fluid flows, incompressible and compressible, and to pinpoint the salient features of the new LBM/FDLBM in this detailed review. These objectives are accomplished in the following sections.

In Section 2, the MBE with its new continuous f^{eq} is derived. Section 3 focuses on the development of a new LBE and lattice f^{eq}, while Section 4 discusses the extension of the LBE to hydrodynamic flow simulations. Section 5 discusses the new LBM, the relevant boundary conditions, an immersed boundary method (IBM) for the new LBM, and the splitting method together with the associated numerical technique used to solve the MBE. Section 6 reviews and discusses the FDLBM simulation results of aeroacoustics, different kinds of flow problems, and work by others on magnetohydrodynamics. Fluids considered include Newtonian, non-Newtonian and nanofluids. Finally, Section 7 draws conclusions on the strengths and range of applications of the new LBM/FDLBM.

2. Modeled Boltzmann Equation (MBE) and a New Continuous f^{eq}

As discussed in the Introduction, the new MBE and FDLBM thus developed are able, in principle and in practice, to handle a wide range of gas and fluid dynamic problems, including aeroacoustics, hydrodynamics, magnetohydrodynamics, nano-fluid flows with simple as well as complex boundary geometries. Since aeroacoustics disturbances are order of magnitude smaller than aerodynamic disturbances, the choice of characteristic parameters used to normalize the Euler and N-S equations has to be chosen carefully, so that the aeroacoustics terms are still explicitly included in the governing equations after normalization. Consequently, Lele [57] proposed to choose the following characteristic parameters to normalize the Euler and N-S

equations in order to recover the acoustic scaling form of these equations. These parameters are: $L = x_0/Kn$ for length, c_r for velocity, τ_0 for time, ρ_r for density, and $c_r^2/\left(C_p\right)_r$ for temperature. From this point on, the same characteristic parameters are used to normalize all variables in the BE and the LBE.

2.1 MBE for Diatomic Gas

In order to recover the acoustic scaling form of the Euler and N-S equations correctly from the MBE, the same characteristic parameters as those used to normalize the Euler and N-S equations are also used to normalize the BGK-type MBE, which is given by

$$\frac{\partial \hat{f}}{\partial \hat{t}} + \hat{\boldsymbol{\xi}} \cdot \nabla_{\hat{x}} \hat{f} = -\frac{1}{\hat{\tau}}\left(\hat{f} - \hat{f}^{eq}\right) \quad . \tag{1}$$

At this point, the particle equilibrium distribution function $\hat{f}^{eq}$ has not been defined. Since the current objective is to require the new MBE to have the ability to yield the correct thermodynamic properties for diatomic gas, the conventional proposal to represent $\hat{f}^{eq}$ by a Maxwellian distribution might not be appropriate. Therefore, in the present approach, the correct recovery of the thermodynamic properties, such as γ, Pr, etc. is specified as a condition in the derivation of a representation for $\hat{f}^{eq}$.

If the dimensionless symbols are represented by the same symbols without a hat, they can be written as,

$$\boldsymbol{x} = \frac{\hat{\boldsymbol{x}}}{\hat{x}_o / Kn} = \frac{\hat{\boldsymbol{x}}}{\hat{L}} \quad , \quad t = \frac{\hat{t}}{\hat{\tau}_o / Kn} = \frac{\hat{t}}{\hat{L}/\hat{c}_r} \quad , \quad \tau = \frac{\hat{\tau}}{\hat{\tau}_o} \quad , \quad p = \frac{\hat{p}}{\hat{\rho}_r \hat{c}_r^2} \quad ,$$

$$\rho = \frac{\hat{\rho}}{\hat{\rho}_r} \quad , \quad e = \frac{\hat{e}}{\hat{c}_r^2} \quad , \quad \boldsymbol{u},\ \boldsymbol{\xi} = \frac{\hat{\boldsymbol{u}},\ \hat{\boldsymbol{\xi}}}{\hat{c}_r} \quad , \quad T = \frac{\hat{T}}{\hat{c}_r^2/\left(\hat{C}_p\right)_r} \quad ,$$

$$\theta = \frac{\hat{\theta}}{\hat{c}_r^2} \quad , \quad f,\ f^{eq} = \frac{\hat{f},\ \hat{f}^{eq}}{\hat{\rho}_r / \hat{c}_r^D} \quad , \quad f^{(n)} = \frac{\hat{f}^{(n)}}{\hat{\rho}_r Kn^n / \hat{c}_r^D} \quad , \quad n \geq 0 \quad , \tag{2}$$

where bold face letters and subscripts *i* and *j* are used to represent vectors and their components. In order to recover the Euler and N-S equations correctly from the MBE, it is necessary to employ the Chapman-Enskog expansion in terms of *Kn* to the variables in Eq. (1). Thus,

expanding x_i, t and f in terms of Kn, the following expressions for these variables and their derivatives with respect to x_i, and t are obtained,

$$x_i = x_i^{(1)} + Knx_i^{(2)} + O(Kn^2) \quad , \tag{3a}$$

$$t = t^{(1)} + Knt^{(2)} + O(Kn^2) \quad , \tag{3b}$$

$$f = f^{(0)} + Knf^{(1)} + Kn^2 f^{(2)} + O(Kn^3) \quad , \tag{3c}$$

$$\frac{\partial}{\partial t} = \frac{\partial}{\partial t^{(1)}} + Kn\frac{\partial}{\partial t^{(2)}} \quad , \tag{3d}$$

$$\frac{\partial}{\partial x_i} = \frac{\partial}{\partial x_i^{(1)}} \quad . \tag{3e}$$

These expansions are sufficient under the dense gas assumption, i.e., $Kn << 1$. Therefore, only the first three elements, $f^{(0)}$, $f^{(1)}$, and $f^{(2)}$ in the f expansion need to be determined. Collecting same order terms to $O\left(Kn^2\right)$, the equations for $f^{(0)}$, $f^{(1)}$, and $f^{(2)}$ are obtained:

$$f^{(0)} = f^{eq} \quad , \quad \text{to } O(Kn^0) \quad , \tag{4}$$

$$\frac{\partial f^{(0)}}{\partial t^{(1)}} + \boldsymbol{\xi}\cdot\nabla_{x^{(1)}} f^{(0)} = -\frac{f^{(1)}}{\tau} \quad , \quad \text{to } O(Kn^1) \quad , \tag{5}$$

$$\frac{\partial f^{(1)}}{\partial t^{(1)}} + \frac{\partial f^{(0)}}{\partial t^{(2)}} + \boldsymbol{\xi}\cdot\nabla_{x^{(1)}} f^{(1)} = -\frac{f^{(2)}}{\tau} \quad , \quad \text{to } O(Kn^2) \quad . \tag{6}$$

Only Eqs. (4) and (5) are required for the recovery of the Euler equations; therefore, solutions of these two equations are sought for $f^{(0)}$ and $f^{(1)}$ under certain macroscopic conditions. These conditions are the correct recovery of the thermodynamic properties such as γ, mass ρ, linear momentum ρu_i, and the internal energy e. According to Li et al. [36], if these properties were to be recovered correctly, the rotational degree of freedom of the particle also has to be considered in the collision and transport processes of the particles. In other words, D_T and D_R have to be taken into consideration in the evaluation of the total energy e_t of the particles. In mathematical form, these conditions can be written as:

$$\rho = \int f^{eq} d\boldsymbol{\xi} \quad , \tag{7}$$

$$\rho u_i = \int f^{eq} \xi_i d\boldsymbol{\xi} \quad , \tag{8}$$

$$\rho e_t = \rho e + \frac{1}{2}\rho |\boldsymbol{u}|^2 = \frac{D_T + D_R}{D} \int \frac{1}{2} f^{eq} |\boldsymbol{\xi}|^2 d\boldsymbol{\xi} \quad , \tag{9}$$

where the integral is evaluated over the entire velocity space. If the number of internal degree of freedom K is defined as $K = D_T + D_R - D$, Eq. (9) can be recast as

$$\rho e_t = \rho e + \frac{1}{2}\rho |\boldsymbol{u}|^2 = \frac{D_T + D_R}{D} \int \frac{1}{2} f^{eq} |\boldsymbol{\xi}|^2 d\boldsymbol{\xi}$$

$$\Rightarrow \quad \rho e_t = \int \frac{1}{2} f^{eq} |\boldsymbol{\xi} - \boldsymbol{u}|^2 d\boldsymbol{\xi} + \frac{K}{D} \int \frac{1}{2} f^{eq} |\boldsymbol{\xi}|^2 d\boldsymbol{\xi} + \frac{1}{2}\rho |\boldsymbol{u}|^2 \quad . \tag{10}$$

In Eq. (10), $(\boldsymbol{\xi} - \boldsymbol{u})$ is defined as the peculiar velocity of the particle. Thus expanded, the first term on the right of Eq. (10) represents the internal energy derived from the translational motion of the particle, while the second term that of the rotational motion of the particle, and the third term represents the kinetic energy of the flow. It can be seen that this energy model is different from that stipulated in the BGK model [6]. Finally, higher order terms like $f^{(n)}$ are given by,

$$\int f^{(n)} d\boldsymbol{\xi} = 0 \quad , \tag{11a}$$

$$\int f^{(n)} \boldsymbol{\xi} d\boldsymbol{\xi} = 0 \quad , \tag{11b}$$

$$\frac{D_T + D_R}{D} \int \frac{1}{2} f^{(n)} |\boldsymbol{\xi}|^2 d\boldsymbol{\xi} = 0 \quad \text{for all } n \geq 1 \quad . \tag{11c}$$

2.1.1 *Recovery of Thermodynamic Properties for Diatomic Gas*

The ideal gas law for diatomic gas is given by $p = \rho\theta$. Upon invoking the equipartition theorem, the internal energy can be written as,

$$e = \frac{D_T + D_R}{2}\theta = \frac{\theta}{\gamma - 1} \quad \text{where} \quad \gamma = \frac{D_T + D_R + 2}{D_T + D_R} . \tag{12}$$

It can be seen that this gives rise to a correct expression for the internal energy e, and a specific heat ratio γ that does not depend on problem dimension, D. For the problem under consideration $D_T = 3$ and $D_R = 2$; therefore, for any given D, $\gamma = 7/5$ is obtained. Also, the

sound speed is given by $c^2 = \gamma\theta$, so once θ is known, the sound speed can be determined correctly. Once c and γ are recovered correctly, the next step is to examine the recovery of the Euler equations and the formulation of a continuous f^{eq}.

2.2 Recovery of the Euler Equations

The first objective of the current study is to improve the Maxwellian distribution so that it can be correctly applied to monatomic as well as diatomic gases. Most gas flow problems deal with diatomic gases; therefore, an MBE that relies on a monatomic gas assumption is not appropriate. The rationale and methodology on how to accomplish this objective can be best illustrated by considering the recovery of the Euler equation first. Once established, the same methodology can be used to seek an improved Maxwellian distribution for recovery of the N-S equations. Besides, the current objective is mainly focused on the development of a lattice Boltzmann method to solve the MBE; the example on how to seek an improved Maxwellian distribution for viscous flow will be more appropriately addressed in the section that considers the lattice Boltzmann equation.

In order to recover the Euler equations correctly, the first step is to recover the continuity equation and then the momentum and energy equations. Integrating Eq. (5), setting $f^{(0)} = f^{eq}$, $t = t^{(1)}$ and $x_j = x_j^{(1)}$, the recovered continuity equation, with no other restrictions, is obtained:

$$\int\left[\frac{\partial f^{eq}}{\partial t} + \frac{\partial}{\partial x_j}\left(\xi_j f^{eq}\right) = -\frac{f^{(1)}}{\tau}\right]d\boldsymbol{\xi} \quad \Rightarrow \quad \frac{\partial \rho}{\partial t} + \frac{\partial}{\partial x_j}\left(\rho u_j\right) = 0 \quad . \tag{13}$$

Similarly, multiplying Eq. (5) by ξ_i gives the momentum equation as,

$$\int\left[\frac{\partial f^{eq}}{\partial t} + \frac{\partial}{\partial x_j}\left(\xi_j f^{eq}\right) = -\frac{f^{(1)}}{\tau}\right]\xi_i d\boldsymbol{\xi} \quad \Rightarrow \quad \frac{\partial\left(\rho u_i\right)}{\partial t} + \frac{\partial}{\partial x_j}\left(P_{ij} + \rho u_i u_j\right) = 0 \quad , \tag{14}$$

where $\int\left(\xi_i\right)\left(\xi_j\right)f^{eq}d\boldsymbol{\xi} = P_{ij} + \rho u_i u_j$ and $P_{ij} = \int\left(\xi_i - u_i\right)\left(\xi_j - u_j\right)f^{eq}d\boldsymbol{\xi}$ have been substituted. Since the trace of P_{ij} is not zero, rather, it is given by the static pressure p, this suggests that P_{ij} can be rewritten as $P_{ij} = p\,\delta_{ij} + P'_{ij}$ where P'_{ij} is defined as

$$P'_{ij} = \int \left(\xi_i\right)\left(\xi_j\right) f^{eq} d\boldsymbol{\xi} - \rho u_i u_j - p\delta_{ij} \quad , \tag{15a}$$

and P'_{ij} has to satisfy the condition

$$\partial P'_{ij} / \partial x_j = 0 \quad . \tag{15b}$$

Condition (15b) is sufficient to warrant the correct recovery of the inviscid momentum equation from Eq. (14). Under these stipulated conditions, Eq. (14) is reduced to

$$\frac{\partial\left(\rho u_i\right)}{\partial t} + \frac{\partial}{\partial x_j}\left(\rho u_i u_j\right) = -\frac{\partial p}{\partial x_i} \quad . \tag{16}$$

Finally, the energy equation is obtained by multiplying Eq. (5) by $\left(\left|\boldsymbol{\xi}\right|^2 / 2\right)\left[\left(D_T + D_R\right) / D\right]$ to give

$$\int\left[\frac{\partial f^{eq}}{\partial t} + \frac{\partial}{\partial x_j}\left(\xi_j f^{eq}\right) = -\frac{f^{(1)}}{\tau}\right]\frac{\left|\boldsymbol{\xi}\right|^2}{2}\left(\frac{D_T + D_R}{D}\right) d\boldsymbol{\xi}$$

$$\Rightarrow \quad \frac{\partial}{\partial t^{(1)}}\left(\rho e + \frac{1}{2}\rho\left|\boldsymbol{u}\right|^2\right) + \frac{D_T + D_R}{D}\frac{\partial}{\partial x_j}\left(Q_j + u_j\left\{\frac{1}{2}\rho\left|\boldsymbol{u}\right|^2 + \frac{1}{2}P_{kk}\right\} + u_k P_{jk}\right) = 0 \quad , \tag{17}$$

where $Q_j = \left[\int\left(\xi_j - u_j\right)\left|\boldsymbol{\xi} - \boldsymbol{u}\right|^2 f^{eq} d\boldsymbol{\xi}\right] / 2$ has been assumed and this leads to

$$\frac{1}{2}\int\left(\xi_j\right)\left|\boldsymbol{\xi}\right|^2 f^{eq} d\boldsymbol{\xi} = Q_j + u_j\left(\frac{1}{2}\rho\left|\boldsymbol{u}\right|^2 + \frac{1}{2}P_{kk}\right) + u_k P_{jk} \quad . \tag{18}$$

These simplifications together with $p = \rho\theta = \left(\gamma - 1\right)\rho e$, $P_{ij} = p\,\delta_{ij} + P'_{ij}$, and Eq. (15b) lead to the following equation for *e*;

$$\frac{\partial}{\partial t}\left(\rho e + \frac{1}{2}\rho\left|\boldsymbol{u}\right|^2\right) + \frac{\partial}{\partial x_j}\left[u_j\left(\rho e + p + \frac{1}{2}\rho\left|\boldsymbol{u}\right|^2\right)\right] +$$

$$\frac{\partial}{\partial x_j}\left[\frac{D_T + D_R}{D}Q_j + \frac{D_T + D_R - D}{D}u_j\left(\frac{1}{2}\rho\left|\boldsymbol{u}\right|^2\right) + \frac{D_T + D_R - D}{D}pu_j\right.$$

$$\left. + \frac{D_T + D_R}{D}\frac{1}{2}u_j P'_{kk} + \frac{D_T + D_R}{D}u_k P'_{jk}\right] = 0$$

$$\Rightarrow \frac{\partial}{\partial t}\left(\rho e + \frac{1}{2}\rho\left|\boldsymbol{u}\right|^2\right) + \frac{\partial}{\partial x_j}\left[u_j\left(\rho e + p + \frac{1}{2}\rho\left|\boldsymbol{u}\right|^2\right)\right] + \frac{\partial}{\partial x_j}\left(Q'_j\right) = 0 \quad . \tag{19}$$

In this representation, all terms inside the square bracket are represented by Q'_j. With this simplification, it is obvious that the energy equation can be recovered identically with either $\partial Q'_j / \partial x_j = 0$ or $Q'_j = 0$ is assumed. If $Q'_j = 0$ is assumed, the definition of Q'_j will lead to

$$Q_j = -\left[\frac{D_T + D_R - D}{D_T + D_R} u_j \left(\frac{1}{2}\rho|\boldsymbol{u}|^2\right) + \frac{D_T + D_R - D}{D_T + D_R} p u_j + \frac{1}{2} u_j P'_{kk} + u_k P'_{jk}\right] \quad , \tag{20}$$

and Q_j can be determined once P'_{ij} is known.

The following derivation of a continuous f^{eq} lends support to the assumption $Q'_j = 0$. It can be seen that knowledge of f^{eq} would allow P'_{ij} to be evaluated or vice versa. As such, the derivation of an new modeled Boltzmann equation is reduced to seeking an appropriate representation for the continuous f^{eq}.

2.3 New Continuous f^{eq} for 3-D Flows

The approach adopted here is to follow the theoretical foundation lay out in [17,18,19], especially that given by Wang-Chang et al. [17], in the formulation of f^{eq} that could point the way to a solution of P'_{ij}. If the leading term in the f^{eq} expansion is not a Maxwellian, it might not approach the limit for monatomic gas correctly. On the other hand, if it is a Maxwellian distribution, it cannot recover the correct thermodynamic properties for diatomic gas. Therefore, the simplest leading term in the f^{eq} expansion should be a modified Maxwellian that has the following properties. First, in the limit of a monatomic gas, the BGK model for f^{eq} is recovered. Second, other terms in the expansion should make up of the moments of $\boldsymbol{\xi}$ with unknown parameters so that the mean flow velocity $\boldsymbol{u}$ will not appear in any terms in the expansion. That way, M will not appear anywhere in the f^{eq} expansion and the MBE will not be subjected to the condition $M << 1$. Third, the unknown parameters should reflect the energy effects arising from particle-particle collisions that are resulted from translational and rotational motions. Therefore, these unknown parameters could be scalars, vectors, and/or tensors representing flow properties such as the velocity and temperature field and their gradients. Fourth, sufficient number of moments of $\boldsymbol{\xi}$ and the unknown parameters should be present so

that all elements of P'_{ij} can be determined. Based on the work of [17] and the conditions stipulated above, an expansion for f^{eq} with a scalar α_0, three vectors α_j, a_j, and b_i, a second-order tensor β_{mn}, and an unknown parameter η, can be formulated as,

$$f^{eq} = \alpha_0 exp\left[-\eta\sum_{k=1}^{D}\left(\xi_k - b_k\right)^2\right] + \sum_{i=1}^{D}\alpha_i\xi_i exp\left[-\eta\left|\boldsymbol{\xi}\right|^2\right] + \sum_{m,n=1}^{D}\beta_{mn}\xi_m\xi_n exp\left[-\eta\left|\boldsymbol{\xi}\right|^2\right]$$

$$+ \sum_{j=1}^{D}a_j\xi_j\left|\boldsymbol{\xi}\right|^2 exp\left[-\eta\left|\boldsymbol{\xi}\right|^2\right] \quad . \tag{21}$$

Equations for determining the scalars, vectors, tensors, and η can be derived from the conditions stipulated in Eqs. (7-9), (15a) and (20). After some tedious algebra, they lead to the following equations for the unknown scalars, vectors, tensors, and η,

$$\rho = \left(\alpha_0 + \sum_{m}^{D}\frac{\beta_{mm}}{2\eta}\right)\sqrt{\frac{\pi}{\eta}}^D \quad , \tag{22a}$$

$$\rho u_j = \left[\alpha_0 b_j + \frac{\alpha_j}{2\eta} + \frac{(D+2)a_j}{4\eta^2}\right]\sqrt{\frac{\pi}{\eta}}^D \quad , \tag{22b}$$

$$\frac{2D}{D_T + D_R}\left(\rho e + \frac{1}{2}\rho\left|\boldsymbol{u}\right|^2\right) = \frac{\rho D}{2\eta} + \sum_{k}^{D}\alpha_0 b_k^2\sqrt{\frac{\pi}{\eta}}^D + \sum_{m}^{D}\frac{\beta_{mm}}{2\eta^2}\sqrt{\frac{\pi}{\eta}}^D \quad , \tag{22c}$$

$$\rho u_i u_j + p\delta_{ij} + P'_{ij} = \frac{\rho\delta_{ij}}{2\eta} + \alpha_0 b_i b_j\sqrt{\frac{\pi}{\eta}}^D + \frac{\beta_{ij}+\beta_{ji}}{4\eta^2}\sqrt{\frac{\pi}{\eta}}^D \quad , \tag{22d}$$

$$\left(\frac{D}{2} + \frac{D}{D_T + D_R}\right)pu_j + \frac{D}{D_T + D_R}\frac{1}{2}\rho\left|\boldsymbol{u}\right|^2 u_j = \left(1 + \frac{D}{2}\right)\frac{\rho u_j}{2\eta}$$

$$+ \frac{\alpha_0 b_j}{2}\sum_{k}^{D}b_k^2\sqrt{\frac{\pi}{\eta}}^D + \frac{a_j}{8\eta^3}(D+2)\sqrt{\frac{\pi}{\eta}}^D \quad . \tag{22e}$$

From Eq. (22d), it can be seen that an expression for η can be obtained by assuming $p = \rho/2\eta$. For diatomic gas $p = \rho\theta$, therefore, it follows that $\eta = 1/2\theta$ is the appropriate value for η in this formulation for f^{eq}. The remaining scalars, vectors and tensor can be determined once a solution for $P'_{i,j}$ is found.

2.3.1 *3-D Solution for* P'_{ij}

A three-dimensional (3-D) solution for P'_{ij} is necessary for the proposed new MBE if the resultant FDLBM were to be applicable to a wide range of fluid dynamic, aerodynamic, and aeroacoustics problems. In this section, a 3-D solution for P'_{ij} in Cartesian coordinates is sought. Using Cartesian tensor notation, the three components of Eq. (15b) governing P'_{ij} can be decomposed into their component forms as

$$\frac{\partial P'_{11}}{\partial x} + \frac{\partial P'_{12}}{\partial y} + \frac{\partial P'_{13}}{\partial z} = 0 \quad , \tag{23a}$$

$$\frac{\partial P'_{21}}{\partial x} + \frac{\partial P'_{22}}{\partial y} + \frac{\partial P'_{23}}{\partial z} = 0 \quad , \tag{23b}$$

$$\frac{\partial P'_{31}}{\partial x} + \frac{\partial P'_{32}}{\partial y} + \frac{\partial P'_{33}}{\partial z} = 0 \quad . \tag{23c}$$

An equation for the trace of P'_{ij} can be deduced by exploiting its symmetric property. Invoking the symmetric condition to simplify Eq. (15a), an expression can be deduced for the trace of P'_{ij}. It can be written as

$$\sum_{i=1}^{D} P'_{ii} = \frac{D - \left(D_T + D_R\right)}{D_T + D_R} \rho \left|\boldsymbol{u}\right|^2 \quad . \tag{24}$$

Another equation for the three off-diagonal elements of P'_{ij} can be derived by taking the derivative of Eq. (23a) with respect to y and z, that of Eq. (23b) with respect to x and z, and that of Eq. (23c) with respect to x and y. Summing up these three equations and then making use of Eq. (24), the following equation for the three off-diagonal elements P'_{12}, P'_{13}, P'_{23} is obtained. The result is

$$\frac{\partial^3}{\partial x \partial y \partial z}\left[\frac{D - \left(D_T + D_R\right)}{D_T + D_R}\rho\left|\boldsymbol{u}\right|^2\right] + \frac{\partial}{\partial z}\left(\frac{\partial^2}{\partial x^2} + \frac{\partial^2}{\partial y^2}\right)P'_{12} + \frac{\partial}{\partial y}\left(\frac{\partial^2}{\partial x^2} + \frac{\partial^2}{\partial z^2}\right)P'_{13}$$
$$+ \frac{\partial}{\partial x}\left(\frac{\partial^2}{\partial y^2} + \frac{\partial^2}{\partial z^2}\right)P'_{23} = 0 \quad . \tag{25}$$

Altogether, Eq. (23) and Eq. (24) give four independent equations for the determination of P'_{ij} which has six independent components, P'_{11}, P'_{22}, P'_{33}, P'_{12}, P'_{13}, P'_{23}. Consequently, the number of available equations is less than the number of unknowns; therefore, further simplifications and/or assumptions can be made for this formulation. In order to gain insight into the kind and type of simplifications required for this problem, consider a 2-D case first. For a 2-D case, Eq. (25) can be shown to reduce to

$$\frac{\partial^2}{\partial x \partial y}\left[\frac{D-\left(D_T+D_R\right)}{\left(D_T+D_R\right)}\rho\left|\boldsymbol{u}\right|^2\right]+\left(\frac{\partial^2}{\partial x^2}+\frac{\partial^2}{\partial y^2}\right)P'_{12}=0 \quad , \tag{26}$$

Analogously, the same isotropic assumption can be made for the 3-D case, thus leading to the following equations for P'_{12}, P'_{13}, P'_{23},

$$\frac{\partial^2}{\partial x \partial y}\left[\frac{D-\left(D_T+D_R\right)}{3\left(D_T+D_R\right)}\rho\left|\boldsymbol{u}\right|^2\right]+\left(\frac{\partial^2}{\partial x^2}+\frac{\partial^2}{\partial y^2}\right)P'_{12}=0 \quad , \tag{27a}$$

$$\frac{\partial^2}{\partial x \partial z}\left[\frac{D-\left(D_T+D_R\right)}{3\left(D_T+D_R\right)}\rho\left|\boldsymbol{u}\right|^2\right]+\left(\frac{\partial^2}{\partial x^2}+\frac{\partial^2}{\partial z^2}\right)P'_{13}=0 \quad . \tag{27b}$$

The third equation is obtained by substituting Eqs. (27a, b) into Eq. (25), and the result is

$$\frac{\partial^3}{\partial x \partial y \partial z}\left[\frac{D-\left(D_T+D_R\right)}{3\left(D_T+D_R\right)}\rho\left|\boldsymbol{u}\right|^2\right]+\frac{\partial}{\partial x}\left(\frac{\partial^2}{\partial y^2}+\frac{\partial^2}{\partial z^2}\right)P'_{23}=0 \quad . \tag{27c}$$

These choices are not unique. Presumably, the isotropic assumption could be made for the pair P'_{12} and P'_{23}, or P'_{13} and P'_{23}, while Eq. (25) is again used to deduce the third equation for these two pairs of equations obtained from the analogous isotropic assumption. Thus formulated, six equations are available for the six unknowns arising from the second order tensor, P'_{ij}. Once solutions for $P'_{12}, P'_{13}, P'_{23}$ are obtained, $P'_{11}, P'_{22}, P'_{33}$ can be deduced by solving Eqs. (23a-c).

The Poisson equations as given in Eqs. (27a-c) could be solved for an infinite domain $\mathbf{R}^D\left(-\infty < x_i < \infty\right)$, and the solution is given by

$$P'_{ij} = \frac{1}{2\pi}\int_{-\infty}^{\infty}\int_{-\infty}^{\infty} f\left(x'_i, x'_j\right) \ln \frac{1}{\sqrt{\left(x_i - x'_i\right)^2 + \left(x_j - x'_j\right)^2}}\, dx'_i\, dx'_j \quad \text{for} \quad i \neq j \quad , \tag{28a}$$

$$P'_{ij} = -\int \sum_{k\neq i}^{D} \frac{\partial P'_{ik}}{\partial x_k}\, dx_i \quad \text{for} \quad i = j \quad , \tag{28b}$$

where $$f\left(x'_i, x'_j\right) = \frac{D - \left(D_T + D_R\right)}{D_0\left(D_T + D_R\right)}\left[\frac{\partial^2 \rho \left|\boldsymbol{u}\right|^2}{\partial x'_i \partial x'_j}\right] \quad , \tag{28c}$$

and $D_0 = 1$ for 2-D flow and $D_0 = 3$ for 3-D flow.

Once the solution for P'_{ij} has been obtained, the parameters α_0, α_j, a_j, b_i and b_{mn} can be determined from Eqs. (22a-e). The result for D = 2 or 3 is

$$\alpha_0 = \frac{\rho}{\sqrt{2\pi\theta}^D} - \frac{D - \left(D_T + D_R\right)}{\left(D_T + D_R\right)\theta\sqrt{2\pi\theta}^D}\left[\frac{1}{2}\rho\left|\boldsymbol{u}\right|^2\right] \quad , \tag{29a}$$

$$\alpha_j = \frac{1}{\theta}\left[\frac{\rho u_j}{\sqrt{2\pi\theta}^D} - \alpha_0 b_j - \left(D+2\right)\theta^2 a_j\right] \quad , \tag{29b}$$

$$a_j = \frac{1}{\left(D+2\right)\theta^3\sqrt{2\pi\theta}^D}\left[u_j p\left\{\frac{D - \left(D_T + D_R\right)}{\left(D_T + D_R\right)}\right\} - \frac{b_j}{2}\rho\left|\boldsymbol{u}\right|^2 + \frac{D}{\left(D_T + D_R\right)} u_j \frac{1}{2}\rho\left|\boldsymbol{u}\right|^2\right] \quad , \tag{29c}$$

$$b_i = \frac{\pm u_i}{\sqrt{1 - \frac{D - \left(D_T + D_R\right)}{\left(D_T + D_R\right)\theta}\left(\frac{1}{2}\left|\boldsymbol{u}\right|^2\right)}} \quad , \tag{29d}$$

$$\beta_{ij} = \frac{P'_{ij}}{2\theta^2\sqrt{2\pi\theta}^D} \quad , \tag{29e}$$

At this point, all parameters (scalars, vectors, tensors, and η) in Eq. (21) are known; thus, an new continuous f^{eq} to replace the Maxwellian distribution function in the original BGK

model has been formulated. Note that for monatomic gas, $D_T = 3$, $D_R = 0$, and $P'_{ij} = 0$ for i, j = 1….D. The vector b_i can be evaluated from Eq. (29d) by taking the solution with the "+" sign. Under this condition, the parameters as specified in Eq. (21) will take on the following solutions; $b_i = u_i$, $\alpha_0 = \rho / \sqrt{2\pi\theta}^D$, $\alpha_i = a_i = 0$, and $\beta_{ij} = 0$ for i, j = 1....D. It can be shown that f^{eq} as given in Eq. (21) with the parameters substituted by these solutions will reduce to the Maxwellian distribution function in the original BGK model. Therefore, an important objective set out in the formulation of an new continuous f^{eq} has been achieved; refer to [42] for more details.

Note that in the process of deriving Eq. (21), no condition has been imposed on the relaxation time $\hat{\tau}$ in the original BE (i.e. Eq. (1)), which was derived by adopting the BGK model with a Maxwellian distribution function for f^{eq}. This suggests that the new MBE is not restricted to a particular $\hat{\tau}$, therefore, its solution might not require adjustments to be made to $\hat{\tau}$ as suggested by investigators for certain class of problems. Furthermore, f^{eq} as given in Eq. (21) will allow the acoustic scaling form of the Euler and N-S equations to be recovered with no additional assumption invoked other than the dense gas assumption, i.e., $Kn << 1$. Consequently, Eq. (21) is better formulated for aeroacoustics simulations compared to conventional LBM.

3. Lattice Boltzmann Equation (LBE) and a New Lattice f_α^{eq}

The new continuous f^{eq} derived in Section 2 does not change the character of the MBE; it is still a linear scalar equation. However, both the translational and the rotational nonlinear particle collision effects are modeled in the new continuous f^{eq}. These improvements are made to broaden the applications of the new MBE and to free it of the major restrictions inherent in the conventional BGK-type MBE. Therefore, it is anticipated that the new MBE could more accurately reflect the physics of aerodynamic-aeroacoustics interactions and other more complicated flow problems. Different numerical methods, such as the finite difference schemes proposed in [14 -16], can be used to solve the MBE. Since the MBE is a linear equation, its solution can also be easily handled using a velocity lattice method [1- 3]. In the velocity lattice

method, or commonly labeled the lattice Boltzmann method (LBM), a lattice counterpart of the continuous f^{eq} is sought. The current approach also proposes to solve the MBE using LBM; therefore, derivation of the lattice counterpart of the continuous f^{eq} is presented in this section. Next, the recovery of the Euler equations is discussed assuming a D2Q13 velocity lattice; then a D2Q13 lattice is invoked in the recovery of the N-S equations. The choice of lattice models for the recovery of the Euler or the N-S equations is arbitrary; they are selected to illustrate the independence of the methodology on the choice of lattice model. It is further shown that the f_α^{eq} thus derived for the recovery of the Euler and/or N-S equations is identical, once μ and κ is set to zero in the N-S equations case.

3.1 New Lattice f_α^{eq} for the Euler Equations

In most conventional velocity lattice method used to solve the MBE [1-3, 58], a Taylor expansion of the Maxwellian distribution function [1] is commonly assumed. The expansion is usually made in terms of the inner product of the particle and fluid flow velocity, given by $\boldsymbol{\xi} \bullet \boldsymbol{u}$ [20, 21]. As in the case of the continuous f^{eq}, the requirement that the proposed f_α^{eq} will lead to the correct recovery of the Euler and/or the N-S equations is invoked. Consequently, the expansion for $\boldsymbol{\xi} \bullet \boldsymbol{u}$ normally terminates after the second or third order, depending on whether the Euler or the N-S equations are to be recovered. Furthermore, the expansion coefficients of the Taylor series are determined by requiring a full and correct recovery of either the Euler or N-S equations. It is the expansion of the Maxwellian distribution in terms of $\boldsymbol{\xi} \bullet \boldsymbol{u}$ that renders the lattice f_α^{eq} dependent on M; hence, the subsequent restriction of $M << 1$ on the LBM [1-3, 58]. If the present method were to be free of this assumption, another approach to derive a lattice f_α^{eq} that does not depend on an expansion in terms of $\boldsymbol{\xi} \bullet \boldsymbol{u}$ has to be found. Support for this requirement can be found in the continuous f^{eq} given in Eq. (21). This distribution function can be expanded in a polynomial series and terms up to second order of $\boldsymbol{\xi}$ can be collected to represent the lattice f_α^{eq}. Each term in the series is weighted by coefficients that can be scalars, vectors or tensors depending on the nature of the term. These coefficients are determined by requiring a full and exact recovery of the Euler or N-S equations. A parallel can also be seen

from the approach taken by Philippi et al. [41]. Instead of expanding f_α^{eq} in terms of $\boldsymbol{\xi} \bullet \boldsymbol{u}$, a polynomial series in $\boldsymbol{\xi}$ up to its second order was assumed. Once the expansion is freed of the presence of $\boldsymbol{u}$ and its products with $\boldsymbol{\xi}$, the dependence on *M* and hence the restriction $M << 1$ will vanish. Thus, with this understanding, derivation of the lattice f_α^{eq} can proceed as follows.

In the following, a 2-D flow is considered. The corresponding 3-D derivation follows essentially the same rationale and methodology. The 2-D velocity space is discretized using a velocity lattice. The corresponding discrete lattice form of Eq. (1) can be written as

$$\frac{\partial f_\alpha}{\partial t} + \xi_\alpha \bullet \nabla_x f_\alpha = -\frac{1}{\tau Kn}\left(f_\alpha - f_\alpha^{eq}\right) \quad , \tag{30}$$

where the subscript α is used to indicate the index for the lattice velocity, and f_α is the component of f at index α. Assuming that a D2Q13 velocity lattice model is sufficient to yield accurate resolution for aeroacoustics simulations, the methodology for the derivation of a D2Q13 lattice f_α^{eq} is given below. The lattice velocity for such a model is given by

$$\xi_0 = 0, \quad \alpha = 0 \quad , \tag{31a}$$

$$\xi_\alpha = \sigma\left\{\cos\left[\pi\left(\alpha-1\right)/4\right],\ \sin\left[\pi\left(\alpha-1\right)/4\right]\right\}, \qquad \alpha = 1,3,5,7 \quad , \tag{31b}$$

$$\xi_\alpha = \sqrt{2}\sigma\left\{\cos\left[\pi\left(\alpha-1\right)/4\right],\ \sin\left[\pi\left(\alpha-1\right)/4\right]\right\}, \quad \alpha = 2,4,6,8 \quad , \tag{31c}$$

$$\xi_\alpha = 2\sigma\left\{\cos\left[\pi\left(\alpha-1\right)/2\right],\ \sin\left[\pi\left(\alpha-1\right)/2\right]\right\}, \quad \alpha = 9,10,11,12 \quad , \tag{31d}$$

where σ is a parameter to be determined or specified. It is assumed that f_α^{eq} can be expressed as a polynomial series of the particle lattice velocity ξ_α. To second order, the series in 2-D Cartesian form is given by

$$f_\alpha^{eq} = A_\alpha + \left(\xi_\alpha\right)_x Ax_\alpha + \left(\xi_\alpha\right)_y Ay_\alpha + \left(\xi_\alpha\right)_x^2 Bxx_\alpha + \left(\xi_\alpha\right)_y^2 Byy_\alpha + \left(\xi_\alpha\right)_x \left(\xi_\alpha\right)_y Bxy_\alpha \quad , \tag{32}$$

where the coefficients, A_α, Ax_α, Bxx_α, etc., can be scalars, vectors and tensors. This lattice f_α^{eq} is different from conventional ones, which are expansion of the Maxwellian distribution function in terms of $\boldsymbol{\xi} \bullet \boldsymbol{u}$ up 2nd order [20] or 3rd order [59-61]. The present approach proposes a

polynomial in terms of $\left(\xi_\alpha\right)$ and leaves the inclusion of $\boldsymbol{u}$ in the coefficients of Eq. (32). Consequently, it is not limited by the $M << 1$ assumption.

These coefficients can be determined by invoking the conditions stipulated for the exact recovery of the Euler equations in the continuous f^{eq} case. These conditions are given by Eqs. (22a-22e). Only nine equations can be deduced from Eqs. (22a-22e) for the determination of the coefficients, A_α, Ax_α, Bxx_α, etc. Furthermore, one of these nine equations is a duplicate of the kinetic energy equation; thus further reducing the number of available equations to eight. It should also be noted that among the unknowns in these equations are the elements of P'_{ij}, which for a 2-D flow are reduced to P'_{xx}, P'_{xy} and P'_{yy}. Their values can be determined by solving Eqs. (22a-b) and Eq. (26). For 2-D flows, Eqs. (22a-b) are reduced to

$$\frac{\partial P'_{11}}{\partial x} + \frac{\partial P'_{12}}{\partial y} = 0 \quad , \tag{33a}$$

$$\frac{\partial P'_{21}}{\partial x} + \frac{\partial P'_{22}}{\partial y} = 0 \quad , \tag{33b}$$

while Eq. (26) remains the same because it has already been written for a 2-D flow.

Even then, only 8 equations are available for determining the components resulting from the coefficients, A_α, Ax_α, Bxx_α, etc.; therefore, further assumption has to be made to reduce the number of unknowns. A reasonable assumption is to consider the coefficients with the same "energy cell" of the lattice velocities to be the same. Since the number of unknowns resulting from a complete expansion of the coefficients A_α, Ax_α, Bxx_α, etc. is 19 for the D2Q13 lattice, there is certain flexibility in making further assumptions to reduce the number of unknowns to 8. As a first attempt, 11 of the coefficients are assumed zero for the D2Q13 velocity lattice. The resulting set of solutions for these coefficients is:

$$A_0 = \rho - \frac{2p}{\sigma^2} - \left(\gamma - 1\right)\frac{\rho\left|\boldsymbol{u}\right|^2}{\sigma^2} \quad , \qquad A_1 = A_2 = A_9 = 0 \quad , \tag{34a}$$

$$Ax_1 = \frac{2}{3}\frac{\rho u}{\sigma^2} - \frac{1}{3}\frac{\gamma p u}{\sigma^4} - \left(\gamma - 1\right)\frac{1}{6}\frac{\rho\left|\boldsymbol{u}\right|^2 u}{\sigma^4} \quad , \qquad Ax_2 = 0 \quad , \tag{34b}$$

$$Ax_9 = -\frac{1}{24}\frac{\rho u}{\sigma^2} + \frac{1}{12}\frac{\gamma p u}{\sigma^4} + (\gamma - 1)\frac{1}{24}\frac{\rho |\boldsymbol{u}|^2 u}{\sigma^4} \quad , \tag{34c}$$

$$Ay_1 = \frac{2}{3}\frac{\rho v}{\sigma^2} - \frac{1}{3}\frac{\gamma p v}{\sigma^4} - (\gamma - 1)\frac{1}{6}\frac{\rho |\boldsymbol{u}|^2 v}{\sigma^4} \quad , \qquad Ay_2 = 0 \quad , \tag{34d}$$

$$Ay_9 = -\frac{1}{24}\frac{\rho v}{\sigma^2} + \frac{1}{12}\frac{\gamma p v}{\sigma^4} + (\gamma - 1)\frac{1}{24}\frac{\rho |\boldsymbol{u}|^2 v}{\sigma^4} \quad , \tag{34e}$$

$$Bxx_1 = \frac{1}{2\sigma^4}\left(p + \rho u^2 + P'_{xx}\right) \quad , \qquad Bxx_2 = Bxx_9 = 0 \quad , \tag{34f}$$

$$Byy_1 = \frac{1}{2\sigma^4}\left(p + \rho v^2 + P'_{yy}\right) \quad , \qquad Byy_2 = Byy_9 = 0 \quad , \tag{34g}$$

$$Bxy_2 = \frac{1}{4\sigma^4}\left(\rho uv + P'_{xy}\right) \quad , \qquad Bxy_1 = Bxy_9 = 0 \quad . \tag{34h}$$

It should be recognized that the solutions given in Eqs. (34a-h) for the coefficients in Eq. (32) are not unique. Eqs. (34a-h) are taken to represent the most obvious solutions that can be found, and effort to seek new sets of solutions to those given in Eqs. (34a-h) has not been made. It should be pointed out that this set of solutions has been tested against multiple aeroacoustics, aerodynamic and hydrodynamic flow problems and they lead to stable, yet correct and accurate, results compared to experimental measurements, theoretical solutions, and/or direct numerical simulation results of the same problems [39, 41-54]. As such, there is no reason to doubt the validity and reliability of the solution set Eqs. (34a-h), for more details refer to [39].

These results are derived based on recovery of the Euler equations. However, the general nature of this approach can be illustrated by recovering the N-S equations in the next section.

3.2 New Lattice f_α^{eq} for the N-S Equations

Instead of starting with the Euler equations, the N-S equations written in the acoustic scaling form suggested by Lele [57] are used. The tensor form of the N-S equations are given by

$$\frac{\partial \rho}{\partial t} + \frac{\partial \rho u_i}{\partial x_i} = 0 \quad , \tag{35}$$

$$\frac{\partial \rho u_i}{\partial t} + \frac{\partial \rho u_i u_j}{\partial x_j} = -\frac{\partial p}{\partial x_i} - \frac{\partial \tau_{ij}}{\partial x_j} \quad , \tag{36}$$

$$\frac{\partial \rho e_t}{\partial t} + \frac{\partial \rho u_i e_t}{\partial x_i} = -\frac{\partial p u_i}{\partial x_i} - \frac{\partial \tau_{ij} u_i}{\partial x_j} - \frac{\partial q_i}{\partial x_i} \quad , \tag{37}$$

where, for convenience, indices are used to represent vectors and tensors. As before, the state equation is given by Eq. (12), i.e. $p = \rho e(\gamma - 1)$ and the total energy e_t is defined by Eq. (9a), i.e. $e_t = e + (1/2)|\boldsymbol{u}|^2$. The viscous tensor and the heat flux vector are defined as

$$\tau_{ij} = -\frac{M_\infty}{Re_\infty}\left\{2\mu\left(S_{ij} - \frac{1}{3}\delta_{ij} S_{kk}\right)\right\} \quad , \tag{38a}$$

$$q_i = -\frac{\gamma M_\infty}{Re_\infty Pr_\infty}\left(\kappa \frac{\partial e}{\partial x_i}\right) \quad , \tag{38b}$$

where the tensor S_{ij} can be written as $S_{ij} = \left(\partial u_i / \partial x_j + \partial u_j / \partial x_i\right)$ and the following dimensionless parameters have been defined: $M_\infty = \hat{u}_\infty / \hat{c}_\infty$, $Re_\infty = \hat{\rho}_\infty \hat{L} \hat{u}_\infty / \hat{\mu}_\infty$, $Pr_\infty = \hat{\mu}_\infty \left(\hat{c}_p\right)_\infty / \hat{\kappa}_\infty$, $\mu = \hat{\mu} / \hat{\mu}_\infty$, and $\kappa = \hat{\kappa} / \hat{\kappa}_\infty$. It should be pointed out that the local values of μ and κ vary with space and time according to physical laws to be specified for the relevant fluid of the flow. These are the equations that the LBE should in principle recover fully, if the MBE and f_α^{eq} were deemed completely viable for diatomic gas.

The starting point is Eq. (30); again the dense gas assumption (*Kn* << 1) is invoked. Just as in the case of the Euler equations, the following conditions for the definition of mass, momentum, and total energy have to be satisfied. These conditions are valid for diatomic gas where $D_T = 3$ and $D_R = 2$; therefore, the state equation with $\gamma = 1.4$ is correctly recovered. The definitions for mass, momentum and total energy are given in Eqs. (7-9) and in discrete form are:

$$\rho = \sum_{\alpha=0}^{N} f_\alpha \quad , \tag{39a}$$

$$\rho u_i = \sum_{\alpha=0}^{N} f_\alpha \left(\xi_\alpha\right)_i \quad , \tag{39b}$$

$$\frac{4}{D_T + D_R}\left(\rho e_t\right) = \sum_{\alpha=0}^{N} f_\alpha \left(\xi_\alpha\right)_i^2 \quad . \tag{39c}$$

For purpose of illustration, only a D2Q9 lattice model is used to derive the coefficients in the expansion assumed for f_α^{eq}. As discussed above, the same rationale and methodology can be used to deduce these coefficients for other velocity lattice models. For a D2Q9 lattice model, the lattice velocity is given by

$$\xi_\alpha = 0, \quad \alpha = 0 \quad , \tag{40a}$$

$$\xi_\alpha = \sigma\left\{\cos\left[\pi\left(\alpha-1\right)/4\right], \quad \sin\left[\pi\left(\alpha-1\right)/4\right]\right\} \quad , \qquad \alpha = 1,3,5,7 \quad , \tag{40b}$$

$$\xi_\alpha = \sqrt{2}\,\sigma\left\{\cos\left[\pi\left(\alpha-1\right)/4\right], \quad \sin\left[\pi\left(\alpha-1\right)/4\right]\right\} \quad , \qquad \alpha = 2,4,6,8 \quad . \tag{40c}$$

As in the case of the Euler Equations, a polynomial series in terms of $\left(\xi_\alpha\right)_i$ up to second order is assumed for the discretized form of f_α^{eq}. The polynomial is again given by Eq. (32). Therefore, it is not subject to the restrictions of conventional polynomial assumed for f_α^{eq} [20, 59-61]. In the recovery of the Euler equations, the above derivation shows that u_i appears in the coefficients of Eq. (32). For recovery of the N-S equations, it is anticipated that not only will u_i appear in the coefficients, the viscous stress tensor S_{ij} and the heat flux vector q_i also will be present in the coefficients.

Just as in the case for the recovery of the Euler equations, the next step is to demonstrate that Eq. (32) with the coefficients properly determined is equivalent to Eqs. (35) – (37) with a D2Q9 lattice model and a Chapman-Enskog expansion for f_α. The derivation can be carried out in a manner similar to that outline above for the Euler equations recovery. As before, it is assumed that for each α, f_α can be expanded in terms of *Kn* to yield

$$f_\alpha = f_\alpha^{(0)} + Kn^1 f_\alpha^{(1)} + Kn^2 f_\alpha^{(2)} + O\left(Kn^3\right) \quad . \tag{41}$$

The equations governing the transport of $f_\alpha^{(i)}$ can be obtained for i = 0 - 2 by substituting Eq. (41) into Eq. (30) and then collecting terms with the same order of *Kn*. The results are

$$f_\alpha^{(0)} = f_\alpha^{eq} \qquad \text{to } O\left(Kn^0\right) \quad , \tag{42a}$$

$$\frac{\partial f_\alpha^{(0)}}{\partial t} + \left(\xi_\alpha\right)_i \frac{\partial f_\alpha^{(0)}}{\partial x_i} = -\frac{f_\alpha^{(1)}}{\tau} \qquad \text{to } O\left(Kn^1\right) \quad , \tag{42b}$$

$$\frac{\partial f_\alpha^{(1)}}{\partial t} + \left(\xi_\alpha\right)_i \frac{\partial f_\alpha^{(1)}}{\partial x_i} = -\frac{f_\alpha^{(2)}}{\tau} \qquad \text{to } O\left(Kn^2\right) \quad . \tag{42c}$$

In conventional approach, only Eq. (42b) is required to established equivalence with the Euler equations. On the other hand, Eqs. (42b) and (42c) are both used to recover the N-S equations. In the present approach, Eq. (42c) is not required in establishing equivalence with the N-S equations if the macroscopic properties defined by Eqs. (39a) – (39c) are used to determine the coefficients in Eq. (32). For 2-D flows with a D2Q9 lattice, the results are

$$\sum_{\alpha=0}^{N} f_\alpha^{eq} = \rho \quad , \tag{43a}$$

$$\sum_{\alpha=0}^{N} f_\alpha^{eq}\left(\xi_\alpha\right)_x = \rho u \quad , \tag{43b}$$

$$\sum_{\alpha=0}^{N} f_\alpha^{eq}\left(\xi_\alpha\right)_y = \rho v \quad , \tag{43c}$$

$$\sum_{\alpha=0}^{N} f_\alpha^{eq}\left\{\left(\xi_\alpha\right)_x^2 + \left(\xi_\alpha\right)_y^2\right\} = \frac{4}{D_T + D_R}\left(\rho e_t\right) \quad , \tag{43d}$$

$$\sum_{\alpha=0}^{N} f_\alpha^{eq}\left(\xi_\alpha\right)_x^2 = \rho u^2 + p + \tau_{xx} + P'_{xx} \quad , \tag{44a}$$

$$\sum_{\alpha=0}^{N} f_\alpha^{eq}\left(\xi_\alpha\right)_y^2 = \rho v^2 + p + \tau_{yy} + P'_{yy} \quad , \tag{44b}$$

$$\sum_{\alpha=0}^{N} f_\alpha^{eq}\left(\xi_\alpha\right)_x\left(\xi_\alpha\right)_y = \rho uv + \tau_{xy} + P'_{xy} \quad , \tag{44c}$$

$$\sum_{\alpha=0}^{N} f_\alpha^{eq}\left\{\left(\xi_\alpha\right)_x^2 + \left(\xi_\alpha\right)_y^2\right\}\left(\xi_\alpha\right)_x = \frac{4}{D_T + D_R}\left[u\left(p + \rho e_t\right) + u\tau_{xx} + v\tau_{xy} + q_x\right] \quad , \tag{45a}$$

$$\sum_{\alpha=0}^{N} f_\alpha^{eq}\left\{\left(\xi_\alpha\right)_x^2+\left(\xi_\alpha\right)_y^2\right\}\left(\xi_\alpha\right)_y=\frac{4}{D_T+D_R}\left[v\left(p+\rho e_t\right)+u\tau_{xy}+v\tau_{yy}+q_y\right] \quad . \tag{45b}$$

For a D2Q9 lattice, N = 8 just as in the inviscid flow case, and P'_{xx}, P'_{yy}, P'_{xy} are the elements of a second order tensor P'_{ij} in 2-D flows. The physical meaning of these conditions can be interpreted as follows. Eqs. (43a-d) are the 2-D equivalent of Eqs. (39a-c), while Eqs. (44a-c) are the conditions derived by requiring Eq. (36) to be recovered identically and Eqs. (45a-b) are obtained by requiring Eq. (37) to be satisfied correctly. These last two conditions, taken together, ensure that Eq. (30) is equivalent to the N-S equations correct to order *Kn*. Higher order terms are assumed to be negligibly small so they can be taken to be essentially zero. Mathematically, they are represented by

$$\sum_{\alpha=0}^{N} f_\alpha^{(n)}=0 \qquad \text{for } n\geq 1 \quad , \tag{46a}$$

$$\sum_{\alpha=0}^{N} f_\alpha^{(n)}\left(\xi_\alpha\right)_x=0 \qquad \text{for } n\geq 1 \quad , \tag{46b}$$

$$\sum_{\alpha=0}^{N} f_\alpha^{(n)}\left(\xi_\alpha\right)_y=0 \qquad \text{for } n\geq 1 \quad , \tag{46c}$$

$$\frac{D_T+D_R}{4}\sum_{\alpha=0}^{N} f_\alpha^{(n)}\left\{\left(\xi_\alpha\right)_x^2+\left(\xi_\alpha\right)_y^2\right\}=0 \qquad \text{for } n\geq 1 \quad . \tag{46d}$$

Finally, the N-S equations in component form are given by multiplying Eq. (30) with $\left\{1,\ \left(\xi_\alpha\right)_i,\ \left(\left|\left(\xi_\alpha\right)_i\right|^2\right)\left(D_T+D_R\right)/4\right\}^T$, take summation over α, and then substitute Eq. (41) into the resulting equations. After invoking the conditions given by Eqs. (43a-d) to Eqs. (46a-d), the final macro transport equations for a 2-D flow in Cartesian coordinates are given by,

$$\frac{\partial\rho}{\partial t}+\frac{\partial\rho u}{\partial x}+\frac{\partial\rho v}{\partial y}+O(Kn)=0 \quad , \tag{47a}$$

$$\frac{\partial\left(\rho u\right)}{\partial t}+\frac{\partial}{\partial x}\left(\rho u^2+p+\tau_{xx}+P'_{xx}\right)+\frac{\partial}{\partial y}\left(\rho uv+\tau_{xy}+P'_{xy}\right)+O(Kn)=0 \quad , \tag{47b}$$

$$\frac{\partial(\rho v)}{\partial t} + \frac{\partial}{\partial x}\left(\rho uv + \tau_{xy} + P'_{xy}\right) + \frac{\partial}{\partial y}\left(\rho v^2 + p + \tau_{yy} + P'_{yy}\right) + O(Kn) = 0 \quad , \tag{47c}$$

$$\frac{\partial}{\partial t}\left(\rho e_t\right) + \frac{\partial}{\partial x}\left[u\left(\rho e_t + p\right) + u\tau_{xx} + v\tau_{xy} + q_x\right] + \frac{\partial}{\partial y}\left[v\left(\rho e_t + p\right) + u\tau_{xy} + v\tau_{yy} + q_y\right] + O(Kn) = 0 \quad , \tag{47d}$$

In order to recover the full set of N-S equations correct to $O(Kn)$, the second order tensor P'_{ij} has to satisfy the divergence condition $\left(\partial P'_{ij}/\partial x_j\right) = 0$, which is identical to the condition given in Eq. (15b) in the development of a continuous f^{eq}.

The coefficients, A_α, Ax_α, Bxx_α, etc., in the expansion for f_α^{eq} given by Eq. (32) are still not known and need to be determined. Following the assumption and procedure used in Section 3.1, i.e., the coefficients with the same "energy cell" of the lattice velocities are taken to be the same, the following simplifications for the coefficients in Eq. (32) can be deduced. These simplifications can be specified as:

$$\begin{aligned} A_1 &= A_3 = A_5 = A_7, \\ A_2 &= A_4 = A_6 = A_8, \end{aligned} \quad , \tag{48a}$$

$$\begin{aligned} Ax_1 &= Ax_3 = Ax_5 = Ax_7, \\ Ax_2 &= Ax_4 = Ax_6 = Ax_8, \end{aligned} \quad , \tag{48b}$$

$$\begin{aligned} Ay_1 &= Ay_3 = Ay_5 = Ay_7, \\ Ay_2 &= Ay_4 = Ay_6 = Ay_8, \end{aligned} \quad , \tag{48c}$$

$$\begin{aligned} Bxx_1 &= Bxx_3 = Bxx_5 = Bxx_7, \\ Bxx_2 &= Bxx_4 = Bxx_6 = Bxx_8, \end{aligned} \quad , \tag{48d}$$

$$\begin{aligned} Byy_1 &= Byy_3 = Byy_5 = Byy_7, \\ Byy_2 &= Byy_4 = Byy_6 = Byy_8, \end{aligned} \quad , \tag{48e}$$

$$\begin{aligned} Bxy_1 &= Bxy_3 = Bxy_5 = Bxy_7, \\ Bxy_2 &= Bxy_4 = Bxy_6 = Bxy_8. \end{aligned} \tag{48f}$$

Therefore, the number of unknowns resulting from A_0 plus the coefficients for a D2Q9 lattice is 13, while the number of independent equations that can be found is 8. Consequently, 5 coefficients out of 13 have to be assumed zero in order to render the equations governing the remaining coefficients become a determinate set. These five coefficients are A_1, A_2, Bxx_2, Byy_2 and Bxy_1, and they are assumed zero. Then the other 8 coefficients are given by the following:

$$A_0 = \rho - \frac{2p}{\sigma^2} - (\gamma - 1)\frac{\rho|\boldsymbol{u}|^2}{\sigma^2}, \qquad A_1 = A_2 = 0 \quad , \tag{49a}$$

$$Ax_1 = \frac{\rho u}{\sigma^2} - \frac{\gamma p u}{\sigma^4} - (\gamma - 1)\frac{1}{2}\frac{\rho|\boldsymbol{u}|^2 u}{\sigma^4} - (\gamma - 1)\frac{q_x + u\tau_{xx} + v\tau_{xy}}{\sigma^4} \quad , \tag{49b}$$

$$Ax_2 = -\frac{1}{4}\frac{\rho u}{\sigma^2} + \frac{1}{2}\frac{\gamma p u}{\sigma^4} + (\gamma - 1)\frac{1}{4}\frac{\rho|\boldsymbol{u}|^2 u}{\sigma^4} + (\gamma - 1)\frac{q_x + u\tau_{xx} + v\tau_{xy}}{2\sigma^4} \quad , \tag{49c}$$

$$Ay_1 = \frac{\rho v}{\sigma^2} - \frac{\gamma p v}{\sigma^4} - (\gamma - 1)\frac{1}{2}\frac{\rho|\boldsymbol{u}|^2 v}{\sigma^4} - (\gamma - 1)\frac{q_y + u\tau_{xy} + v\tau_{yy}}{\sigma^4} \quad , \tag{49d}$$

$$Ay_2 = -\frac{1}{4}\frac{\rho v}{\sigma^2} + \frac{1}{2}\frac{\gamma p v}{\sigma^4} + (\gamma - 1)\frac{1}{4}\frac{\rho|\boldsymbol{u}|^2 v}{\sigma^4} + (\gamma - 1)\frac{q_y + u\tau_{xy} + v\tau_{yy}}{2\sigma^4} \quad , \tag{49e}$$

$$Bxx_1 = \frac{1}{2\sigma^4}\left(p + \rho u^2 + \tau_{xx} + P'_{xx}\right) \quad , \qquad Bxx_2 = 0 \quad , \tag{49f}$$

$$Byy_1 = \frac{1}{2\sigma^4}\left(p + \rho v^2 + \tau_{yy} + P'_{yy}\right) \quad , \qquad Byy_2 = 0 \quad , \tag{49g}$$

$$Bxy_2 = \frac{1}{4\sigma^4}\left(\rho uv + \tau_{xy} + P'_{xy}\right) \quad , \qquad Bxy_1 = 0 \quad . \tag{49h}$$

The choice of setting these 5 coefficients, A_1, A_2, Bxx_2, Byy_2, Bxy_1, to zero is not unique. For the present case, it is guided by necessity to recover an f_α^{eq} expansion similar to those given by previous researchers [20, 21, 59-61] who expanded the Maxwellian distribution function to give similarly expanded f_α^{eq}. With this understanding, Eq. (32) can be recast into a form similar to those given in [20, 21, 59-61]. Again, omitting all details, the result is:

$$f_\alpha^{eq} = C_\alpha + C_{0\alpha}\left|\boldsymbol{u}\right|^2 + \left(\xi_\alpha\right)_x C_{1\alpha x} + \left(\xi_\alpha\right)_y C_{1\alpha y} + \left(\xi_\alpha\right)_x u C_{2\alpha xx} + \left(\xi_\alpha\right)_x v C_{2\alpha xy}$$
$$+ \left(\xi_\alpha\right)_y u C_{2\alpha yx} + \left(\xi_\alpha\right)_y v C_{2\alpha yy} + \left(\xi_\alpha\right)_x \left|\boldsymbol{u}\right|^2 u C_{3\alpha xx} + \left(\xi_\alpha\right)_x \left|\boldsymbol{u}\right|^2 v C_{3\alpha xy}$$
$$+ \left(\xi_\alpha\right)_x^2 C_{4\alpha xx} + \left(\xi_\alpha\right)_y^2 C_{4\alpha yy} + \left(\xi_\alpha\right)_x \left(\xi_\alpha\right)_y C_{4\alpha xy} + \left(\xi_\alpha\right)_x^2 u^2 C_{5\alpha xx}$$
$$+ \left(\xi_\alpha\right)_y^2 v^2 C_{5\alpha yy} + \left(\xi_\alpha\right)_x \left(\xi_\alpha\right)_y uv C_{5\alpha xy} \quad . \qquad (50)$$

It should be pointed out that in the present expansion, coefficients represented by Eqs. (49a-h) will give rise to terms involving u_i, $\left(\xi_\alpha\right)_i$ and their products. Only terms up to second order of u_i, $\left(\xi_\alpha\right)_i$ and their products are shown in Eq. (50). This expansion is similar to those given in [20, 21, 59, 60], but is different from that derived by Watari [61] in two ways. For example, this expansion does not include 3rd order terms in $\left(\xi_\alpha\right)_i$, u_i and their products; instead, it includes terms such as $\left(\xi_\alpha\right)_x C_{1\alpha x}$, $\left(\xi_\alpha\right)_y C_{1\alpha y}$, $\left(\xi_\alpha\right)_x^2 C_{4\alpha xx}$, $\left(\xi_\alpha\right)_y^2 C_{4\alpha yy}$, and $\left(\xi_\alpha\right)_x \left(\xi_\alpha\right)_y C_{4\alpha xy}$. Therefore, the current approach yields an new method to derive an expansion for f_α^{eq} that resulted in coefficients given by Eqs. (48a-h). The mean flow velocities are enclosed inside the expansion coefficients and do not appear explicitly as products with the particle velocities. Consequently, the expansion is not subject to the $M << 1$ condition; for more details refer to [47]. The solution of P'_{ij} for a 3-D flow has already been given in Section 2.3.1. Using the same methodology, a P'_{ij} solution for 2-D flows can also be obtained. Note also that for inviscid flows with μ and κ set to zero, Eqs. (47a) – (47d) reduce identically to Eqs. (13), (16) and (19). It appears that the approach and methodology outline in Section 3.2 for the N-S equations is sufficiently general to yield both the Euler and N-S equations dependent on whether μ and κ are set to zero or not. It should be noted that the expansion for f_α^{eq} given by Eq. (32) is applicable for both inviscid (i.e. recovery of Euler equations) and viscous (i.e. recovery of N-S equations) flows except that the coefficients in Eq. (32) would take on different forms.

Another point to note is that the recovery of the N-S equations is being accomplished by assuming one lattice distribution function only; therefore, the coefficients in the f_α^{eq} expansion (Eq. (32)), besides dependent on the velocity and pressure field, are also functions of both the

shear stress and the heat flux. Consequently, it is only necessary to set 5 of the 13 coefficients given in Eqs. (49a-h) to zero because two more equations are available for the coefficients in Eq. (32). On the other hand, for isothermal incompressible flow, there is no need to recover the e or T equation and two more coefficients in Eq. (32) need to be set to zero. This means that 7 of the 13 coefficients (in a D2Q9 lattice) need to be set to zero (for details refer to Section 6 under the Subsection Incompressibility). In the development of this new LBM, it is further found that irrespective of whether 5 or 7 coefficients are set to zero for the respective flow, the same set of coefficients is always valid for all flow types belonging to the same class. The current formulation is not the only way to account for thermal effect in a flow. Another new is to treat the energy equation separately by postulating a different distribution function for e or T. This option is discussed in detail in Subsection 4.1.2.

Up to this point, no mention of the initial and boundary conditions (be they free stream or wall boundary conditions) have been given. In anticipation of the fact that a splitting method is used to solve Eq. (30) and Eq. (32) for both steady and unsteady flows, a detail discussion of these conditions is given in Section 5. Therefore, it is sufficient to point out here that the initial and boundary conditions of f_α under the present scheme are calculated from the macroscopic variables given or deduced at these boundaries. Consequently, the no-slip condition at the wall is satisfied identically and mass leakage is avoided completely.

4. Extension to Hydrodynamic Flows

Since the development of the LBM as a numerical simulation tool, it has been focused on gas flows where an ideal gas law exists. For liquid and/or fluid flows with multiple components and phases, the use of conventional LBM to simulate such flows is inappropriate, not to mention that it might not be valid because a gas equation of state does not apply here. Since then, different remedies have been sought to improve and/or replace the conventional LBM. One such remedy is to extend the mean-field approximation for liquid theory [62] to treat fluid flows with phase transition, and binary immiscible fluids [63-66]. Another approach is to approximate liquid flows by a systematic discretization of the Boltzmann kinetic equation, i.e., constructing

higher-order LBE models [67]. As such, this alternate approach offers a way to recover the N-S equations based on kinetic level of representation. In principle, this approach is not subject to the assumption of an ideal gas law; hence, it can be used to treat incompressible flow of liquids such as double diffusive phenomena found in ocean layers [68-70]. Although Shan et al. [67] had shown that the Hermite expansion can be used to construct higher-order LBE, its extension to more complicated flows, such as ocean currents where diffusion due to salinity and temperature difference exist, might not be straightforward. Hence, there is a need to seek a different approach that makes use of the simplicity of the LBM, and yet is capable of simulating liquid flows where a state equation is not necessary and fluid density is constant in the flow field.

From the above discussion, it is clear that all LBE approaches or their variants proposed to remedy liquid flow problems cannot be implemented just as easily as the LBM. Therefore, a new approach to derive a BGK-type modeled LBE that can recover the N-S equations fully and correctly is sought. In the following, the BGK-type modeled LBE is derived based on a discrete flux scheme (DFS). A two-equation approach much like that outlined in [71, 72] is pursued. One equation is for $\hat{f}$, which is a distribution function used to represent an intrinsic flow property in an infinitesimally small control volume; another distribution function $\hat{g}$ is used to represent the total thermal energy of the same infinitesimally small control volume. In anticipation of the fact that the velocity lattice method is used to solve $\hat{f}$ and $\hat{g}$, the outline below gives the derivation for the lattice counterpart of these two functions, $\hat{f}_\alpha$ and $\hat{g}_\alpha$. In order to claim validity of this two-equation approach, it is necessary to establish equivalency between this approach and that outline in Section 3.2 for incompressible flows. Once this is accomplished, the two-equation LBM approach is free of the $M << 1$ condition, and can also be used to treat thermal and buoyant problems with and without heat transfer, as well as stratification in salinity or other properties.

4.1 Discrete Flux Scheme (DFS)

It is noted that the DFS is a numerical scheme proposed for solving the N-S equations. If the solution of the DFS scheme were to be equivalent to that given by the N-S equations, it is

necessary to show that the governing equations for $\hat{f}_\alpha$ and $\hat{g}_\alpha$ are essentially equivalent to the mass, momentum and energy transport equations in the set of N-S equations. Therefore, $\hat{f}_\alpha$ and $\hat{g}_\alpha$ have to satisfy conditions similar to those previously proposed to establish equivalency between the MBE and the N-S equations. This success will reduce the set of vector and tensor N-S equations to a finite number of scalar equations. Thus the set of scalar equations can be solved using the same numerical method employed to solve the MBE listed in Sections 2 and 3. The work discussed in this Section can be found in [50]; readers can refer to it for details.

4.1.1 *Discrete Flux Representation of the Mass and Momentum Equation*

Let $\hat{\Omega}$ represents a finite volume of fluid with an arbitrary shape Ω fixed in space (Fig. 1). The center of Ω is located at coordinates (*x, y, z*), and the fluid is assumed to move through Ω. The corresponding mass $\hat{m}$ inside Ω is assumed to move with a group velocity $\hat{\boldsymbol{\xi}}$. Therefore, fluid density $\hat{\rho}$ of Ω at (*x, y, z*) can be defined as,

$$\hat{\rho}\left(x, y, z\right) = \frac{1}{\hat{\Omega}} \int_{\Omega} \hat{m}\, d\hat{\boldsymbol{\xi}} \quad , \tag{51a}$$

while the velocity $\hat{\boldsymbol{u}}$ of the fluid at (*x, y, z*) is defined as,

$$\hat{\boldsymbol{u}}\left(x, y, z\right) = \frac{\frac{1}{\hat{\Omega}} \int_{\Omega} \hat{m}\, \hat{\boldsymbol{\xi}}\, d\hat{\boldsymbol{\xi}}}{\frac{1}{\hat{\Omega}} \int_{\Omega} \hat{m}\, d\hat{\boldsymbol{\xi}}} \quad . \tag{51b}$$

Following the derivation of the conventional LBE, a discrete representation is proposed. Only a finite number of velocities $\hat{\boldsymbol{\xi}}_\alpha$ need be considered; therefore, fluid density is given by summing up an intrinsic property $\hat{f}_\alpha$ relating to fluid density of a group of fluid masses moving with the same $\hat{\boldsymbol{\xi}}_\alpha$, or

$$\hat{\rho} = \sum_{\alpha} \hat{f}_\alpha \quad . \tag{52a}$$

Similarly, the linear momentum of the same fluid mass is given by,

$$\hat{\rho}\, \hat{\boldsymbol{u}} = \sum_{\alpha} \hat{f}_\alpha\, \hat{\boldsymbol{\xi}}_\alpha \quad . \tag{52b}$$

where $\hat{f}_\alpha = W_\alpha \hat{m}_\alpha / \hat{\Omega}$ and $\hat{m}_\alpha$ in discrete form represents the distribution function $\hat{f}$ and the mass $\hat{m}$, respectively. Under the discrete flux model, the number of velocity component $\hat{\xi}_\alpha$ takes on a very large number. In principle, it can vary from a finite number to infinity. Therefore, it is convenient to introduce a weighting function W_α to account for the summation, which acts like a numerical integration. The weighting function W_α may be negative, hence, $\hat{f}_\alpha$ may also be negative. However, the sum of $\hat{f}_\alpha$ should always be positive. All properties including $\hat{\xi}_\alpha$ are represented by a discrete model; therefore, the flux of all flow properties is similarly represented, hence, the name "discrete flux method" is used.

Under this model, each component of $\hat{f}_\alpha$ will move with the same component velocity $\hat{\xi}_\alpha$. The velocity of these masses of fluid will vary as a result of collision and/or the effect of intermolecular forces between fluid molecules; therefore, the total rate of change of $\hat{f}_\alpha$ in Ω, represented by $\left(\partial \hat{f}_\alpha / \partial \hat{t} + \hat{\boldsymbol{\xi}}_\alpha \bullet \nabla \hat{f}_\alpha\right)$, is not necessarily zero. Along the line of the argument used to derive the LBE, $\hat{f}_\alpha$ will also reach a "local equilibrium" state denoted by $\hat{f}_\alpha^{eq}$. As $\hat{f}_\alpha$ reaches its local equilibrium state, its rate of change $\left(\partial \hat{f}_\alpha / \partial \hat{t} + \hat{\boldsymbol{\xi}}_\alpha \bullet \nabla \hat{f}_\alpha\right)$ will vanish. When the masses of fluid inside Ω are not in their local equilibrium states, it is argued that they will rearrange their velocities to approach $\hat{f}_\alpha^{eq}$ as a result of collision and/or the effect of intermolecular forces as mentioned before. The time required for this rearrangement can again be designated by $\hat{\tau}$, the "relaxation time", which is substantially smaller than the flow characteristic time $\hat{t}_0$, much like that proposed in the BGK model for the conventional LBE. Following the argument of the BGK model, it is further assumed that $\left(\partial \hat{f}_\alpha / \partial \hat{t} + \hat{\boldsymbol{\xi}}_\alpha \bullet \nabla \hat{f}_\alpha\right)$ is proportional to the difference between $\hat{f}_\alpha$ and $\hat{f}_\alpha^{eq}$, or

$$\frac{\partial \hat{f}_\alpha}{\partial \hat{t}} + \hat{\boldsymbol{\xi}}_\alpha \bullet \nabla \tilde{f}_\alpha = -\frac{\hat{f}_\alpha - \hat{f}_\alpha^{eq}}{\hat{\tau}} \quad . \tag{53}$$

After normalizing $\hat{f}_\alpha$ and other variables by their corresponding characteristic parameters, $\hat{\rho}_0$, $\hat{\xi}_\alpha$ $\hat{u}_0$, $\hat{t}_0$, and $\hat{L}_0$, respectively, the dimensionless form of Eq. (53) is given by

$$\frac{\partial f_\alpha}{\partial t} + \boldsymbol{\xi}_\alpha \cdot \nabla f_\alpha = -\frac{f_\alpha - f_\alpha^{eq}}{\varepsilon \tau} \quad , \tag{54}$$

where ε is a small parameter that can be interpreted as similar to *Kn*. It is shown later that this interpretation is consistent with the continuum assumption.

If, in addition, it is assumed that the deviation of f_α from f_α^{eq} is very small, then f_α can be written in terms of f_α^{eq} plus a small non-equilibrium component f_α^{neq}, such that

$$f_\alpha = f_\alpha^{eq} + \varepsilon f_\alpha^{neq} \quad . \tag{55}$$

Thus defined, f_α^{eq} can be determined if certain conditions are met. These conditions are put forward with the objective that the f_α^{eq} thus obtained can be used in Eq. (54) to recover the mass and momentum equation in the set of N-S equations. These conditions are:

$$\sum_\alpha f_\alpha^{eq} = \rho \quad , \tag{56a}$$

$$\sum_\alpha f_\alpha^{eq} \left(\xi_\alpha\right)_i = \rho\, u_i \quad , \tag{56b}$$

$$\sum_\alpha f_\alpha^{eq} \left(\xi_\alpha\right)_{\mathrm{i}} \left(\xi_\alpha\right)_{\mathrm{j}} = \rho u_{\mathrm{i}} u_{\mathrm{j}} + p\,\delta_{\mathrm{ij}} - \tau_{\mathrm{ij}} \quad . \tag{56c}$$

The first two conditions are similar to the mass and linear momentum definitions given in Eqs. (52a-b) and those listed in Eqs. (39a-b) for the evaluation of an equilibrium particle distribution function of the LBM [3]. The third condition is proposed to ensure the correct recovery of the momentum equation in the N-S equations. In Eq. (56c), the dimensionless viscous stress tensor τ_{ij}, is given by

$$\tau_{ij} = -\frac{M_\infty}{Re_\infty}\left\{2\mu\left(S_{ij} - \frac{1}{3}\delta_{ij} S_{kk}\right)\right\} \quad , \tag{56d}$$

where the strain tensor S_{ij} is again defined by $S_{ij} = \left(\partial u_i / \partial x_j + \partial u_j / \partial x_i\right)/2$. Multiplying Eq. (54) by $\left\{1, \left(\xi_\alpha\right)_i\right\}^T$, taking summation over α, and using the expressions given in Eqs. (56a-c), the exact mass conservation and momentum equation accurate to order ε are obtained:

$$\frac{\partial \rho}{\partial t} + \sum_j \frac{\partial \rho u_j}{\partial x_j} = \frac{D\rho}{Dt} + \rho \sum_j \frac{\partial u_j}{\partial x_j} = 0 \quad , \tag{57}$$

$$\frac{\partial\left(\rho u_i\right)}{\partial t} + \sum_j \frac{\partial}{\partial x_j}\left(\rho u_i u_j + p\delta_{ij} + \tau_{ij}\right) = O\left(\varepsilon\right) \quad . \tag{58}$$

It can be seen that if ε is interpreted as *Kn*, the correct N-S equations for a continuum fluid are recovered correctly. The next step is to recover the energy equation in the N-S equations.

4.1.2 *Discrete Flux Representation of the Energy Equation*

Similar to f_α, another flux distribution function, g_α, representing the total thermal energy e_t is introduced. This is given by

$$\rho e_t = \rho\left(e + \frac{1}{2}|\boldsymbol{u}|^2\right) = \sum_\alpha g_\alpha \quad , \tag{59}$$

where e_t and e, and g_α have been normalized by $\hat{u}_0^2$ and $\hat{\rho}_0\hat{u}_0^2$, respectively, to make them dimensionless. Similar to the argument made for f_α, although g_α is related to the total energy, its individual value can be negative due to the finite number of discrete velocities assumed. The equilibrium state of g_α is g_α^{eq}. Similarly, g_α can be written in terms of g_α^{eq} plus a non-equilibrium state g_α^{neq}, i.e.

$$g_\alpha = g_\alpha^{eq} + \varepsilon g_\varepsilon^{neq} \quad . \tag{60}$$

The equation that governs the transport of g_α can again be derived in a manner similar to that for f_α. The result is

$$\frac{\partial g_\alpha}{\partial t} + \boldsymbol{\xi}_\alpha \cdot \nabla g_\alpha = -\frac{g_\alpha - g_\alpha^{eq}}{\varepsilon\tau} \quad . \tag{61}$$

If the thermal energy equation in the N-S equations were to be recovered correctly, g_α^{eq} has to satisfy the following conditions;

$$\sum_\alpha g_\alpha^{eq} = \rho\left(e + \frac{1}{2}|\boldsymbol{u}|^2\right) \quad , \tag{62a}$$

$$\sum_\alpha g_\alpha^{eq}\left(\xi_\alpha\right)_i = u_i\left(p + \rho e + \frac{1}{2}\rho|\boldsymbol{u}|^2\right) + \sum_j u_j\tau_{ij} + q_i \quad , \tag{62b}$$

where the heat flux vector q_i is given by

$$q_i = -\frac{\gamma M_\infty}{Re_\infty Pr_\infty}\left(\kappa \frac{\partial e}{\partial x_i}\right) \quad , \tag{62c}$$

Pr_∞ is a reference Prandtl number, and κ is the fluid coefficient of thermal conductivity made dimensionless by a reference $\hat{\kappa}_0$. Eq. (62a) is similar to the definition of e_t given in Eq. (59), while Eq. (62b) just ensures that the energy equation in the N-S equations is correctly recovered. Summing up Eq. (61) over α, and substituting the expressions given by Eqs. (62a-b), the thermal energy equation is recovered, i.e.,

$$\frac{\partial}{\partial t}\left(\rho e + \frac{1}{2}\rho|\boldsymbol{u}|^2\right) + \sum_j \frac{\partial}{\partial x_j}\left[u_j\left(\rho e + \frac{1}{2}\rho|\boldsymbol{u}|^2 + p\right) + \sum_k u_k \tau_{jk} + q_j\right] = O(\varepsilon) \quad . \tag{63}$$

From the above derivation, it is clear that solving Eq. (54) and Eq. (61) simultaneously is equivalent to solving the N-S equations given by Eqs. (57), (58) and (63). For compressible gas flows, an equation of state is required to close the equation set; however, for incompressible flows of gas or liquid, no such requirement is necessary. Before proceeding to discuss the numerical methods used to solve Eq. (54) and Eq. (61), an extension of this general approach to treat flows with external body forces is outlined below. The method proposed is general enough for any external body force, including that created by irregular immersed boundaries [73]. This is discussed in detail in Section 4.1.3.

4.2 Extension of Methodology to Flows with External Body Force

The effect of an external body force, such as buoyancy or salinity, can be easily accounted for in the discrete flux formulation. It is accomplished by modifying Eq. (54) to read:

$$\frac{\partial f_\alpha}{\partial t} + \boldsymbol{\xi}_\alpha \cdot \nabla f_\alpha + F_\alpha = -\frac{f_\alpha - f_\alpha^{eq}}{\varepsilon \tau} \quad , \tag{64}$$

where F_α is the dimensionless rate of change of density of fluid elements moving with velocity ξ_α in the control volume Ω due to the applied force field. It has to satisfy the following conditions,

$$\sum_\alpha F_\alpha = 0 \quad , \tag{65a}$$

$$\sum_{\alpha} F_{\alpha} \boldsymbol{\xi}_{\alpha} = \boldsymbol{F}_b \quad . \tag{65b}$$

Here, $\boldsymbol{F}_b$ is the dimensionless external body force applied to the flow field. The condition given in Eq. (65a) implies that the body force does not affect the total mass inside Ω. In Eq. (65b), F_α multiplies by ξ_α is the rate of change of momentum due to the external force field; thus, it is the body force itself. Therefore, this approach can be used to recover the buoyant force in the corresponding N-S equations. For problems with irregular immersed boundaries [73], a balance of fluid forces acting on the boundary can be used to represent the immersed boundary and the above approach is equally applicable.

5. Finite Difference LBM and Immersed Boundary Method

In this section, the following topics are discussed. These are the lattice Boltzmann method; the initial conditions, and wall and free stream boundary conditions; the splitting and finite difference methods used to treat the model Boltzmann equation; and the immersed boundary method used to handle wall boundaries with complex geometry.

5.1 New Lattice Boltzmann Method (LBM)

The lattice Boltzmann method essentially consists of solving Eq. (30) with f_α^{eq} given by Eq. (32), while the coefficients in this equation are calculated from Eqs. (34a-h). In addition, P'_{ij} is determined by solving Eq. (15b), i.e. $\partial P'_{ij} / \partial x_j = 0$, or by solving Eqs. (26 and 33a-b). Once the coefficients in the expansion for f_α^{eq} are known, Eq. (32) is well defined. Note that these equations are given for the case of a D2Q13 velocity lattice (Fig. 2a). Equations similar to Eqs. (34a-h) can also be derived for other velocity lattice models, such as a D2Q9 lattice model (Fig. 2b). For this case, f_α^{eq} is still given by Eq. (32), while the velocity lattices are defined by Eqs. (31a-c). Since the number of equations available for determining A_α, Ax_α, Bxx_α, etc. is still eight, only five of these coefficients need to be assumed zero. This choice of zero assumption for the five coefficients is not unique; however, the choice does work well for all validations cases attempted. Once these coefficients are set to zero and others are determined by solving the relevant equations for a particular 2-D or 3-D problem, they remain valid for any class of 2-D or

3-D problems and do not have to change from one problem to the next. Therefore, the coefficients are not problem dependent, and the new LBM is more general in this sense.

With an new lattice f_α^{eq} proposed for both Euler and N-S equations, the BGK-type MBE is readily applicable to a wide range of physical problems using an appropriate numerical scheme. In a numerical simulation, a finite computational domain is adopted. Well-defined initial conditions, properly formulated boundary conditions, with a space-time accurate and efficient numerical scheme, are the foundation of numerical simulations. Since the conventional MBE are confined to simulations with low Mach number, the corresponding numerical methods are also with low order accuracy, normally second-order in both space and time. Hence, the open boundary conditions are commonly reduced to first or zero order of accuracy. If the improved BGK-type MBE is to be extended to solve a wide range of physical problems, the order of accuracy for the corresponding numerical schemes, including the treatment of both solid and open boundary conditions, should be adequate to resolve the physical properties in the truncated computational domain.

5.2 Initial Conditions, Wall and Free Stream Boundary Conditions

Throughout the numerical simulation by using LBM, the evolution of f_α is described, where the corresponding macroscopic quantities are evaluated via moment of f_α. To start the simulation, however, the information at mesoscopic level is not directly available. Instead, the initial known quantities, i.e. the macroscopic ones, are inputted and transformed into the corresponding f_α^{eq} for every node in the computational domain.

On the other hand, two main types of boundaries are commonly involved in numerical simulations, namely solid and open boundaries. For the wall boundary conditions, a conventional bounce-back hypothesis of f_α at mesoscopic level leads to mass leakage at the wall [26-34]. Similar to the case in posing initial conditions, only macroscopic quantities are known at the wall boundaries, upon which the mesoscopic information has to be determined. It renders the bounce-back scheme at mesoscopic level inappropriate for an accurate address of the boundary conditions at walls, which eventually hinders the application of LBM to simulations

involve solid boundaries. Therefore, a properly imposed wall boundary condition should be constructed with reference to the macroscopic quantities at the solid surface. In view of this, slip / no-slip, isothermal / adiabatic wall boundary conditions are imposed for wall boundaries, where the macroscopic quantities or their derivatives are defined, and the corresponding f_α^{eq} are calculated. Thus configured, the mass leakage problem is resolved.

Due to limitation of computational resources, a finite domain is invoked for numerical simulations. The challenge comes from the fact that the boundary of the domain has to be transparent to the quantities being simulated, such that they can pass through the boundary without reflecting back and contaminating the domain. Via a thorough investigation for different types of open boundary conditions [39], an absorbing boundary condition (ABC) was established, which was proofed to be the most effective for simulations require high order of accuracy, such as aeroacoustics problems. Similar to the non-reflecting boundary conditions (NRBC) in direct numerical simulations (DNS), ABC adopts the concept of directing the outgoing disturbances towards a prescribed, desirable value within a buffer region, such that the reflection is minimized. For LBM, a prescribed, desirable value of the distribution function at the boundary, f_α^{eq}, is determined from the prescribed macroscopic quantities (usually mean flow), and is then implemented into the formulation for the buffer zone:

$$\frac{\partial f_\alpha}{\partial t} + \xi_\alpha \bullet \nabla_x f_\alpha + \sigma_d \left(f_\alpha^{eq} - f_\alpha \right) = -\frac{1}{\tau Kn} \left(f_\alpha - f_\alpha^{eq} \right) \quad , \tag{66}$$

where f_a has the same structure as σ in the lattice velocity, σ_d as the damping coefficient where $\sigma_d = \sigma_m \left(\delta / D_d \right)^2$, σ_m is a constant to be specified to tailor for different cases. Thus formulated, the ABC is proofed to have successfully duplicated the results as that obtained by DNS for various aeroacoustics problems with negligible discrepancies [42, 39, 48].

5.3 Splitting Method and Finite Difference LBM

The inhomogeneous partial differential equation (PDE) of Eq. (30) can be solved by using a splitting method [76, 77], where the equation is divided into two PDEs, one

homogeneous and one diffusion type equation, and are being solved as two initial value problems:

$$1^{st}\ PDE: \quad \frac{\partial f_\alpha}{\partial t} + \xi_\alpha \bullet \nabla_x f_\alpha = 0 \quad , \tag{67}$$

$$2^{nd}\ PDE: \quad \frac{\partial f_\alpha}{\partial t} = -\frac{1}{\tau Kn}\left(f_\alpha - f_\alpha^{eq}\right) \quad . \tag{68}$$

These two PDEs describe the streaming step, given by Eq. (67), and the collision step, given by Eq, (68). The initial values of $f_\alpha^{0,eq}\left(x,t\right)$ are determined from Eq. (32) and Eq. (34) using the initial macroscopic primitive variables.

The streaming step begins by making use of $f_\alpha^{0,eq}\left(x,t\right)$ to start the solution of Eq. (67). This will lead to intermediate f_α^I for all interior points, but not the boundary points. Macroscopic variables such as u^I, v^I, p^I are then calculated from equations such as those given in Eq. (43a-d) and Eq. (44a-c). The boundary conditions for the macroscopic variables are then set according to problem specifications. Finally, using the macroscopic quantities thus determined in the domain and the boundaries, the intermediate value for the equilibrium distribution function, $f_\alpha^{I,eq}$, are calculated from Eq. (30) and Eq. (32) where the coefficients are determined from Eq. (34a-h).

The collision step involves solving Eq. (68). Employing the Euler method, where Δt is set equal to τKn for temporal discretization, the finite difference counterpart of Eq. (68) becomes

$$\frac{f_\alpha\left(x,t+\Delta t\right) - f_\alpha\left(x,t\right)}{\Delta t} = \frac{1}{\tau Kn}\left[f_\alpha\left(x,t\right) - f_\alpha^{eq}\left(x,t\right)\right] \Rightarrow f_\alpha\left(x,t+\Delta t\right) = f_\alpha^{eq}\left(x,t\right) \quad , \tag{69}$$

This equation leads to the ability to set f_α at time $(t+\Delta t)$ as $f_\alpha^{I,eq}$. In other words, the macroscopic variables at $(t+\Delta t)$ are essentially given by u^I, v^I, p^I. Therefore, the collision step does not take up any computing resource. Time marching is then achieved by repeating the procedure outlined above for the streaming and collision step.

In principle, any finite difference numerical schemes suitable for solving PDEs, such as Eqs. (67, 68), can be adopted according to the required order of accuracy for the target physical problem. The LBM thus is collectively called the finite-difference LBM (FDLBM). The FDLBM is so developed to avoid any ad-hoc improvisation in numerical simulations.

5.4 Immersed Boundary Method (IBM) and FDLBM

In view of the fact that wall boundary values of f_α are determined from the macroscopic quantities (ρ, u, v, p), the new LBM could be extended to treat flows with complex geometry using numerical schemes that are commonly employed to solve the N-S equations directly. Two schemes stand out among the many available; they are the body-fitted geometry method and the immersed boundary method. However, these two schemes are quite cumbersome, especially when the wall boundary is changing with time. One illustrative example is blood flow through arteries with plaque build up (Fig. 3). For this type of flow, the LBM numerical solution can no longer be easily carried out using Cartesian grids, which works best for flows whose boundaries can be well defined by Cartesian coordinates. Another complication is that blood is a non-Newtonian fluid; any attempt to approximate it by a Newtonian assumption would greatly compromise the simulated flow behavior [56]. For wall boundary with complex geometry changing with time, the applicability and suitability of using body-fitted geometry method with LBM for blood flow simulations has been widely explored by researchers [78, 79, 80, 81, 82, 83]. In these studies, the grids are generated *a priori* [80]. For a time dependent problem, the geometry of the plaque build up will also vary with time; therefore, the computer-generated grids have to be checked (either manually or through computation) to ensure integrity of the simulated results [79]. These additional tasks render the body-fitted geometry method very time consuming. Therefore, the combined LBM and body-fitted geometry method fails to yield any advantage compared to solving the N-S equations directly using other numerical methods. The next step is to explore the advantage of deploying the IBM with the new LBM.

In the following sub-sections, the rationale for the IBM is first justified, then its implementation into the new LBM with changing wall boundary that is either stationary or time

dependent is discussed. Next, the procedure on how to implement the IBM into an LBM for stationary flow is formulated, which is then followed by a discussion on its extension to time dependent problems.

5.4.1 *IBM and Its Implementation into the new LBM*

As outlined in Sections 2-4 & 5, an FDLBM that provides a convenient algorithm for setting the boundary condition using a splitting method to solve the LBE has been presented. This FDLBM, based on the new LBM, is free of the inherent compressibility effect of conventional LBM [44]. It is capable of simulating flows of Newtonian and non-Newtonian fluids with (or without) external body forces [56], and in micro-channels [45]. Using this numerical approach, a wide variety of governing equations for aeroacoustics, aerodynamics and hydrodynamics flows can be similarly treated [50]. The FDLBM thus developed was originally aimed at micro-channel flows along the line suggested in [84], but its application is actually much broader [56]. The FDLBM has one drawback though, i.e. its solution relies on Cartesian grids, even for 2-D flows with complex boundary geometry. An new is to devise a scheme to integrate the IBM into the FDLBM so that the combined numerical technique can properly handle unsteady flows with complex boundary geometry (such as in blood flow with plaque build up). Once proven, the numerical scheme would give rise to a computational tool that could handle complex boundaries using Cartesian grids only for any 2-D, axisymmetric and 3-D flows. In the following, a procedure, different from those given in [73, 85, 86, 87, 88], to implement the general IBM concept into the new LBM is discussed [52, 53].

From the above discussion, it can be seen that blood flow through arteries with plaque build up is an appropriate example to use to illustrate how valid wall boundary conditions with changing geometry could be developed for the new LBM. Development of the IBM is based on the pioneering work of Peskin [89, 90], who studied cardiac mechanics and the associated blood flow. The IBM was used to solve the N-S equations in the presence of moving immersed boundaries (in this case the heart-valve leaflets), which moved at a local fluid velocity and exerted forces locally on the fluid. This suggests that the boundary should be modelled as a set

of elements linked by springs. In developing the IBM, Peskin [89] required that a fixed Cartesian grid should again be used to carry out the numerical simulation. Through the introduction of an external body force field, which was designed to simultaneously satisfy the no-slip condition at blood vessel wall and also mimic the changing wall geometry due to plaque build up, the wall geometry could be modeled correctly. Thus formulated, wall boundary with complex geometry (moving or stationary), and even fluid-structure interaction (FSI) problems, could be treated by this IBM [73, 91].

In order to illustrate how the IBM can handle boundary with complex geometries, moving and even elastic [73], the flow through a pipe with varying constriction is chosen as an example [52, 53]. The IBM is formulated using Cartesian coordinates where the constricted boundary inside the computational domain is called the immersed boundary. The immersed boundary is represented by a set of massless points, $\boldsymbol{X}_k = \left(X_k, Y_k\right)$ with index $k = 1 \ldots N$ that moves with the local fluid velocity $\boldsymbol{u} = \left(u, v\right)$. Hence, their tracking is Lagrangian in nature, i.e.

$$\frac{\partial \boldsymbol{X}_k}{\partial t} = \boldsymbol{u}\left(\boldsymbol{X}_k, t\right) \quad . \tag{71}$$

For this example, the Euler method is used to solve the above equation; thus, the local fluid velocity is given by

$$\boldsymbol{u}\left(\boldsymbol{X}_k, t\right) = \int_{\boldsymbol{x}\in\Omega} \boldsymbol{u}\left(\boldsymbol{x}, t\right) \delta\left(\left|\boldsymbol{x} - \boldsymbol{X}\right|\right) \quad , \tag{72a}$$

and in discretized form Eq. (68a) can be written as

$$\boldsymbol{u}\left(\boldsymbol{X}_k, t\right) = \sum_{i,j} \boldsymbol{u}^{ij}\, \delta_d\left(x^{ij} - X_k\right) \delta_d\left(y^{ij} - Y_k\right) \Delta x \Delta y \quad , \tag{72b}$$

where $\boldsymbol{u}^{ij}$ is the velocity vector at the position indexed by i and j, calculated from the Cartesian grid, $\left(x^{ij}, y^{ij}\right)$ is the Cartesian coordinate positions indexed by i and j.. The Dirac delta function δ appears as a kernel in each of the equations in which a transition is made from boundary to fluid quantities or vice versa, and δ_d is the discrete counterpart of δ. The choice of δ will affect

the accuracy of different types of governing equations [92]. For the present formulation, Peskin's [89] choice for δ is adopted; it is given by

$$\delta_d\left(r\right) = \begin{cases} \dfrac{1+cos\left(\pi r / 2h\right)}{4h} & , \quad \left|r\right| < 2h \\ 0 & , \quad \left|r\right| \geq 2h \end{cases} \quad , \tag{73}$$

According to simulations reported in [52, 53], good results for all cases tested are reported.

The effect of the immersed boundary on the surrounding fluid is transmitted through a localized forcing term $\boldsymbol{F}^{ib} = \left(F_x^{ib}, F_y^{ib}\right)$. This is added as a body force in the momentum equations and is given by

$$\boldsymbol{F}^{ib}\left(\boldsymbol{x}, t\right) = \frac{1}{N}\sum_{k=1}^{N} \boldsymbol{F}_k\left(t\right)\, \delta_d\left(\left|\boldsymbol{x} - \boldsymbol{X}_k\right|\right) \quad , \tag{74a}$$

in continuous form while its counterpart in discrete form is,

$$\boldsymbol{F}^{ib}\left(\boldsymbol{x}, t\right) = \frac{1}{N}\sum_{k=1}^{N} \boldsymbol{F}^{ib}\left(\boldsymbol{X}_k, t\right)\, \delta_d\left(x^{ij} - X_k\right)\, \delta_d\left(y^{ij} - Y_k\right) \quad . \tag{74b}$$

The relation between $\boldsymbol{X}_k$ and $\boldsymbol{F}_k$ depends on the material properties of the immersed boundary. For all CFD examples reported in [52, 53], the immersed boundary is considered as a rigid wall, and is simulated using the method employed in [90, 92].

The immersed boundary points $\boldsymbol{X}_k$ are assumed to attach to a fictitious fixed equilibrium location $\boldsymbol{X}_k^e$ by a spring with a restoring force $\boldsymbol{F}_k$ given by

$$\boldsymbol{F}_k\left(t\right) = -\mathrm{K}\left[\boldsymbol{X}_k\left(t\right) - \boldsymbol{X}_k^e\right] \quad , \tag{75}$$

where K is a positive spring constant. When K is large, the displacement between $\boldsymbol{X}_k^e$ and $\boldsymbol{X}_k$ is negligible. Therefore, the immersed boundary is relatively stable; thus simulating a rigid wall defined by $\boldsymbol{X}_k$. In practice, K should be as large as possible; however, large K results in a stiff system that might lead to numerical instability [73]. Although the IBM is only used to simulate a

rigid wall in this example, it is obvious that modifying the "material properties" could allow elastic and/or moving boundaries with complex geometry to be simulated also.

5.4.2 *Steady LBM/IBM*

A first attempt to implement the IBM into an LBM/FDLBM framework was carried out in [85, 86]. In these studies, the immersed points were used to simulate some moving inelastic particulates. An external force created by the deformation of the particulates was computed by deploying the penalty method [85] or the direct forcing scheme [86]. A similar idea was put forward in [74] and [87]. However, Niu et al. [87] incorporated the IBM with a multi-relaxation collision LBM; consequently, the forcing term was calculated using the momentum exchange method. A similar concept has also been used to treat problems with a moving boundary in 2-D and 3-D flows [88].

In the current formulation, the IBM can be built into the new LBM through the addition of an external body force in the N-S equations. This requires recovery of the N-S equations with a body force included; the procedure of which has been outlined in Section 4.1.3. Consequently, the only work required here is to modify the distribution function for the external body force F_α to account for the forcing function of the immersed boundary points. It can be seen that Eq. (64) is also applicable for the LBM/IBM technique provided F_α in Eq. (64) is interpreted as the body force created by the immersed boundary. Therefore, conditions that the distribution function F_α have to satisfy can be similarly derived as in Section 4.2; the result is

$$\sum_{\alpha=0}^{8} F_\alpha = 0 \quad , \tag{76a}$$

$$\sum_{\alpha=0}^{8} F_\alpha \xi_{\alpha x} = F_x^{ib} \quad , \tag{76b}$$

$$\sum_{\alpha=0}^{8} F_\alpha \xi_{\alpha y} = F_y^{ib} \quad , \tag{76c}$$

$$\sum_{\alpha=0}^{8} F_\alpha \left(\xi_{\alpha x}^2 + \xi_{\alpha y}^2\right) = 0 \quad . \tag{76d}$$

If a minimal form of Eq. (32) is assumed for F_α, such as

$$F_\alpha = A_\alpha + \xi_{\alpha x} Ax_\alpha + \xi_{\alpha y} Ay_\alpha \quad , \tag{77}$$

the coefficients in Eq. (73) can be determined to give

$$A_0 = A_1 = A_2 = 0 \quad , \tag{78a}$$

$$Ax_1 = \frac{F_x^{ib}}{2\sigma^2}, \; Ax_2 = 0 \quad , \tag{78b}$$

$$Ay_1 = \frac{F_y^{ib}}{2\sigma^2}, \; Ay_2 = 0 \quad . \tag{78c}$$

It can be seen that time-varying and/or complex wall boundary can be dealt with by solving the MBE with an additional body force without compromising the numerical advantage of the new LBM.

As pointed out in [91], most IBM uses the restoring force technique; therefore, some streamlines may pass through the solid body because the no-slip condition is only approximately satisfied. In the present method, the no-slip condition at the boundary is satisfied by the primitive variables and the particle distribution function is determined from these primitive variables. Therefore, streamline leakage might not be a factor like that mentioned in [91].

5.4.3 *Unsteady LBM/IBM*

The artificial compressibility or the pressure correction method is frequently used to solve the unsteady incompressible N-S equations. Both methods employ pseudo time to make the solution time-accurate by treating the time-dependent terms in pseudo time [93]. Real physical time terms are added in the governing equations and the solution is iterated to a pseudo-time convergence at each real time step. When the pseudo-time terms vanish, the solution obtained satisfies the complete time-dependent equations. For the sake of brevity, this approach is denoted as the pseudo-time approach. Detailed discussion of this approach can be found in [93]. The same approach is also used in [45] to solve the unsteady N-S equations by extending the steady FDLBM to a time-accurate FDLBM; refer to Section 6.2 for details. Only the

formulation for a time-accurate FDLBM is given here. It is not necessary to repeat the case for a time-accurate FDLBM/IBM because the extension is fairly straightforward.

Only the Cartesian form of Eq. (64) is considered. In this equation, as explained above, the body force F_α is used to represent a real, physical time term in the pseudo-time approach. Following the procedure used to determine F_α in the stationary case, it can be easily shown that F_α for this pseudo-time approach has to satisfy the following constraints. It can be easily shown that assuming a D2Q9 lattice model for illustration purpose, these constraints are determined as

$$\sum_{\alpha=0}^{8} F_\alpha = \frac{\partial \rho}{\partial t'} \quad , \tag{79a}$$

$$\sum_{\alpha=0}^{8} F_\alpha \xi_{\alpha x} = \frac{\partial \rho u}{\partial t'} \quad , \tag{79b}$$

$$\sum_{\alpha=0}^{8} F_\alpha \xi_{\alpha y} = \frac{\partial \rho v}{\partial t'} \quad , \tag{79c}$$

$$\sum_{\alpha=0}^{8} F_\alpha \left(\frac{\xi_{\alpha x}^2 + \xi_{\alpha y}^2}{2} \right) = \frac{\sigma^2}{2} \frac{\partial \rho}{\partial t'} \quad , \tag{79d}$$

where t' is the real physical time and t is the pseudo-time for iteration purpose. Following the derivation given in [45], Eq. (64) is multiplied by $\left(1, \boldsymbol{\xi}_\alpha, \left|\boldsymbol{\xi}_\alpha\right|^2 / 2\right)^T$, then taking summation over α, and using Eqs. (75a-d), the following equations are obtained:

$$\frac{\partial \rho}{\partial t'} + \frac{\partial}{\partial t}\left(\sum_\alpha f_\alpha \right) + \frac{\partial \rho u}{\partial x} + \frac{\partial \rho v}{\partial y} = -\frac{1}{Kn\,\tau}\left(\sum_\alpha f_\alpha - \rho \right) \quad , \tag{80a}$$

$$\frac{\partial \rho u}{\partial t'} + \frac{\partial \rho u}{\partial t} + \frac{\partial \rho u^2 + p - \tau_{xx}}{\partial x} + \frac{\partial \rho uv - \tau_{xy}}{\partial y} = O\left(Kn\right) \quad , \tag{80b}$$

$$\frac{\partial \rho v}{\partial t'} + \frac{\partial \rho v}{\partial t} + \frac{\partial \rho uv - \tau_{xy}}{\partial x} + \frac{\partial \rho v^2 + p - \tau_{yy}}{\partial y} = O\left(Kn\right) \quad , \tag{80c}$$

$$\frac{\partial}{\partial t}\left[\left(p - \frac{\tau_{xx} + \tau_{yy}}{2} \right) + \frac{1}{2}\rho\left(u^2 + v^2\right) \right] + \frac{\sigma^2}{2}\left(\frac{\partial \rho}{\partial t'} + \frac{\partial \rho u}{\partial x} + \frac{\partial \rho v}{\partial y} \right) = O\left(Kn\right) \quad . \tag{80d}$$

After reaching steady state with respect to the pseudo-time *t*, all pseudo-time terms vanish. Eqs. (80b-d) become the continuity and momentum equations of the N-S equations, respectively. The sum of the distribution function f_α, as shown in Eq. (80a), is the density.

Following the procedure outlined in Section 5.3.2, the IBM can again be integrated into the new LBM by solving Eq. (64) with an assumption that a minimal form for F_α is given by Eq. (77). Following the same rules as those used to deduce the coefficients in Eq. (77), one possible set of solutions for this unsteady case is

$$A_0 = 0,\ A_1 = \frac{1}{4}\frac{\partial \rho}{\partial t'},\quad A_2 = 0 \quad , \tag{81a}$$

$$Ax_1 = \frac{1}{2\sigma^2}\frac{\partial \rho u}{\partial t'},\quad Ax_2 = 0 \quad , \tag{81b}$$

$$Ay_1 = \frac{1}{2\sigma^2}\frac{\partial \rho v}{\partial t'},\quad Ay_2 = 0 \quad . \tag{81c}$$

The physical time derivative term can be approximated by any finite difference method; however, the simple Euler method is used here, i.e.,

$$\frac{\partial Z}{\partial t'} = \frac{Z - Z_0}{\Delta t'} \quad , \tag{82}$$

where Z is the updated physical quantity (e.g. $\rho,\ \rho u,\ \rho v$) iterating in pseudo-time, Z_0 is the physical quantity in the previous physical time step and $\Delta t'$ is the step size of the physical time. For incompressible flow where density is a constant, the density derivative is simply zero.

6. Discussions on Validation Cases

6.1 Prologue

To demonstrate the viability and uniqueness of the new LBM/FDLBM, a series of validation test cases have already been carried out and reported in open literature [42-54]. The test cases were selected to highlight the validity, accuracy and uniqueness of the special characteristics of the new LBM. Before settling down on the choice of these cases, it is prudent to recall that the conventional LBM has been used to simulate aeroacoustic problems and the results are more than wanting [36-40], especially in its simulation of acoustic scattering by a

vortex [46]. The results were improved after different nonreflecting boundary conditions were attempted with corrections made to ensure the transport coefficients, such as μ, γ, and c of the fluid, were recovered correctly for diatomic gas. Further, the relaxation time scale in the LBE has to be replaced by an effective relaxation time that is made up of the time scales of the intermolecular potential and the weak repulsive potential. This tailoring is valid for the problems under consideration; however, the tailoring might have to be modified for different problems. Therefore, the fine tunings made to conventional LBM are not unique and are problem dependent.

On the other hand, the new LBM is formulated to rectify the inadequacies of conventional LBM. These inadequacies are the conventional LBM's inability to satisfy the zero-velocity divergence condition for incompressible flow, mass leakage at the wall, and dependence of the mean flow on M for incompressible flow, and justification required in using the conventional LBM to simulate hydrodynamic flows where the fluid medium is liquid instead of gas. The most important improvement in the new LBM is its ability to satisfy the zero-velocity divergence condition for incompressible flows. It is this feature that puts the new LBM on solid ground for incompressible flow simulations.

Since pressure is the primary driving force in any incompressible flow, the pressure field should be part of the solution and should not be specified in the form of a state equation much like that stipulates in conventional LBM. Therefore, validation cases to demonstrate this unique property of the new LBM should include simple isothermal incompressible flow [44] as well as thermal incompressible flow [51] and flow with uncertainty [49]. Once completed, the ability of the new LBM to replicate incompressible flow in microchannel is attempted [45]. The next step is to demonstrate the ability of the new LBM to resolve compressible flows correctly including its ability to capture shocks [43] and to resolve their structures [47]. In view of these successes, the new LBM is then applied to simulate aeroacoustics and thermo-aeroacoustics with/without vortex and thermal scattering [42, 46, 54, 55] and flows with immersed boundaries as in blood flow through arteries where blood fluid is non-Newtonian [52, 53]. Finally, the new LBM is used to simulate buoyant and double diffusive flows in oceans where the medium is water [50]. These publications were mainly derived from two PhD theses, one on aeroacoustics [55], and

another on blood flow through arteries [56]. In these simulations using the new LBM, the results are found to be in excellent agreement with theoretical analysis and/or measurements, and DAS and DNS simulations whenever available.

All calculations were carried out using the same numerical technique and method, and identical velocity lattice model was adopted; i.e., a D2Q9 model for 2-D flows, and a D3Q15 model for 3-D flows. Most simulations carried out were either 1-D or 2-D; however, a few 3-D cases were also attempted. Laminar flow was assumed in each of the simulations, and examples were carefully chosen to highlight characteristics that are representative of the salient features of the new LBM. Three different types of fluids had been examined, Newtonian, non-Newtonian, and nanofluid. A majority of the flow cases studied was steady while a few unsteady cases had also been carried out. These choices were chosen to illustrate the general nature and ability of the new LBM. Most simulations were carried out to 10^{-4} accuracy. Since aereoacoustics disturbances are at least two-order of magnitude smaller than any aerodynamic disturbances, a sixth-order accurate finite difference scheme put forward by Lele [57] was built into the FDLBM code to resolve the aeroacoustics disturbances correctly.

Results of these studies have already been published in the open literature [42-54]. Instead of carrying out a complete replication of these published results again in this paper, a summary discussion of their unique results is organized to bring out the salient features of each flow group attempted. The flow groups chosen in the validation cases can be briefly classified as: incompressible, compressible, complex boundary geometry, aeroacoustics and scattering, and flow uncertainty. Results for these flow groups are discussed and analyzed under the subsection headings: (2) incompressibility, (3) compressibility, (4) complex boundary geometry, (5) aeroacoustics and scattering, and (6) flow uncertainty. In addition, the numerical advantage of the new FDLBM numerical scheme is discussed in Subsection 6.7. Furthermore, Kefayati and his group at Flinders University of South Australia, Adelaide, have adopted the computer code developed by Drs. S. C. Fu and E. W. S. Kam [55, 56] to extend the new FDLBM to treat magnetohydrodynamics flows where the medium can be nanofluid or non-Newtonian fluid. In order to enhance completeness of this paper, Subsection 6.8 will focus on a brief discussion of Kefayati's successful LBM simulations of magnetohydrodynamics flows [94-102].

6.2 Incompressibility

Broadly speaking, the FDLBM based on the new LBM has been tested against wide variety of flows; very good to excellent agreement with DNS, DAS, and measurements results were obtained [44, 45, 49-53]. Although the ability of the new LBM to correctly simulate incompressible flow has previously been demonstrated [44], this salient feature of the new LBM warrants special attention. Therefore, the proof that this property is inherent in the formulation of the new LBM is summarized here for reference; only a broad outline is given, interested readers should refer to [44] for details.

In this case, it is only necessary to consider the 2-D laminar N-S equations for incompressible flow. The starting point is the normalized discrete Boltzmann equation, Eq. (30), with f_α^{eq} given by Eq. (32). However, in this case, all variables are made dimensionless with reference to L, ρ_0, u_0, and ρu_0^2, which are used to normalize length, density, velocity, and pressure and stresses, respectively. As before, a D2Q9 lattice model is assumed and the lattice velocities are defined as:

$$\xi_0 = \left(0,0\right), \quad \alpha = 0 \quad , \tag{83a}$$

$$\xi_\alpha = \sigma\left(cos\left[\pi\left(\alpha-1\right)/4\right],\ sin\left[\pi\left(\alpha-1\right)/4\right]\right) \quad , \quad \alpha = 1, 3, 5, 7 \quad , \tag{83b}$$

$$\xi_\alpha = \sqrt{2}\sigma\left(cos\left[\pi\left(\alpha-1\right)/4\right],\ sin\left[\pi\left(\alpha-1\right)/4\right]\right) \quad , \quad \alpha = 2, 4, 6, 8 \quad , \tag{83c}$$

where σ is a scaling parameter to be defined later. A Chapman-Enskog type expansion is assumed for f_α, which to 2nd order can be written as,

$$f_\alpha = f_\alpha^{eq} + \varepsilon f_\alpha^{(1)} + \varepsilon^2 f_\alpha^{(2)} + O\left(\varepsilon^3\right) \quad , \tag{84a}$$

and $$\sum_{\alpha=0}^{8} f_\alpha^{(n)} = \sum_{\alpha=0}^{8} f_\alpha^{(n)} \xi_{\alpha x} = \sum_{\alpha=0}^{8} f_\alpha^{(n)} \xi_{\alpha y} = 0 \ , \quad n \geq 1 \quad , \tag{84b}$$

has been assumed. Here, ε is taken to be *Kn*, which is assumed very small. Multiply Eq. (30) by $\left(1,\xi\right)^{\mathrm{T}}$ and take summation over α, the laminar incompressible N-S equations without assuming steady flow yet:

$$\frac{\partial\rho}{\partial t}+\frac{\partial\rho u}{\partial x}+\frac{\partial\rho v}{\partial y}=0 \quad , \tag{85a}$$

$$\frac{\partial\rho u}{\partial t}+\frac{\partial\rho u^2}{\partial x}+\frac{\partial\rho uv}{\partial y}=-\frac{\partial p}{\partial x}+\frac{\partial\tau_{xx}}{\partial x}+\frac{\partial\tau_{xy}}{\partial y}+O\left(\varepsilon\right) \quad , \tag{85b}$$

$$\frac{\partial\rho v}{\partial t}+\frac{\partial\rho uv}{\partial x}+\frac{\partial\rho v^2}{\partial y}=-\frac{\partial p}{\partial y}+\frac{\partial\tau_{xy}}{\partial x}+\frac{\partial\tau_{yy}}{\partial y}+O\left(\varepsilon\right) \quad . \tag{85c}$$

are recovered subject to the following conditions:

$$\sum_{\alpha=0}^{8}f_\alpha^{eq}=\rho=\text{constant} \quad , \tag{86a}$$

$$\sum_{\alpha=0}^{8}f_\alpha^{eq}\xi_{\alpha x}=\rho u \quad , \tag{86b}$$

$$\sum_{\alpha=0}^{8}f_\alpha^{eq}\xi_{\alpha y}=\rho v \quad , \tag{86c}$$

$$\sum_{\alpha=0}^{8}f_\alpha^{eq}\xi_{\alpha x}^2=\rho u^2+p-\tau_{xx} \quad , \tag{86d}$$

$$\sum_{\alpha=0}^{8}f_\alpha^{eq}\xi_{\alpha y}^2=\rho v^2+p-\tau_{yy} \quad , \tag{86e}$$

$$\sum_{\alpha=0}^{8}f_\alpha^{eq}\xi_{\alpha x}\xi_{\alpha y}=\rho uv-\tau_{xy} \quad . \tag{86f}$$

Using Eqs. (86a-f) and following the procedure outlined in Section 3.2, the coefficients in the lattice f_α^{eq} as given in Eq. (32) can be determined to be,

$$A_0=\rho-\frac{2p}{\sigma^2}-\frac{\rho\left|\boldsymbol{u}\right|^2}{\sigma^2}+\frac{\tau_{xx}+\tau_{yy}}{\sigma^2}, \quad A_1=A_2=0 \quad , \tag{87a}$$

$$Ax_1=\frac{\rho u}{2\sigma^2} \ , \quad Ax_2=0 \quad , \tag{87b}$$

$$Ay_1 = \frac{\rho v}{2\sigma^2} \ , \quad Ay_2 = 0 \quad , \tag{87c}$$

$$Bxx_1 = \frac{1}{2\sigma^4}\left(p + \rho u^2 - \tau_{xx}\right) \ , \quad Bxx_2 = 0 \quad , \tag{87d}$$

$$Byy_1 = \frac{1}{2\sigma^4}\left(p + \rho v^2 - \tau_{yy}\right) \ , \quad Byy_2 = 0 \quad , \tag{87e}$$

$$Bxy_2 = \frac{1}{4\sigma^4}\left(\rho uv - \tau_{xy}\right) \ , \quad Bxy_1 = 0 \quad . \tag{87f}$$

This choice of zero coefficients is not arbitrary; other cases attempted show they work well also.

As discussed in Section 5.3, a splitting method is used to solve Eq. (30). Therefore, the temporal and spatial derivatives in Eq. (30) can be discretized in the following manner, or

$$\frac{f_\alpha\left(\vec{x}, t+\Delta t\right) - f_\alpha\left(\vec{x}, t\right)}{\Delta t} + \frac{f_\alpha\left(\vec{x} + \xi_\alpha \Delta t, t+\Delta t\right) - f_\alpha\left(\vec{x}, t+\Delta t\right)}{\Delta t}$$
$$= -\frac{1}{\varepsilon\tau}\left(f_\alpha\left(\vec{x}, t\right) - f_\alpha^{eq}\left(\vec{x}, t\right)\right) \quad . \tag{88}$$

Defining the scaling parameter σ such that the discretized velocity would fit the grid point and setting $\varepsilon = \Delta t$ [44] the following is obtained,

$$f_\alpha\left(\vec{x} + \xi_\alpha \Delta t \ , \ t + \Delta t\right) - f_\alpha\left(\vec{x}, t\right) = -\frac{1}{\tau}\left(f_\alpha\left(\vec{x}, t\right) - f_\alpha^{eq}\left(\vec{x}, t\right)\right) \quad . \tag{89}$$

Up to this point, no condition has been imposed on the relaxation time τ. In this work, $\tau = 1$ is assumed and this allows the derivation of the following simple relation,

$$f_\alpha\left(\vec{x} + \xi_\alpha \Delta t, \ t + \Delta t\right) = f_\alpha^{eq}\left(\vec{x}, t\right) \quad . \tag{90}$$

In fact, τ is arbitrary in the present method and it always appears together with ε. Therefore, using an appropriate normalization τ can logically treated as unity.

As suggested in Section 5.3, a splitting method is used to solve Eq. (30). In the present case, ρ = constant is specified and is not determined by f_α. Therefore, if there is a difference between the given ρ and the value of $\sum_\alpha f_\alpha$, then Eq. (84b) might not be satisfied and the following relation is obtained,

$$\sum_{\alpha}\left(f_{\alpha}-f_{\alpha}^{eq}\right)\begin{pmatrix}1\\ \xi_{\alpha x}\\ \xi_{\alpha y}\\ \dfrac{\xi_{\alpha x}^{2}+\xi_{\alpha y}^{2}}{2}\end{pmatrix}=\begin{pmatrix}\sum_{\alpha}f_{\alpha}-\rho\\ 0\\ 0\\ 0\end{pmatrix} \quad . \tag{91}$$

Consequently, multiplying Eq. (30) with respect to $\left[1,\ \xi,\ \left(\left|\xi\right|^{2}/2\right)\right]^{\mathrm{T}}$, taking summation over α, and invoking Eq. (86a-f) during numerical manipulation, the solution of Eq. (30) will lead to the satisfaction of,

$$\frac{\partial\sum_{\alpha}f_{\alpha}}{\partial t}+\frac{\partial\rho u}{\partial x}+\frac{\partial\rho v}{\partial y}=-\frac{\sum_{\alpha}f_{\alpha}-\rho}{\varepsilon} \quad , \tag{92a}$$

$$\frac{\partial\rho u}{\partial t}+\frac{\partial\rho u^{2}+p-\tau_{xx}}{\partial x}+\frac{\partial\rho uv-\tau_{xy}}{\partial y}=O\left(\varepsilon\right) \quad , \tag{92b}$$

$$\frac{\partial\rho v}{\partial t}+\frac{\partial\rho uv-\tau_{xy}}{\partial x}+\frac{\partial\rho v^{2}+p-\tau_{yy}}{\partial y}=O\left(\varepsilon\right) \quad , \tag{92c}$$

$$\frac{\partial}{\partial t}\left[\left(p-\frac{\tau_{xx}+\tau_{yy}}{2}\right)+\frac{1}{2}\rho\left(u^{2}+v^{2}\right)\right]+\frac{\sigma^{2}}{2}\left(\frac{\partial\rho u}{\partial x}+\frac{\partial\rho v}{\partial y}\right)=O\left(\varepsilon\right) \quad . \tag{92d}$$

The last equation is due to the following relations,

$$\sum_{\alpha=0}^{8}f_{\alpha}^{eq}\frac{\xi_{\alpha x}}{2}\left(\xi_{\alpha x}^{2}+\xi_{\alpha y}^{2}\right)=\frac{\sigma^{2}\rho u}{2} \quad , \tag{93a}$$

$$\sum_{\alpha=0}^{8}f_{\alpha}^{eq}\frac{\xi_{\alpha y}}{2}\left(\xi_{\alpha x}^{2}+\xi_{\alpha y}^{2}\right)=\frac{\sigma^{2}\rho v}{2} \quad , \tag{93b}$$

which are consequence of the choice of parameters in Eqs. (87a-f).

This set of equations, Eqs. (92a-c), is essentially the momentum equations of the incompressible N-S equations Eqs. (85a-c) correct to $O\left(\varepsilon\right)$ provided $\rho=\sum_{\alpha}f_{\alpha}=$ constant. It should be noted that Eq. (92a) is not the mass conservation equation. It will only become the mass conservation equation when ρ is identical to $\sum_{\alpha}f_{\alpha}$. Even if the difference between ρ and

$\sum_{\alpha} f_{\alpha}$ is very small, say of $O(\varepsilon)$, the right hand side of Eq. (92a) is still significant. Treating the evolution as an iteration process and solving the equations until a steady state has been reached, the temporal derivative in Eq. (92d) vanishes. At this point, mass conservation is satisfied, because the second term of Eq. (92d) is also zero.

The salient feature of the new LBM can be gleaned from an understanding of Eq. (92d). The first bracketed term in Eq. (92d) is the pseudo time rate of change of the "mechanical pressure" plus the "dynamic pressure", which can be denoted as the "total pressure head". The second bracketed term in Eq. (92d) is essentially the mass conservation equation. The fluctuation of this term can be used as a convergence criterion for the iteration. As steady state is reached, the artificial density approaches the actual density ρ and mass conservation is satisfied. For a large enough σ, the choice of which depends on numerical stability, iterations could be limited to a few, or perhaps no iteration is required for the satisfaction of Eq. (92a). Thus, the scheme becomes time-accurate [44] compared to the exact solution given in Schlichting [103] (see Stokes' 2nd problem solution in [103]). Taken together, Eq. (92a) and Eq. (92d) functions in a manner similar to the semi-implicit method proposed for pressure correction, i.e., the SIMPLE scheme put forward by Patankar & Spalding [104] for incompressible flow.

Therefore, incompressible flow simulation employing FDLBM with the new LBM integrated into the numerical scheme is equivalent to using SIMPLE to solve the N-S equations directly. In the process, the pressure field is determined without having to rely on the specification of a pressure density relation or a state equation for the fluid. Widely different laminar isothermal/thermal incompressible flow problems have been treated by this new LBM and they include back-step flow and driven cavity flow [45], thermal falling thin film flow, thermal Couette flow, natural convection in a 2-D cavity and in a cube (3-D) [51], and incompressible non-Newtonian fluid flow in a tube with internal constriction [52, 53]. The velocity lattice used in this series of simulations is D2Q9 for 2-D flows and D3Q15 for 3-D flows. No mass leakage has been detected at the boundary or in the flow. Therefore, improvements made to the conventional LBM correct its inadequacy and put the new LBM on a

firm footing as a simple and reliable numerical method to treat a wide variety of flow equations. Further, the simple velocity lattices serve their purpose very well; there is no advantage to use finer velocity lattices, such as D2Q13 for 2-D and D3Q19 for 3-D flows.

6.3 Compressibility

The new LBM is not just applicable to thermal incompressible or low Mach number flow where the state equation, $\rho = p / RT$, is simple and applicable. However, it is also valid for compressible flow where M is high enough to affect the state equation, or to fluid with complicated equation of state. As M increases, the dependence of ρ on p and T becomes more and more complicated, and the LBM's ability to resolve this dependence correctly needs clarification. As an illustration, consider a very complicated state equation in oceanographic flow [105]. In this case, the state equation is given by

$$\rho\left(T, S, p\right) = \rho\left(T, S, 0\right)\left[1 - p / K\left(T, S, p\right)\right]^{-1} \quad , \tag{94}$$

and the functional forms of $\rho\left(T, S, 0\right)$ and $K\left(T, S, p\right)$ accurate to 2nd order of p, T and S are:

$$\begin{aligned} \rho\left(T, S, 0\right) &= 999.842594 + 6.793952\times10^{-2}T + ... \\ &\quad - 1.6546\times10^{-6}T^2S^{1.5} + 4.83140\times10^{-4}S^2 \end{aligned} \quad , \tag{95a}$$

$$\begin{aligned} K\left(T, S, p\right) &= 19652.21 + 148.4206T - 2.327105T^2 + ... \\ &\quad - 2.0816\times10^{-3}Tp^2S + 9.1697\times10^{-10}T^2p^2S \end{aligned} \quad . \tag{95b}$$

Thus, fluid density ρ cannot be considered a constant; rather it is defined by the complex state equation. This problem is completely different from buoyant flow where the Bossinesq approximation can be invoked. Under this complex ρ condition, it is essential to satisfy mass conservation instead of volume conservation, such as in natural convection problem where Bossinesq approximation is still valid [51]. In the present case, the density thus calculated from Eqs. (95a) has to be iterated to a prescribed accuracy with that derived from the new LBM. Once ρ is known, it is used in the splitting method where mass conservation is assured after steady state has been reached in the pseudo-time. Therefore, the new FDLBM is equally applicable to

thermal incompressible flow where the simple state equation is no longer valid, and compressible flow with large M. Indeed, the FDLBM is able to capture shocks correctly in 1-D and 2-D flows up to $M = 1.961$ [43] and to resolve shock structure correctly up to $M = 1.55$ [47].

6.4 Complex Boundary Geometry

In all cases attempted under Sections 6.1 and 6.2, only wall boundary with simple geometry has been carried out. The reason for this choice of problems is to exploit the advantage that the lattice method works best with Cartesian coordinates. However, in order to test the general nature of the LBM, it is necessary to demonstrate the ease with which LBM can simulate flow problems with complex boundary geometry. As discuss in Section 5.4, the adoption of body-fitting coordinates is not the best option because the method is not time efficient and might not work well for elastic boundary and/or boundary with complex geometry.

An alternative is the IBM, an immersed boundary method proposed by Peskin [89]. The method can be made to work well using Cartesian grids in a Cartesian coordinate system. A force balance approach is used to define the boundary geometry and that leads to another LBE type equation for the additional force used to create the boundary. Formulations of an IBM scheme for steady and unsteady flow, respectively, have been detailed in Sections 5.4.2 and 5.4.3; they will not be repeated here. Consequently, Cartesian grids can again be used in the formulation of the LBM with a D2Q9 lattice adopted. In order to test the effectiveness of the LBM/IBM combined scheme, flow through a pipe with immersed restriction has been carried out [52, 53, 56]. Not all flow cases simulated are steady; some time dependent cases have also been attempted. Fluid considered is not limited to Newtonian, non-Newtonian fluid is also investigated. Results thus obtained are in agreement with other numerical and experimental studies [106, 107]. It should be bear in mind that all wall and free surface boundary conditions are given by the primitive variables at these boundaries, while the boundary values for the particle distribution function f_α are evaluated from the given macroscopic variables. As such, specifications of all boundary conditions are essentially the same as those given in a direct numerical simulation of the N-S (or Euler) equations; therefore, no additional complications,

other than solving an additional equation similar to an LBE representing the boundary force, are introduced in the new LBM/IBM approach [56]. Also, computational time is much reduced compared to using a body-fitting coordinates method.

Another salient feature of the methodology used to treat immersed boundary in any flow systems can be further explored. The key part of the methodology is the conversion of the boundary geometry into a force equation that can be treated as an additional body force in the lattice equation, i.e., Eq. (64). This means that any other body force such as buoyancy, salinity, magnetic, or electric can be similarly treated. Therefore, this feature could greatly broaden the application of the new LBM. Besides the above mentioned body forces, another possibility is an extension to turbulent flows, be it incompressible, compressible, stratified, etc. The Reynolds stresses in the Reynolds average N-S equations can be grouped together to form a turbulent force term in the Reynolds average N-S equations. This force could be considered as an additional force term in the LBE; therefore, it can be similarly treated as an additional body force term. Following the methodology outlined above, the Reynolds stresses would be included in the coefficients of the expansion used to represent the lattice force, such as Eq. (32). If, for example, a minimal form similar to that given in Eq. (77) is assumed, the additional force term can be determined. It then follows that any turbulence models, ranging from two-equation to Reynolds-stress models, could be used to calculate the Reynolds stresses that appear in the coefficients of Eq. (77) or some other similar equation. Again, only first order differential equations are added to the scheme; thus, they will not affect the simplicity and stability of the numerical scheme.

6.5 Aeroacoustics and Scattering

In any aeroacoustics computations, it is important that the numerical technique used is able to correctly and accurately resolve sound generation, its propagation, its interaction with disturbances on the path of propagation, and its interaction with boundary reflection. The difficulty lies in the fact that if the mean flow is normalized to be of order 1, it follows that the aerodynamics disturbance is of order 10^{-2}, the acoustics disturbance will be of order 10^{-4}, while the disturbances created by the interaction of the aerodynamics and acoustics disturbance will

become even smaller than the acoustics disturbances. If all these disturbances were to be resolved correctly, the accuracy of the numerical scheme will have to be at least of order 10^{-6} [57]. The disparity in scale accompanied by long propagating distance of acoustic waves lead to computational difficulties in aeroacoustics simulations. This is why direct aeroacoustics simulation (DAS) is still not the numerical technique of choice for aeroacoustics simulations because it is difficult to achieve a numerical simulation accurate to order 10^{-6} and beyond [57].

In developing the new LBM, the suggestion of Lele [57] to normalize the governing equations using acoustic scaling is adopted. With this approach, the numerical simulations of circular pulses in quiescent fluid could achieved an accuracy of at least 10^{-6}; thus allowing the new FDLBM to have the ability to replicate the propagation of these pulses accurately and correctly [42]. The success of this study encourages its extension to simulate acoustics scattering by a single zero circulation vortex [48]. These attempts proof to be quite successful, thus encouraging extension of the present new FDLBM to treat aero-thermoacoustics problems in an enclosure where interactions between aeroacoustics and thermo-aeroacoustics outgoing waves and reflected waves are present in the problem. Furthermore, the walls of the 2-D enclosure are impulsively heated in one vertical wall while it is impulsively cooled in the opposing vertical wall. This setup allows thermal scattering to be investigated simultaneously with interactions among acoustic waves, thermal waves and waves reflected from the solid boundaries. In anticipation that the disturbance waves due to these interactions are even weaker than the outgoing acoustics and reflective acoustics and thermo-aeroacoustics waves, the numerical technique has been improved to have an accuracy of 10^{-7} and 10^{-9} [54]. The LBM simulation results are compared with DAS results as well as known theoretical and numerical solutions. Good agreement has been obtained between the new FDLBM simulations and the DAS and theoretical results. From these studies, it can be seen that the new FDLBM simulations are able to correctly and accurately resolve the outgoing waves, the reflective waves and their interactions.

Since the gas kinetic scheme [24] is based on the conventional LBE, a comparison of this approach with DAS to simulate acoustic scattering by a single heat source could reveal the conventional LBE's potential, or lack thereof, to correctly mimic the real physics. A comparison of this simulation result with available theoretical solution is marginal at best [46, 55]. However, the comparisons between the new FDLBM results, theoretical analysis, and DAS simulations are encouraging because they show that the new FDLBM is just as good as the DAS. On the other hand, the LBE based gas kinetic scheme is not competitive with the new LBM. Besides, the new FDLBM can be extended to deal with complex boundary geometry by incorporating the IBM into the FDLBM, while it is not as easy to extend DAS to domains with complex boundaries, such as aeroacoustics in ducts with flexible walls.

6.6 Flow Uncertainty

Fluid dynamic problems with complicated systems, with uncertainty in the flow, and/or with complexities in initial and boundary conditions are of common occurrence. An example is the mechanism of atherosclerosis formation in arterial system where the initial and boundary conditions of the stenotic plaque are changing with time in an unpredictable manner. In the past, the traditional Monte Carlo (MC) method is employed to study problems similar to this. The MC method requires a tremendous amount of computational resource and is also time consuming. With the advent of computers and the development of efficient uncertainty quantification (UQ) methods, the more efficient Polynomial Chaos (PC) based UQ methods are applied to simulate complicated systems with incomplete knowledge and data, such as given in [108-111]. These PC methods are more efficient and less expansive than a MC method. Since then, methods such as the spectral stochastic finite element method (SSFEM) [111], and the stochastic projection method (SPM) [112] have been developed to focus on fluid dynamics and other flow problems. These stochastic numerical solvers are mostly based on finite difference or finite element numerical solver for the N-S equations. Since the FDLBM has proven to be an efficient numerical solver and is more stable, it would be very attractive to integrate the FDLBM

with either the SSFEM or the SPM to give a stochastic numerical solver to handle flow problems with uncertainty.

An attempt has been made to integrate the new FDLBM with either the SSFEM [111] or the SPM [112] to give a stochastic FDLBM (SFDLBM), and then applied the SFDLBM to simulate flow with one or more random excitation, or with one random process [49]. Interested readers could refer to [49, 56] for details on how to integrate the new FDLBM into a SSFEM or a SPM to give a SFDLBM. Newtonian and non-Newtonian fluid flow problems have been considered. Validation against MC solutions of channel/Couette flow, driven cavity flow, and sudden expansion flow have been carried out [49, 56]. In all these examples, the computational resource required for the SFDLBM is found to be much reduced compared to a MC method. Therefore, the new SFDLBM stochastic numerical solver could serve reliably as an attractive new alternative to other UQ methods in tackling flow problems with uncertainty.

6.7 Numerical Advantage

All numerical simulations attempted, incompressible and compressible flows, convection including natural and forced convection, aeroacoustics with/without scattering, and incompressible flow with uncertainty are found to be stable and can be carried out to a relatively higher order of accuracy to satisfy problem requirements, such as in aeroacoustics simulations where a 10^{-9} accuracy has been achieved with minimum numerical dissipation and without compromising numerical stability [54]. However, computation time could be much reduced if 10^{-7} accuracy is sufficient [54]. Having pointed out the advantage of being able to carry out the simulation to 10^{-7}, the next step is to compare computation time required. Since DAS essentially yields the same accuracy as the new FDLBM [55], it could serve as a benchmark case to compare DAS running time with that of the new FDLBM. In the thermoacoustics study reported in [54], both DAS and FDLBM have been used to simulate the thermoacoustic wave behavior inside a 2-D enclosure where the left wall temperature is twice that of the right wall. The case where the temperature is 1/3 higher has also been carried out. In both simulations, the number of grids in the x and y direction are maintained the same and so is the grid size. In the FDLBM

simulation, besides solving the first order LBE, an additional equation given by Eq. (15b), i.e. $\partial P'_{ij} / \partial x_j = 0$, needs to be solved. A Gauss-Seidel method is normally used to solve this equation for all cases tackled by the FDLBM. This solution takes up a major portion of the time used to solve the FDLBM. Carrying out the solutions to the same accuracy, a running time comparison between DAS and FDLBM for this problem is found to be approximately 2 to 1, i.e., the FDLBM is about 100% more efficient [54, 55]. Another advantage of the FDLBM is its ability to treat problems with complex boundaries through an incorporation of the IBM. The additional effort involves solving one more LBE to account for the additional body force. Thus, the extra time required would not be significant. The same is not necessarily true for DAS or DNS. Similar benefit could also be reaped in the calculation of flow with uncertainty using SFDLBM with SPM or SSFEM. In this later case, the comparison is made with a MC simulation of a driven cavity flow and a sudden expansion flow with two random excitations [49, 56]. The ability to integrate IBM into SFDLBM could give the SFDLBM added advantage, such as modeling blood flow in arteries with constrictions. Therefore, the additional need to solve $\partial P'_{ij} / \partial x_j = 0$ would not appear to be an impediment to the numerical solution.

6.8 Magnetohydrodynamics

The new LBM can treat buoyant flows with ease because the additional buoyant force in the momentum equation can be treated as an external body force; therefore, it can be handled by solving an additional Boltzmann type equation like that given in Eq. (64) with F_α given by Eq. (73). This approach was adopted in the treatment of buoyance and double diffusive effects in [50, 51]. Also, the approach can be extended to treat wall boundary with complex geometry using Cartesian grids much like the technique formulated for the immersed boundary method. This suggests that other external body force terms, such as that encountered in magnetohydrodynamics (MHD) can be similarly treated. The fluid dynamical aspects of MHD can be represented by an additional term in the Euler equation for inviscid flow or in the N-S equations for viscous flow. The additional term is the Lorentz force given by $\mathbf{J} \times \mathbf{B}$ where $\mathbf{J}$ is

the current density and $\mathbf{B}$ is the magnetic field [113]. For example, the modified Euler momentum equation can be written as:

$$\rho \frac{D\boldsymbol{u}}{Dt} = -\nabla p + \rho \boldsymbol{g} + \mathbf{J} \times \mathbf{B} \quad , \tag{96}$$

where D/Dt is the total derivative operating on $\boldsymbol{u}$, and $\boldsymbol{g}$ is the gravitational acceleration vector. In this form, the fluid is considered incompressible. The corresponding lattice Boltzmann equation is still given by Eq. (64) while the additional body force, $\mathbf{F}_{\mathrm{M}} = \mathbf{J} \times \mathbf{B}$, can be represented by Eq. (73). Thus, by following the procedure outlined in Section 4.2, the conditions that the external body forces have to satisfy and the coefficients in Eq. (73) can be determined.

Under the framework of the new LBM, fluid properties are treated as inputs to the FDLBM simulations. This renders the extension to non-Newtonian fluid flows quite simple. As long as the fluid model, such as viscosity, thermal conductivity, etc., are known, they can be specified as inputs and the simulations can be carried out with no other modifications. The formulation is equally applicable to steady and unsteady flows [45, 52, 53, 94, 98, 99]. Its extension to nanofluid flow can be accomplished by considering the nanofluid as a two-phase flow; therefore, in addition to the fluid phase, another equation governing the concentration of the nanofluid phase has to be solved [96, 97, 102]. This means that, besides the LBE for fluid momentum and energy, another LBE for the concentration of the nanofluid has to be solved simultaneously. Extension of the new LBM to simulate MHD, non-Newtonian fluid flow as well as nanofluid flow under the influence of a magnet field has been demonstrated by Kefayati [94-102] who employed the present approach to evaluate the magnetic field effect on Bingham fluid in an internal flow [94, 101], to study double diffusive MHD natural convection and entropy generation in an open cavity with power-law fluids [95, 96], to examine non-Newtonian nanofluid flow through porous media [97], and to understand mixed convection of a Bingham fluid in a driven cavity flow [100, 102] and also non-Newtonian nanofluid flow in an enclosure [98, 99].

The presence of a horizontal magnetic field introduces additional parameters into the flow; these are the Soret and Dufour parameters [95]. Furthermore, the fluids considered are either non-Newtonian nanofluid or simply non-Newtonian. This gives rise to additional equations for the fluids and an additional concentration transport equation for the nanofluid phase. Introduction of these additional parameters in the presence of a horizontal magnetic field greatly complicates the flow; even then, the new LBM handles the simulations without encountering numerical instability problems [e.g. 95, 98, 99]. These MHD simulations further demonstrate the robustness of the new LBM, and render the technique an attractive new to DNS calculations of incompressible and compressible fluid dynamics, hydrodynamics, and magnetohydrodynamics problems, and to DAS problems where high numerical accuracy is required for resolving acoustic disturbances correctly.

7. Conclusions

In view of these successes, the new LBM has proven to be a powerful numerical tool for simulating wide ranges of flow problems involving diatomic gases, different fluids, nanofluids, non-Newtonian fluids, and flows with additional body forces, e.g., buoyant force, magnetic force, electromagnetic force, etc. The FDLBM can be easily integrated with a projection method to deal with uncertainty in the flow or in changing boundary conditions. The new LBM/FDLBM with/without an IBM implementation, and/or with/without an SSFEM/SPM integration is truly a versatile and robust numerical tool. Altogether, progress in the development of this new LBM provides ample evidence to support the claim of versatility, generality, and robustness of the new LBM/FDLBM. In summary, the new LBM improves the capability of conventional LBM. Therefore, advantages of the new LBM can be briefly summarized below:

i. A continuous $\boldsymbol{f}^{eq}$ valid for diatomic gas has been derived for 3-D flows. This modified Maxwellian distribution function approaches the Maxwellian limit correctly for a monatomic gas.

ii. The expansion for the lattice $\boldsymbol{f}_{\alpha}^{eq}$, is expressed in terms of the particle velocity $\boldsymbol{\xi}$ alone; hence, the $M << 1$ assumption inherent in conventional LBM is no longer necessary.

iii. The new LBM/FDLBM is able to simulate the pressure field in an incompressible flow without having to stipulate a pressure density relation or a state equation for the fluid. Further, the calculated divergence of the velocity field is identically zero.

iv. The coefficients in the lattice f_α^{eq} expansion are determined by requiring the exact recovery of the governing flow equations, be they Euler, N-S or the magnetohydrodynamics equations. As a result, 2nd order terms such as dissipation, diffusion, etc. are present only in the coefficients of this expansion; they are not present in the MBE. Their absence in the LBM gives rise to enhance numerical stability in the FDLBM solution.

v. In all cases simulated, a D2Q9 and a D3Q15 lattice model is found to be sufficient for 2-D and 3-D flows, respectively.

vi. The same relaxation time τ in the LBE is valid for all simulations attempted; i.e., τ is not problem dependent. In all flow cases attempted, multiple τ specifications are not necessary.

vii. For the case where only one lattice f_α^{eq} is used to recover the full set of N-S equations using a D2Q9 lattice, 5 coefficients in the expansion for f_α^{eq} need to be set to zero. This set is valid for all flow cases belonging to this family of flow.

viii. In the absence of an energy equation, the full set of N-S equations can also be recovered using a D2Q9 lattice; however, 7 coefficients in the expansion for f_α^{eq} have to be set to zero. Again, this set is valid for all flow cases belonging to this family of flows.

ix. The FDLBM based on the new LBM is equally applicable to thermal incompressible flow and compressible flow with high *M*.

x. All initial and boundary conditions are given by macroscopic variables, while the values of f^{eq} at these boundary locations are evaluated from the macroscopic variable specifications. Therefore, the no-slip condition at the wall can be satisfied identically. Also, mass leakage in the flow due to the $M << 1$ condition is completely eliminated.

xi. Using the LBE to simulate hydrodynamic flows is entirely justified by demonstrating that there is complete equivalence between the present LBE and the LBE type equation obtained through the use of a discrete flux scheme to derive the N-S equations. Therefore, this equivalence permits the use of the new LBM and FDLBM to simulate fluid flows besides those given by diatomic gases.

xii. The new FDLBM has been integrated into either an SSFEM or an SPM to simulate flows with uncertainty successfully. The resulting scheme can handle flows with one or more random excitations and/or with one random process.

xiii. Integrating the IBM into the new LBM could enable the combined LBM/IBM with Cartesian grids to treat flow problems where wall boundaries are defined by complex geometry.

xiv. The additional body force concept inherent in the IBM can be extended to treat flows with other external body forces, such as, buoyancy, salinity, magnetic, electric, and even turbulent flows. Although the method involves solving more than one LBE, it would not add complexity to the numerical solution of the LBE.

xv. All equations involved in the new LBM formulation are first order, second and higher order terms are not present. Thus, employing finite difference technique to solve the first order equations could yield sufficiently high numerical accuracy to allow acoustics waves to be resolved correctly in any simulations of aeroacoustics waves interaction with thermo-aeroacoustics waves.

xvi. Fluid properties are inputs to the new LBM. Consequently, non-Newtonian fluids such as Bingham fluid, blood, and nanofluids can be easily handled as long as their properties are known. In some cases, simultaneous solution of additional LBE's is necessary.

xvii. Thus improved, the new LBM with/without IBM becomes a viable numerical technique for solving the governing equations of any flow dynamics problems. As a numerical technique, the present LBM/IBM has its advantages because all equations solved are first order and can be easily handled with minimum numerical errors. Further, parallel programming could be used to advantage in processing the LBM/IBM equations.

Acknowledgements

The first author is deeply appreciative of the Department of Mechanical Engineering, The Hong Kong Polytechnic University, especially its Heads, Professors Cheng Li and Shi San Qiang, for inviting him to visit the Department every year since 2009 to serve as advisor and to continue his collaboration with staff and students. The support leads to multiple publications on a new LBM/FDLBM, and culminates in this review on the progress in the development of the new LBM/FDLBM and its related validation studies carried out in the past decade. The 2nd author gratefully acknowledges the support given him by the Central Research Grant of The Hong Kong Polytechnic University under Grant Nos. G-YL56, G-YN78, and G-YBGF.

References

[1] Succi S. *Lattice Boltzmann Equation for Fluid Dynamics and Beyond*. Oxford University Press, Oxford, England, U. K., 2001.

[2] Yu D, Mei R, Luo L-S, Shyy W. Viscous Flow Computations with the Method of Lattice Boltzmann Equation. Progress in Aerospace Sciences 2003; 39: 329-67.

[3] Chen S, Doolen G-D. Lattice Boltzmann Method for Fluid Flows. Annual Review of Fluid Mechanics 1998; 30: 329-64.

[4] Harris S. *Introduction to the Theory of the Boltzmann Equation*. Dover, New York, 1999; Chapter 1-4.

[5] Wolf-Gladrow D-A. *Lattice-Gas Cellular Automata and Lattice Boltzmann Models An Introduction*. Springer, New York, 2000, Chap. 5.

[6] Bhatnagar P-L, Gross E-P, Krook M. A Model for Collision Processes in Gases: I. Small Amplitude Processes in Charged and Neutral One-Component Systems. Physical Review 1954; 94(3): 511-25.

[7] Chapman, S. and Cowling, T-G. *The Mathematical Theory of Non-Uniform Gases*. 3rd Ed. Cambridge University Press, 1990.

[8] Chen H, Chen S, Matthaeus W-H. Recovery of the Navier-Stokes Equations Using a Lattice-Gas Boltzmann Method. Physical Review A 1992; 45(8): R5339-R5342.

[9] Qian Y-H, d'Humieres D, Lallemand P. Lattice BGK Models for Navier-Stokes Equation. Europhysics Letters 1992; 17(6): 479-84.

[10] Frisch U, Hasslacher B, Pomeau Y. Lattice-Gas Automata for the Navier-Stokes Equation. Physical Review Letters 1986; 56: 1505–08.

[11] Pohl T, Deserno F, Thurey N, Rude U, Lammers P, Wellein G, Zeiser T. Performance evaluation of parallel large-scale lattice Boltzmann applications on three supercomputing architectures Supercomputing, 2004. Proceedings of the ACM/IEEE SC2004 Conference, 21-21

[12] Wellein G, Zeiser T, Hager G, Donath S. On the Single Processor Performance for Simple Lattice Boltzmann Kernels. Comput and Fluids 2006; 35: 910-919.

[13] Frisch U, d'Humieres D, Hasslacher B, Lallemand P, Pomeau Y, Rivet J-P. Lattice Gas Hydrodynamics in Two and Three Dimensions. Complex Systems 1987; 1(4): 649-707.

[14] Prendergast K-H, Xu K. Numerical Hydrodynamics from Gas-Kinetic Theory. Journal of Computational Physics 1993; 109(1): 53-66.

[15] Xu K, Prendergast, K-H. Numerical Navier-Stokes solution from gas-kinetic theory," Journal of Computational Physics 1994; 114(1): 9-17.

[16] Xu K. A Gas-Kinetic BGK Scheme for the Navier-Stokes Equations and Its Connection with Artificial Dissipation and Godunov Method. Journal of Computational Physics 2001; 171(1): 289-335.

[17] Wang Chang C-S, Uhlenbeck G-E, deBoer J. *Studies in Statistical Mechanics*, Vol. 2 (Editors: deBoer J, Uhlenbeck G-E.); Wiley, New York, 1964.

[18] Morse T-F. Kinetic model for gases with internal degrees of freedom. Physics of Fluids 1964; 7(2): 159-169.

[19] Holway L-H. New statistical models for kinetic theory: methods of construction. Physics of Fluids 1966; 9(9): 1658-1673.

[20] He X, Luo L-S. Theory of the Lattice Boltzmann Method: From the Boltzmann Equation to the Lattice Boltzmann Equation. Physical Review E 1997; 56(6): 6811-17.

[21] Tsutahara M, Kataoka T, Takada N, Kang H-K, Kurita M. Simulations of compressible flows by using the lattice Boltzmann and the finite difference lattice Boltzmann method. Computational Fluid Dynamics Journal 2002; 11(1): 486-493.

[22] Zou Q, Hou S, Chen S, Doolen G-D. An Improved Incompressible Lattice Boltzmann Model for Time-Independent Flows. Journal of Statistical Physics 1995; 81(1/2): 35-48.

[23] Guo Z, Shi B, Wang N. Lattice BGK Model for Incompressible Navier-Stokes Equation. Journal of Computational Physics 2000; 165: 288-306.

[24] Xu K, He X. Lattice Boltzmann Method and Gas-Kinetic BGK Scheme in the Low-Mach Number Viscous Flow Simulations. Journal of Computational Physics 2003; 190: 100-17.

[25] Krüger T, Varnik F, Raabe D. Shear stress in lattice Boltzmann simulations. Physical Review E 2009; 79(4): 46704.

[26] d'Humieres D, Lallemand P. Numerical simulations of hydrodynamics with lattice gas automata in two dimensions. Complex Systems 1987; 1(4): 599-632.

[27] Mei R, Luo L-S, Shyy W. An accurate curved boundary treatment in the lattice Boltzmann method. Journal of Computational Physics 1999; 155(2): 307-30.

[28] Verberg R, Ladd A-J-C. Lattice-Boltzmann model with sub-grid-scale boundary conditions. Physical Review Letters 2000; 84(10): 2148-51.

[29] Rohde M, Kandhai D, Derksen J-J, Van den Akker H-E-A. Improved bounce-back methods for no-slip walls in lattice-Boltzmann schemes: Theory and simulations. Physical Review E 2003; 67(6): 66703.

[30] Chun B, Ladd A-J-C. Interpolated boundary condition for lattice Boltzmann simulations of flows in narrow gaps. Physical Review E 2007; 75(6): 66705.

[31] Bao J, Yuan P, Schaefer L. A mass conserving boundary condition for the lattice Boltzmann equation method. Journal of Computational Physics 2008; 227(18): 8472-87.

[32] Filippova O, Hanel D. Grid refinement for lattice-BGK models. Journal of Computational Physics 1998; 147(1): 219-28.

[33] Chen S-S, Bao Z, Liu J, Li J, Yi C, Zheng C. A heuristic curved-boundary treatment in lattice Boltzmann method. Europhysics Letters (EPL) 2010; 92(5): 54003.

[34] Coupanec E-L, Verschaeve J-C-G. A mass conserving boundary condition for the lattice Boltzmann method for tangentially moving walls. Mathematics and Computers in Simulation 2011; 81(12): 2632-45.

[35] Chen S, Tolke J, Geller S, Krafczyk M. Lattice Boltzmann model for incompressible axisymmetric flows. Phys Rev E 2008; 78: 046703.

[36] Li X-M, Leung R-C-K, So R-M-C. One-step aeroacoustics simulation using lattice Boltzmann method. AIAA Journal 2006; 44(1): 78-89.

[37] Li X-M, So R-M-C, Leung R-C-K. Propagation speed, internal energy and direct aeroacoustics simulation using lattice Boltzmann method. AIAA Journal 2006; 44(12): 2896-2903.

[38] Leung R-C-K, Kam E-W-S, So R-M-C. Recovery of the transport coefficients in the Navier-Stokes equations from the modeled Boltzmann equation. AIAA Journal 2007; 45(4): 737-739.

[39] Kam E-W-S, So R-M-C, Leung R-C-K. Lattice Boltzmann method simulation of aeroacoustics and nonreflecting boundary conditions. AIAA Journal 2007; 45(7): 1703-12.

[40] Kam E-W-S, Leung R-C-K, So R-M-C, Li X-M. A lattice Boltzmann method for computation of aeroacoustics interaction. International Journal of Modern Physics C 2007; 18(4): 463-472.

[41] Philippi P-C, Hegele Jr L-A, dos Santos L-O-E, Surmas R. From the continuous to the lattice Boltzmann equation: the discretization problem and thermal models. Physical Review E 2006; 73: 056702.

[42] Fu S-C, So R-M-C, Leung R-C-K. Modeled Boltzmann Equation and Its Application to Direct Aeroacoustics Simulation. AIAA Journal 2008; 46(7): 1651-62.

[43] So R-M-C, Leung R-C-K, Fu S-C. Modeled Boltzmann equation and its application to shock capturing simulation. AIAA Journal 2008; 46(12): 3038-48.

[44] Fu S-C, So R-M-C. Modeled Lattice Boltzmann equation and the constant density assumption. AIAA Journal 2009; 47(12): 3038-42.

[45] Fu S-C, Leung W-W-F, So R-M-C. A lattice Boltzmann based numerical scheme for microchannel flows. Journal of Fluids Engineering 2009; 131(August): 081401.

[46] Kam E-W-S, So R-M-C, Leung R-C-K. Acoustic scattering by a localized thermal disturbance. AIAA Journal 2009; 47(9): 2039-52.

[47] So R-M-C, Fu S-C, Leung R-C-K. Finite difference lattice Boltzmann method for compressible thermal fluids. AIAA Journal 2010; 48(6): 1059-71.

[48] Kam E-W-S, So R-M-C, Fu S-C, Leung R-C-K. Finite difference lattice Boltzmann method applied to acoustic-scattering problems. AIAA Journal 2010; 48(2): 354-71.

[49] Fu S-C, So R-M-C, Leung W-W-F. Stochastic finite-difference lattice Boltzmann method for steady incompressible viscous flows. Journal of Computational Physics 2010; 229: 6084-6103.

[50] Fu S-C, So R-M-C, Leung W-W-F. A discrete flux scheme for aerodynamic and hydrodynamic flows. Communications in Computational Physics 2011; 9(5): 1257-83.

[51] Fu S-C, So R-M-C, Leung W-W-F. Linearized Boltzmann-type equation based finite difference method for thermal incompressible flow. Computers & Fluids 2012; 69: 67-80.

[52] Fu S-C, Leung W-W-F, So R-M-C. A Lattice Boltzmann and immersed boundary scheme for model blood flow in constricted Pipes: Part 1 - steady flow. Communications in Computational Physics 2013; 14(1): 126-52.

[53] Fu S-C, So R-M-C, Leung W-W-F. A lattice Boltzmann and immersed boundary scheme for model blood flow in constricted pipes: Part 2 - pulsatile flow. Communications in Computational Physics 2013; 14(1): 153-73.

[54] Kam E-W-S, So R-M-C, Fu S-C. One-step simulation of thermoacoustic waves in two-dimensional enclosures. Computers and Fluids 2016; 140: 170-88.

[55] Kam E-W-S, 2007. Prediction of Noise Generation by using Modeled Boltzmann Equation (BE). PhD Thesis, Department of Mechanical Engineering, The Hong Kong Polytechnic University, Hung Hom, Hong Kong.

[56] Fu S-C, 2011. Numerical Simulation of Blood Flow in Stenotic Arteries. PhD Thesis, Department of Mechanical Engineering, The Hong Kong Polytechnic University, Hung Hom, Hong Kong.

[57] Lele S-K. Direct numerical simulations of compressible turbulent flows: fundamentals and application. *Transition, Turbulence and Combustion Modeling* (Editors: Hanifi A, Alfredsson P-H, Johansson A-V, Hennigson D-S.), Kluwer Academic Publishers, London, UK; Chapter 7: 424-429, 1998

[58] Shen X, He X. Discretization of the velocity space in the solution of the Boltzmann equation. Physical Review Letters 1998; 80(1): 65-68.

[59] Kataoka T, Tsutahara M. Lattice Boltzmann model for the compressible Navier-Stokes equations with flexible specific-heat ratio. Physical Review E 2004; 69(3): 035701.

[60] Kataoka T, Tsutahara M. Lattice Boltzmann model for the compressible Euler equations. Physical Review E 2004; 69(5): 056702.

[61] Watari M. Lattice Boltzmann method with arbitrary specific heat ratio applicable to supersonic flow simulations. Physica A: Statistical Mechanics and Its Applications 2007; 382(2): 502-22.

[62] Rowlinson J-S, Widom B. *Molecular Theory of Capillarity*, Clarendon Press, University of Oxford, Oxford, UK, 1982.

[63] Shan X, Chen H. Lattice Boltzmann Model for Simulating Flows with Multiple Phases and Components. Physical Review E 1993; 47: 1815-1820.

[64] Shan X, Chen H. Simulation of Nonideal Gases and Liquid-Gas Phase Transitions by the Lattice Boltzmann Equation. Physical Review E 1994; 49: 2941-2948.

[65] Swift M-R, Osborn W-R, Yeomans J-M. Lattice Boltzmann Simulation of Nonideal Fluids. Physical Review Letters 1995; 75: 830-834.

[66] Chin J, Boek E-S, Coveney P-V. Lattice Boltzmann Simulation of the Flow of Binary Immiscible Fluids with Different Viscosities Using the Shan-Chen Microscopic Interaction Model. Philosophical Transactions of the Royal Society London A 2002; 360: 547-558.

[67] Shan X, Yuan X-F, Chen H. Kinetic Theory Representation of Hydrodynamics: A Way Beyond the Navier-Stokes Equation. Journal of Fluid Mechanics 2006; 550: 413-441.

[68] Phillips O-M. On Flows Induced by Diffusion in a Stably Stratified Fluid. Deep-Sea Research 1970; 17: 435-443.

[69] Chen C-F. Double-Diffusive Convection in an Inclined Slot. Journal of Fluid Mechanics 1975; 72: 721-729.

[70] Fernando H-J-S. The Formation of a Layered Structure when a Stable Salinity Gradient is Heated from Below. Journal of Fluid Mechanics 1987; 182: 525-541.

[71] Guo Z, Shi B, Zheng C. A Coupled Lattice BGK Model for the Boussinesq Equations. International Journal for Numerical Methods in Fluids 2002; 39: 325-342.

[72] Li Q, He Y-L, Wang Y, Tao, W-Q. Coupled Double-Distribution-Function Lattice Boltzmann Method for the Compressible Navier-Stokes Equations. Physical Review E 2007; 76: 056705.

[73] Mittal R, Iaccarino G. Immersed Boundary Methods. Annual Review of Fluid Mechanics 2005; 37: 239-261.

[74] Sterling, J-D, Chen, S. Stability Analysis of Lattice Boltzmann Methods. Journal of Computational Physics 1996; 123(1): 196–206.

[75] He X, Luo L-S. Lattice Boltzmann Model for the Incompressible Navier-Stokes Equation. Journal of Statistical Physics 1997; 88(3/4): 927-944.

[76] Strang G. On the Construction and Comparison of Difference Schemes. SIAM Journal of Numerical Analysis 1968; 5(3): 506-517.

[77] Toro E-F. *Riemann Solvers and Numerical Methods for Fluid Dynamics: A Practical Introduction*, 2nd ed., Springer-Verlag Berlin Heidelberg, New York, 1999; Chapter 15.

[78] Wang D, Bernsdorf J. Lattice Boltzmann Simulation of Steady Non-Newtonian Blood Flow in a 3D Generic Stenosis Case. Computer and Mathematics with Applications 2009; 58(5): 1030-1034.

[79] Chen C, Chen H, Freed D, Shock R, Staroselsky I, Zhang R, Coşkun A-Ü, Stone P-H, Feldman C-L. Simulation of Blood Flow Using Extended Boltzmann Kinetic Approach. Physica A 2006; 362: 174-181.

[80] Krafczyk, M., Cerrolzaz, M., Schulz, M. and Rank, E., 1998, "Analysis of 3D Transient Blood Flow Passing Through an Artificial Aortic Valve by Lattice-Boltzmann Methods," Journal of Biomechanics, **31**(5), pp. 453-462.

[81] Boyd, J., Buick, J. M., Cosgrove, J. A., and Stansell, P., 2004, "Application of the Lattice Boltzmann Method to Arterial Flow Simulation: Investigation of Boundary Conditions for Complex Arterial Geometries," Australasian Physical & Engineering Sciences in Medicine, **27**(4), pp. 207-212.

[82] Ouared, R., Chopard, B., Stahl, B., Rüfenacht, D. A., Yilmaz, H., and Courbebaisse, G., 2008, "Thrombosis Modelling in Intracranial Aneurysms: A Lattice Boltzmann Numerical Algorithm," Computer Physics Communications, **179**(1-3), pp. 128-131.

[83] Bernsdorf, J., Harrison, S. E., Smith, S. M., Lawford, P. V., and Hose, D. R., 2008, "Applying the Lattice Boltzmann Technique to Biofluids: A Novel Approach to Simulate Blood Coagulation," Computers and Mathematics with Applications, **55**(7), pp. 1408-1414.

[84] Lim C-Y, Shu C, Niu X-D, Chew Y-T. Application of Lattice Boltzmann Method to Simulate Microchannel Flows. Physics of Fluids 2002; 14(7): 2299-2308.

[85] Feng Z-G, Michaelides E-E. The Immersed Boundary-lattice Boltzmann Method for Solving Fluid-particles Interaction Problems. Journal of Computational Physics 2004; 195(2): 602-628.

[86] Feng, Z-G, Michaelides E-E. Proteus: a Direct Forcing Method in the Simulations of Particulate Flows. Journal of Computational Physics 2005; 202(1): 20-51.

[87] Niu, X-D, Shu C, Chew Y-T, Peng Y. A Momentum Exchange-based Immersed Boundary-lattice Boltzmann Method for Simulating Incompressible Viscous Flows. Physics Letters A 2006; 354: 173-182.

[88] Strack O-E, Cook B-K. Three-Dimensional Immersed Boundary Conditions for Moving Solids in the Lattice-Boltzmann Method. International Journal for Numerical Methods in Fluids 2007; 55: 103-125.

[89] Peskin C-S. Numerical Analysis of Blood Flow in the Heart. Journal of Computational Physics 1977; 25(3): 220–252.

[90] Lai M-C, Peskin C-S. An Immersed Boundary Method with Formal Second-Order Accuracy and Reduced Numerical Viscosity. Journal of Computational Physics 2000; 160(2): 705-719.

[91] Shu C, Liu N, Chew Y-T. A Novel Immersed Boundary Velocity Correction-Lattice Boltzmann Method and Its application to Simulate Flow Past a Circular Cylinder. Journal of Computational Physics 2007; 226: 1607-1622.

[92] Beyer R-P, Leveque R-J. Analysis of a One-Dimensional Model for the Immersed Boundary Method. SIAM Journal on Numerical Analysis 1992; 29(2): 332-364.

[93] Tannehill J-C, Anderson D-A, Pletcher R-H. *Computational Fluid Mechanics and Heat Transfer*, 2nd ed., Taylor & Francis, Washington D.C. 1997; Chapter 9: 649-776.

[94] Kefayati G-H-R. Mesoscopic simulation of magnetic field effect on Bingham fluid in an internal flow. Journal of Taiwan Institute of Chemical Engineers 2015; 54: 1-10

[95] Kefayati G-H-R. Simulation of double diffusive MHD (magnetohydrodynamic) natural convection and entropy generation in an open cavity filled with power-law fluids in the presence of Soret and Dufour effects (Part I: Study of fluid flow, heat and mass transfer). Energy 2016; 107: 889-916.

[96] Kefayati G-H-R, Nor Azwadi Che Sidik Simulation of natural convection and entropy generation of non-Newtonian nanofluid in an inclined cavity using Buongiorno's mathematical model (Part II: Entropy generation). Powder Technology 2017; 305: 679-703.

[97] Kefayati G-H-R. Heat transfer and entropy generation of natural convection on non-Newtonian nanofluids in a porous cavity. Powder Technology 2016; 299: 127-149.

[98] Kefayati G-H-R. Mixed convection of non-Newtonian nanofluid in an enclosure using Buongiorno's mathematical model. International Journal of Heat and Mass Transfer 2017; 108: 1481-1500.

[99] Kefayati G-H-R. Simulation of natural convection and entropy generation of non-Newtonian nanofluid in a porous cavity using Buongiorno's mathematical model. International Journal of Heat and Mass Transfer 2017; 112: 709-744.

[100] Kefayati G-H-R, Huilgol R-R. Lattice Boltzmann method for simulation of mixed convection of a Bingham fluid in a lid-driven cavity. International Journal of Heat and Mass Transfer 2016; 103: 725-743.

[101] Kefayati G-H-R, Huilgol R-R. Lattice Boltzmann method for the simulation of the steady flow of a Bingham fluid in a pipe of square cross-section. European Journal of Mechanics B/Fluids 2017; 65: 412-422.

[102] Kefayati G-H-R, Tang H. Simulation of natural convection and entropy generation of MHD non-Newtonian nanofluid in a cavity using Buongiorno's mathematical model. International Journal on Hydrogen Energy 2017; 42: 17284-17327.

[103] Schlichting H. *Boundary Layer Theory*, (Translated by Kestin J.) McGraw-Hill Book Co., New York, 4th Edition, 1960; pp. 75.

[104] Patankar S-V, Spalding D-B. A Calculation Procedure for Heat, Mass and Momentum Transfer in Three-Dimensional Parabolic Flows. International Journal of Heat and Mass Transfer 1972; 15: 1787-1806.

[105] Kantha L-H, Clayson C-A. Small Scale Processes in Geophysical Fluid Flows. Academic Press, Cambridge, MA 2000.

[106] Deshpande M-D, Giddens D-P, Mabon R-F. Steady Laminar Flow through Modeled Vascular Stenoses. Journal of Biomechanics 1976; 9(4): 165-74.

[107] Young D, Tsai F. Flow Characteristics in Models of Arterial Stenoses – I Steady Flow. Journal of Biomechanics 1973; 6(4): 395-402.

[108] Wiener S. The Homogeneous Chaos. American Journal of Mathematics 1938; 60: 897-936.

[109] Cameron R, Martin W. The Orthogonal Development of Nonlinear Functionals in Series of Fourier-Hermite Functional. Annals of Mathematics 1947; 48: 385-392.

[110] Chorin A. Hermite Expansions in Monte-Carlo Computation. Journal of Computational Physics 1971; 8: 472-482.

[111] Ghanem R-G, Spanos P-D. *Stochastic Finite Elements: A Spectral Approach*, Springer-Verlag, Berlin/New York, 1991.

[112] Le Maitre O-P, Knio O-M, Najm H-N, Ghanem R-G. A Stochastic Projection Method for Fluid Flow I: Basic Formulation. Journal of Computational Physics 2001; 173: 481-511.

[113] Davidson P-A. An Introduction to Magnetohydrodynamics (Cambridge Texts in Applied Mathematics), Cambridge University Press, Cambridge, UK 2001; ISBN: 0 521 791499.

[114] Ghia U, Ghia K-N, Shin C-T. High-Re Solutions for Incompressible Flow Using the Navier-Stokes Equations and a Multigrid Method. Journal of Computational Physics 1982; 48: 387-411.

[115] Sod G-A. A Survey of Several Finite Difference Methods for Systems of Nonlinear Hyperbolic Conservation Laws. Journal of Computational Physics 1978; 27(1): 1-31.

[116] Harten A. High Resolution Schemes for Hyperbolic Conservation Laws. Journal of Computational Physics 1983; 49(3): 357-93.

[117] Lax P-D, Liu X-D. Solution of Two-Dimensional Riemann Problems of Gas Dynamics by Positive Schemes. SIAM Journal on Scientific Computing 1998; 19(2): 319-340.

[118] Alsmeyer H. Density Profiles in Argon and Nitrogen Shock Waves Measured by the Absorption of an Electron Beam. Journal of Fluid Mechanics 1976; 74: 497-513.

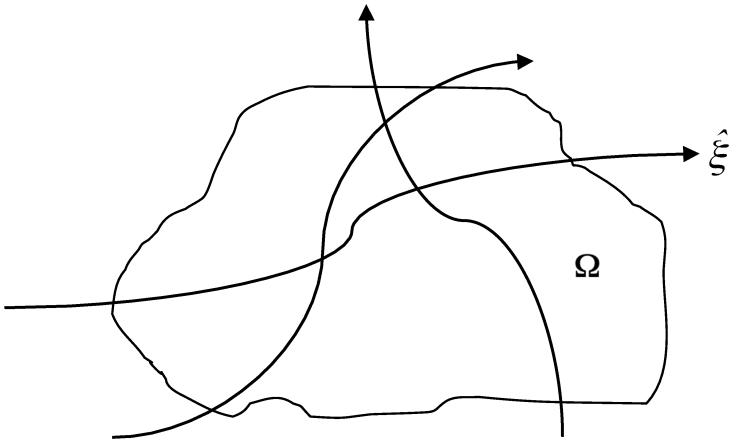

Figure 1. Pictorial representation of the control volume $\hat{\Omega}$ in the flow field.

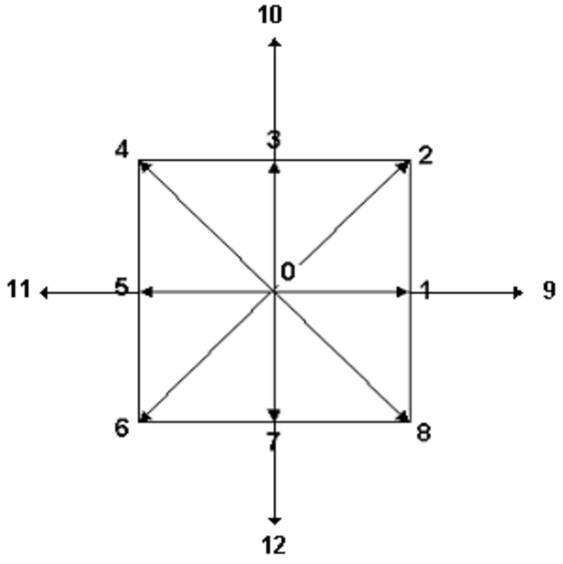

Figure 2a Definition of the D2Q13 lattice velocity model.

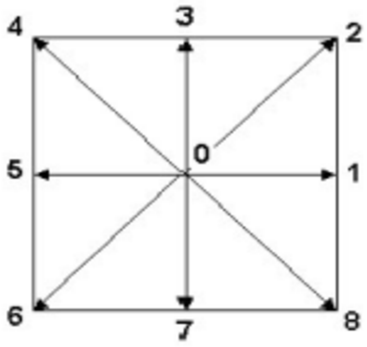

Figure 2b D2Q9 lattice velocity model.

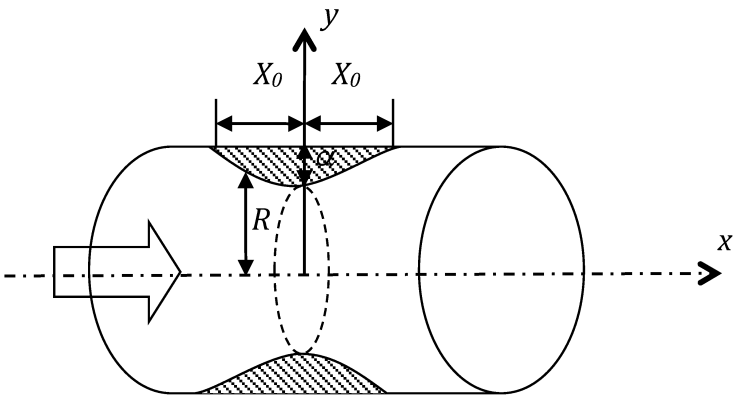

Figure 3. Schematic diagram of pipe flow with constriction.

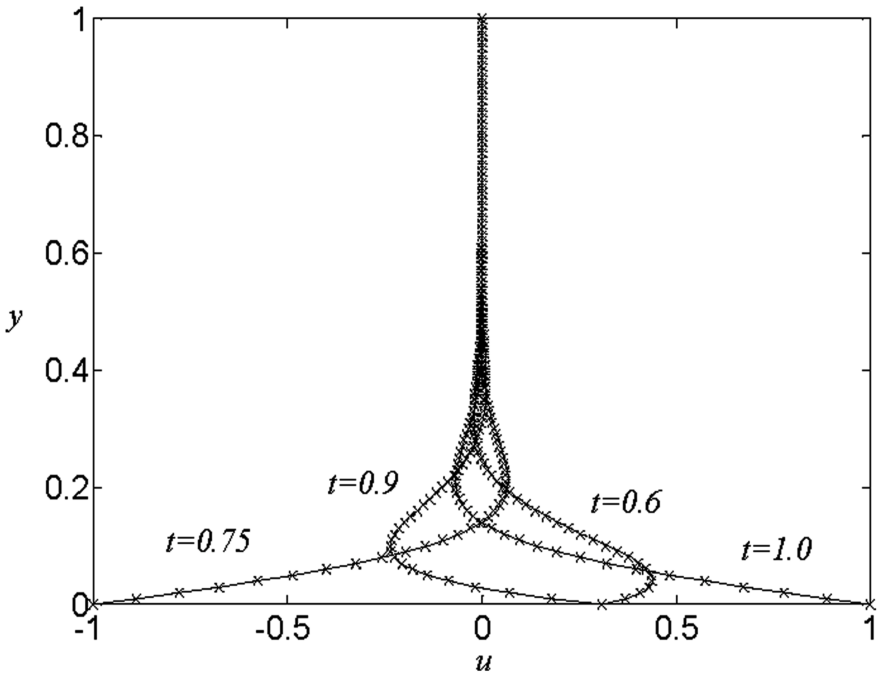

Figure 4 Distribution of u-velocity along the y-axis at various time: solid line represents exact solution [103]; "x" represents FDLBM results.

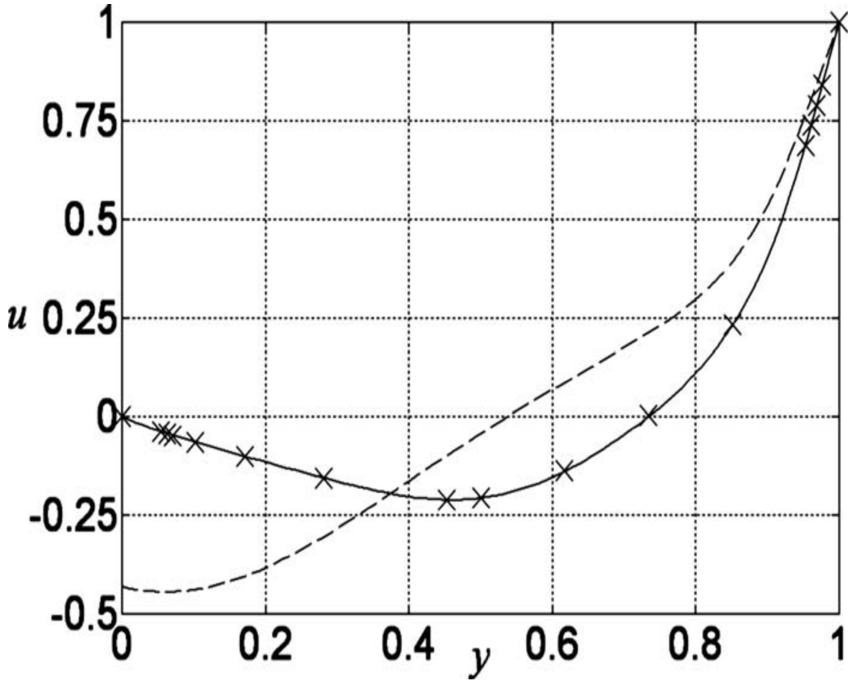

Figure 5 Horizontal velocity, u, of driven cavity flow along y at $x = 0.5$, $Re = 100$: '—', FDLBM with no slip; 'x', Ghia et al. [114] result. '- - -', FDLBM with slip wall.

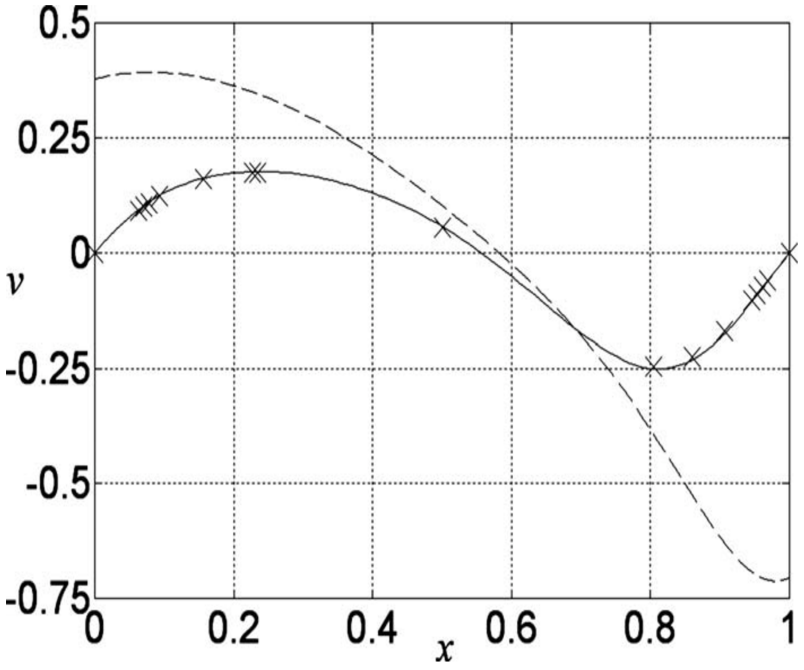

Figure 6 Vertical velocity, v, of driven cavity flow along x at $y = 0.5$, $Re = 100$: solid line '—', FDLBM with no slip; symbol 'x', Ghia et al. [114] result. Dash line '- - -', FDLBM with slip wall.

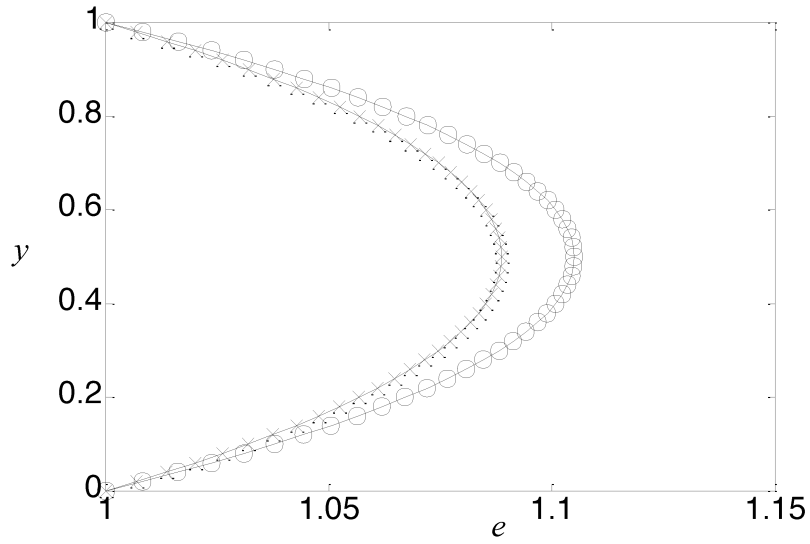

Figure 7 Internal energy distribution of thermal Couette flow for different Pr; solid line '—' is the theoretical solution [51]; Symbols 'x' and 'o' are FDLBM solutions of Pr = 0.71 and 0.84, respectively.

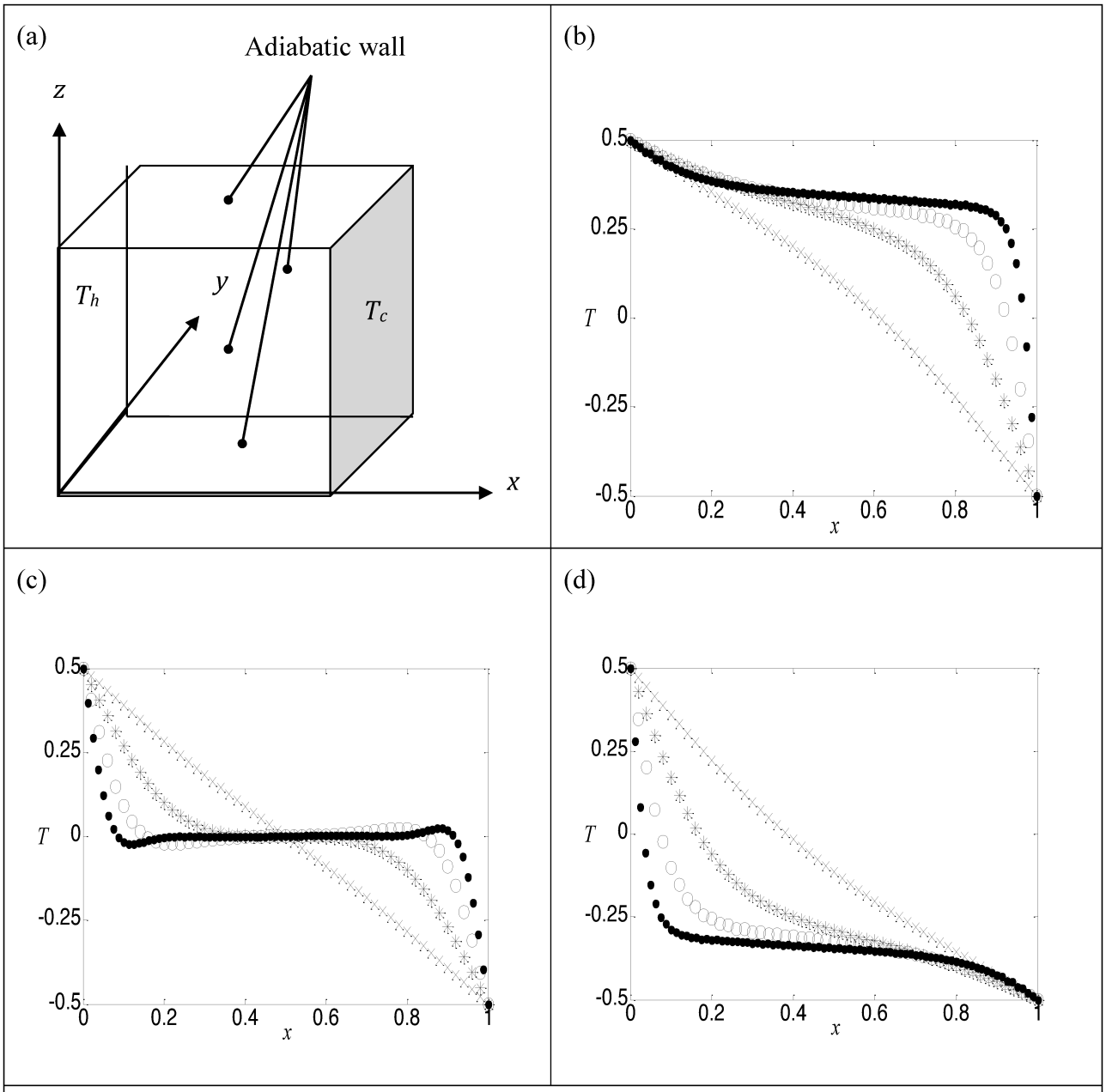

Figure 8 Temperature distribution along the x-direction of natural convection in a cube (a): at (b) $z = 1$, (c) $z = 0.5$ and (d) $z = 0$, for $y = 0.5$, $Pr = 0.71$ and different Ra. Symbols 'x', '*', 'o', and '•' are FDLBM solutions for $Ra = 10^3$, 10^4, 10^5, and 10^6, respectively.

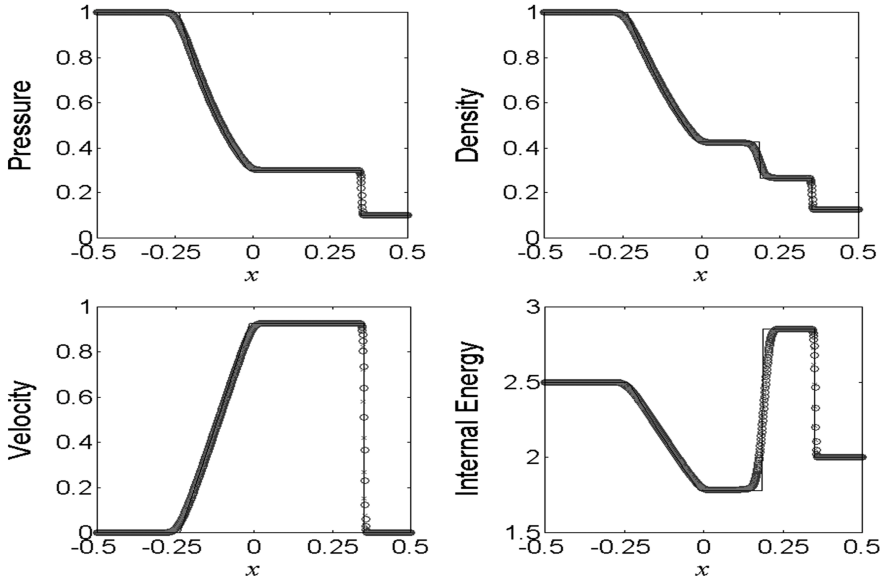

Figure 9 Sod test case [115]: —, exact solution; x, FDLBM simulation; and o, Euler equation solved using 1st order upwind scheme of Harten [116] with flux vector splitting for p, r, u and e at time $t = 0.2$.

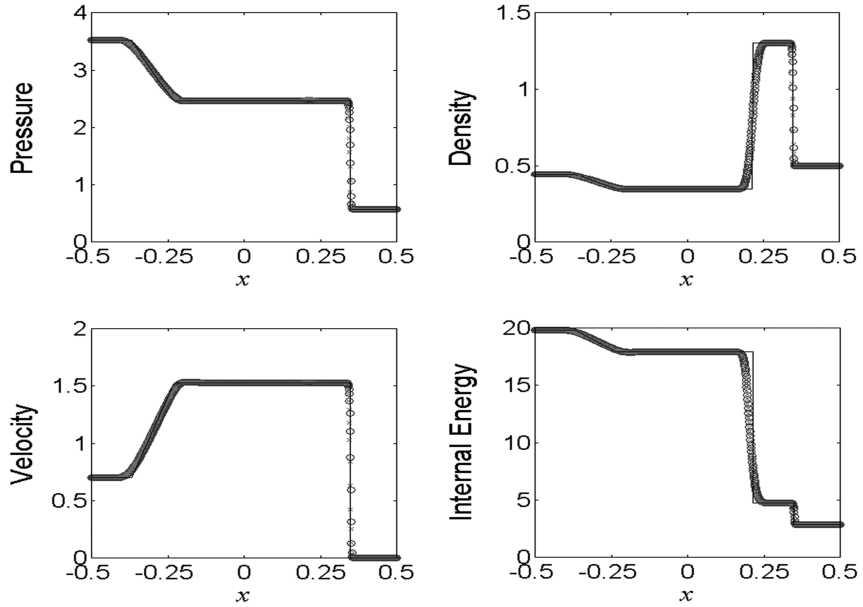

Figure 10 Lax test case [117]: —, exact solution; x, FDLBM simulation; and o, Euler equation solved using the 1st order upwind scheme of Harten [116] with flux vector splitting for p, r, u and e at time $t = 0.14$.

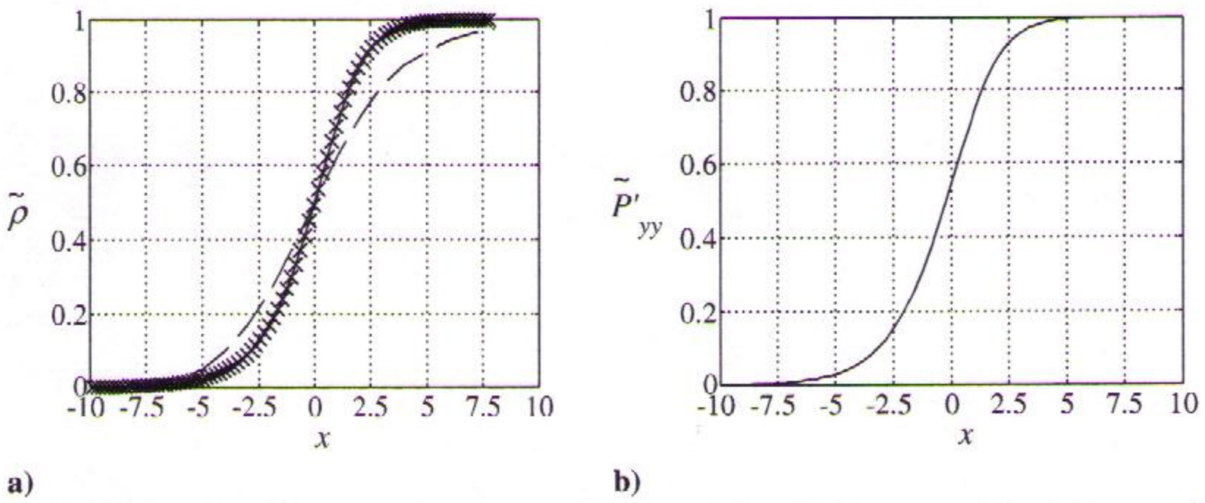

Figure 11 Shock profile for Nitrogen gas with a shock Mach number $M_1 = 1.55$: (a) $\tilde{\rho}$; (b) $\tilde{P}'_{yy}$. Dash line (- - - -) is the experimental result of Alsmeyer [118], cross 'x' is the DNS result, solid line is the FDLBM result. For this 1-D shock $P'_{xx} = P'_{xy} = 0$ and $Pr_\infty = 2/3$, $\gamma = 5/3$, $s = 0.816$, $\Delta x = 0.2$ are specified.

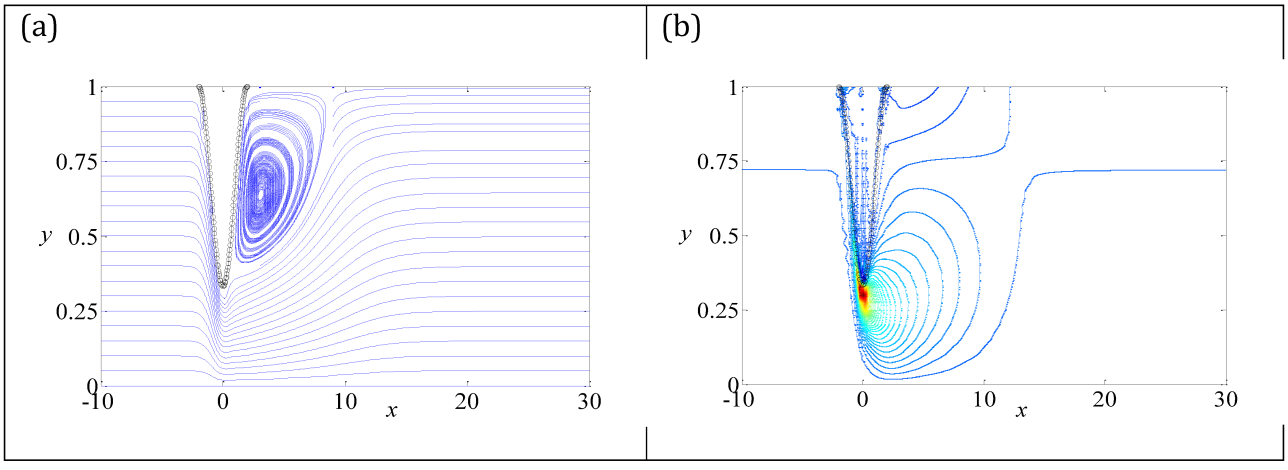

Figure 12 Streamline (a) and vorticity (b) plots for model M3 at Re = 50 from FDLBM simulation. Symbol 'o' denotes immersed boundary points (the area inside the immersed boundary should be ignored). Model M3 is that used in Deshpande et al. [106] with 89% area reduction.

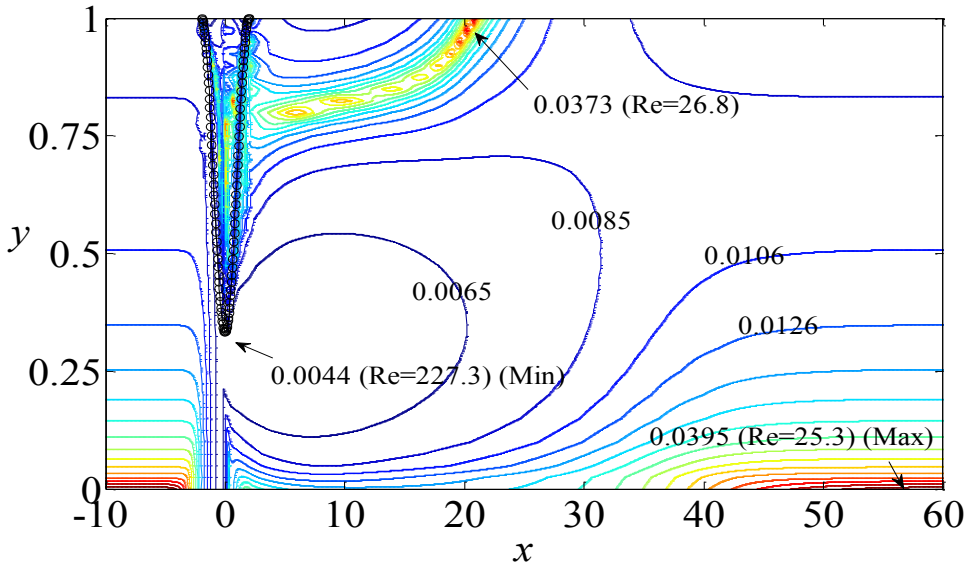

Figure 13 Normalized viscosity (reciprocal of the 'local' Re) contour from FDLBM simulation for model M3 derived from non-Newtonian fluid (CY model [78]). Symbol 'o' denotes immersed boundary points. There are 64 equally distributed contour lines, and the maximum and minimum bounds are 0.0395 and 0.0044.

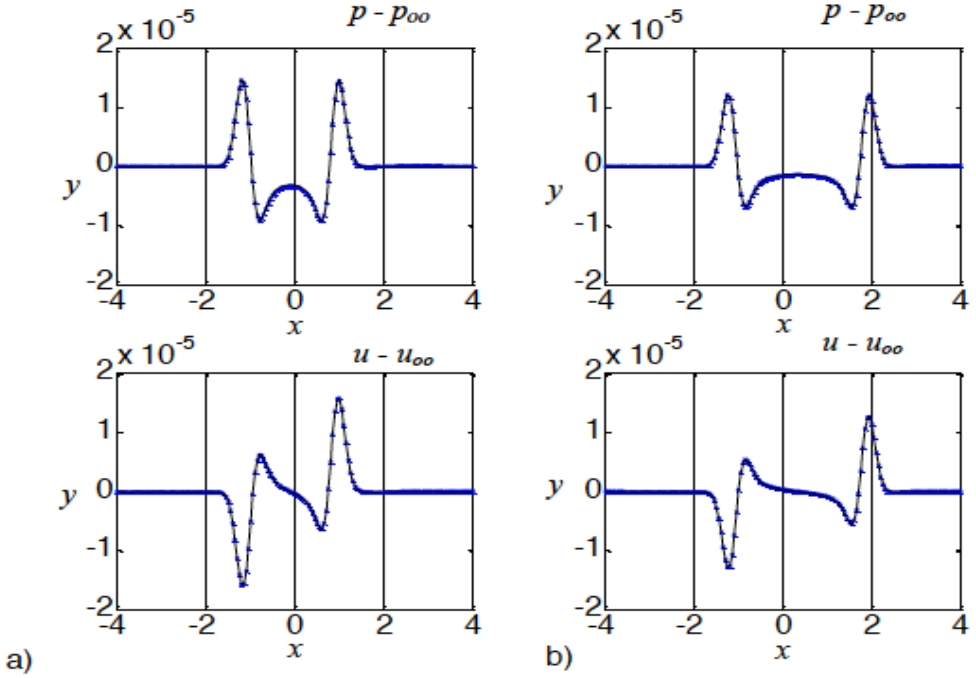

Figure 14 Distributions of p and u fluctuations along x-axis at (a) t = 1.0 and (b) t = 1.5: —, DNS and analytical solution; x, FDLBM solution.

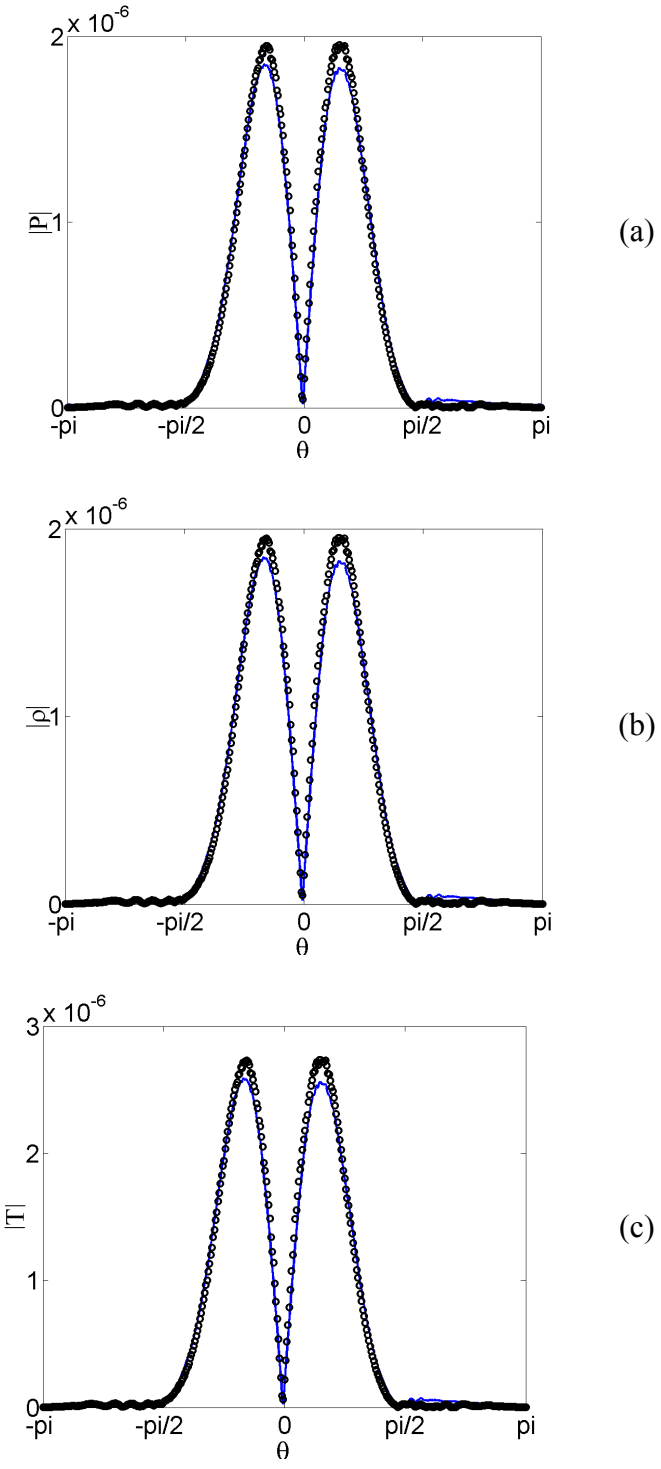

Figure 15

Scattered distributions of (a) p_s; (b) ρ_s; (c) T_s, at $\hat{r}/\hat{\lambda} = 5$ for the $\lambda = 0.5$ vortex-scattering case: "o" FDLBM; "——" DAS.

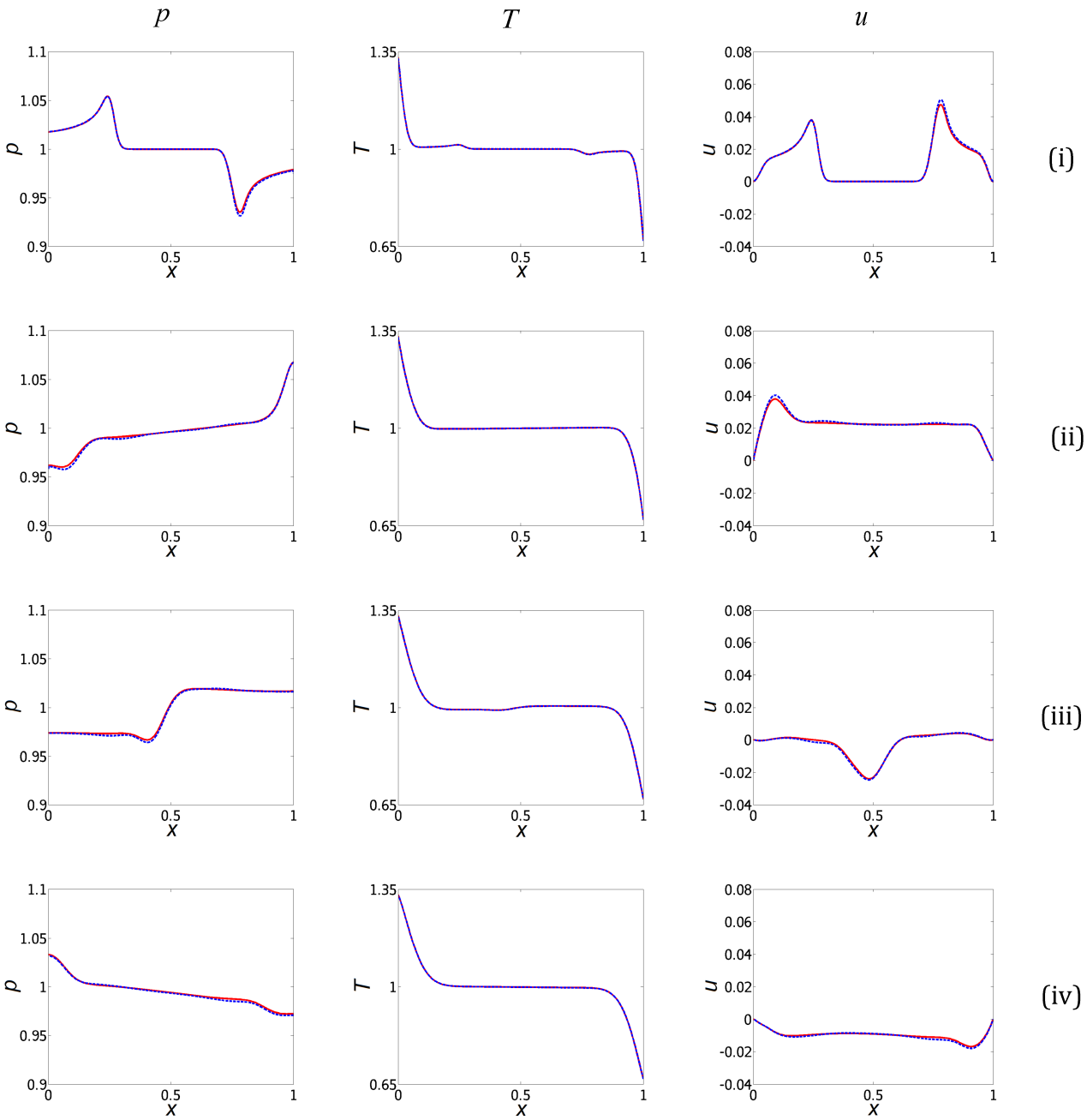

Fig. 16 Case 2, dimensionless p, T, and u variations with x of the thermo-acoustic wave for DAS (blue solid line) and FDLBM (red circles) simulation at (i) $t = 0.25$; (ii) $t = 1.0$; (iii) $t = 1.5$; (iv) $t = 2.0$.

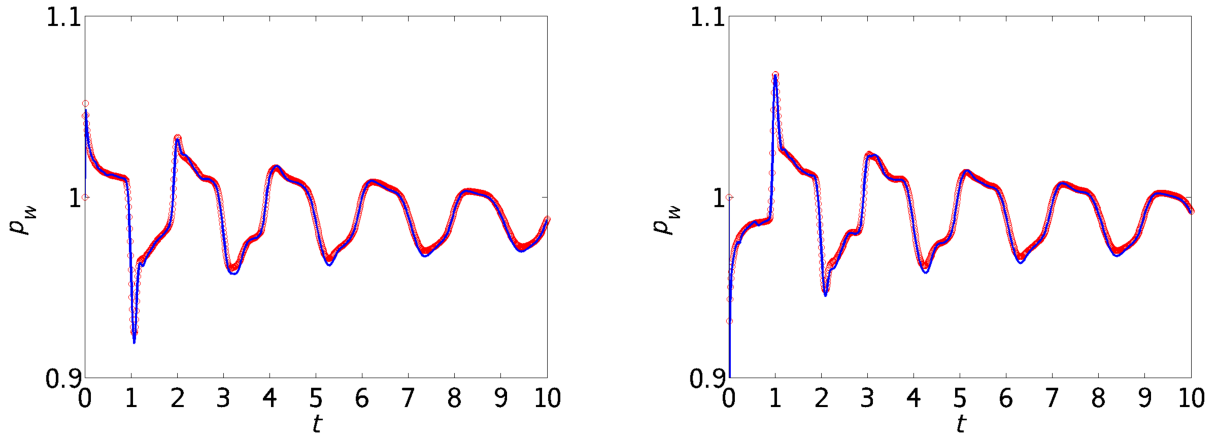

(i) (ii)

Fig. 17a Case 2: dimensionless p_{w} variation with t at the mid-point of (i) left wall, and (ii) right wall: DAS (blue solid line) and FDLBM (red circles) simulation from $t = 0$ to $t = 10$.

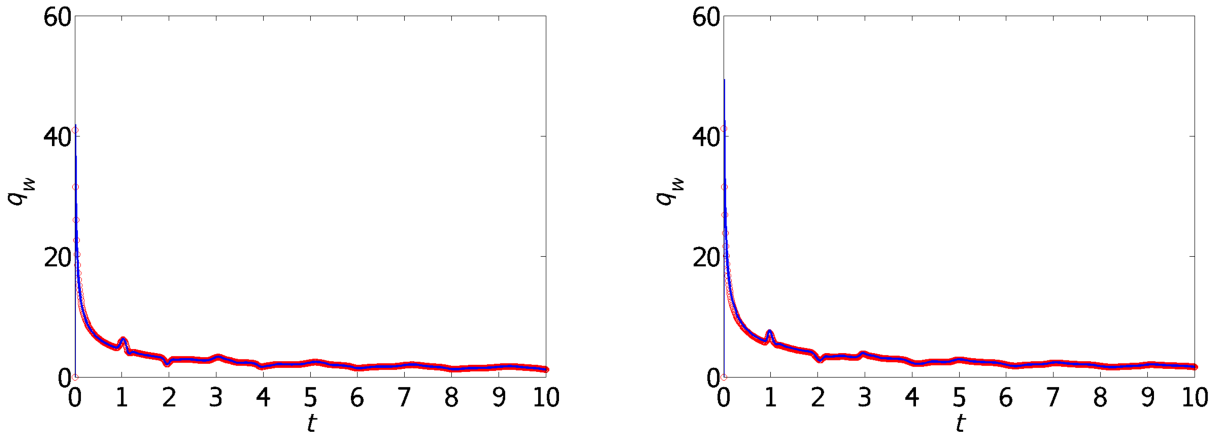

(i) (ii)

Fig.17b Case 2: dimensionless q_w variation with t at the mid-point of (i) left wall, and (ii) right wall: DAS (blue solid line) and FDLBM (red circles) simulation from $t = 0$ to $t = 10$.